Composite Zirconium Phosphate/PTFE Polymer Membranes for Application in Direct Hydrocarbon Fuel Cells

Amani Al-Othman

Thesis submitted to the Faculty of Graduate and Postdoctoral Studies in partial fulfillment of the requirements for the PhD degree in Chemical and Biological Engineering

Department of Chemical and Biological Engineering

Faculty of Engineering

University of Ottawa

Statement of Contributions of Collaborators and/or Co-Authors

I hereby declare that the work presented here is my own effort and I am the sole author of this thesis. I am the one who performed all the experiments and the data analyses under the scientific supervision of Dr. Marten Ternan and Dr. André Tremblay. I have acknowledged other sources of information and assistance in analyses where applicable. The editorial and scientific reviews, as well as the comments were provided by my research project supervisors Dr. Marten Ternan and Dr. André Tremblay.

ABSTRACT

Higher temperature (~ 200°C) operation for proton exchange membrane (PEM) fuel cells would have several advantages including enhanced electrochemical kinetics, useful heat recovery, and improved catalyst tolerance for contaminants. Conventional perfluorosulfonic acid membranes (PFSA), such as Nafion show a dramatic decrease in proton conductivity at temperatures above 80°C. For this reason, there has been an increasing effort toward the development of stable, higher temperature membranes with acceptable proton conductivity. This work is directed toward the development of Nafion free membranes for direct hydrocarbon PEM fuel cells containing zirconium phosphate as the proton conductor component. Hence, composite membranes composed of zirconium-phosphate (ZrP), a solid proton conductor, which was precipitated within the voids of a porous polytetraflouroethylene (PTFE) support were synthesized.

Amorphous-like zirconium phosphate (ZrP) powder was synthesized in this work. ZrP was prepared by precipitation at room temperature via reaction of $ZrOCl_2$ with H_3PO_4 aqueous solutions. The proton conduction properties of ZrP powder were studied under the processing conditions found in direct hydrocarbon fuel cell. Our experimental results showed that the ZrP powder processed at 200°C possess a proton conductivity that is greater by one order of magnitude than the oven-dried samples at 70°C. Thereby, it was possible to avoid the normal decrease in conductivity with increasing temperature by having sufficient water in the vapor phase.

This thesis reports the first synthesis of composite ZrP/PTFE/Glycerol (GLY) membranes. Glycerol (GLY) was introduced into the pores of PTFE with the ZrP proton conductive material using the successive wetting/drying technique. These membranes had reasonable values of proton conductivities (0.045 S cm^{-1}), approaching that of Nafion (0.1 S cm^{-1}) at room temperature. Samples of these composite membranes were processed at the inlet conditions of a propane fuel cell, at 200°C. Experimental results showed that the proton conductivity remained almost unchanged.

This thesis also describes and reports the first synthesis of sulphur “S” or silicon, Si–modified zirconium phosphate (ZrP), porous polytetrafluoethylene (PTFE) and, glycerol (GLY) composite membranes. It was aimed at the substitution of a minor amount of phosphorus “P” in the ZrP by (S or Si) in the ZrP to modify the proton conduction properties. The modification was performed by adding a certain amount of silicic acid or sulphuric acid into phosphoric acid then proceeding with the precipitation in situ. A high proton conductivity, of 0.073 S cm^{-1},i.e. 73% of that of Nafion, was observed for the Si–ZrP/PTFE/GLY composite membrane.

RÉSUMÉ

L'opération à haute température (~ 200°C) de piles à combustible avec membrane échangeuse de protons (PEM) possède plusieurs avantages incluant une amélioration de la cinétique électrochimique, la récupération de chaleur utile et une tolérance accrue des catalyseurs vis à vis les contaminants. Les membranes à acide perfluorosulfonique (PFSA) conventionnelles, tel que le Nafion, démontrent une réduction significative de leur conductivité protonique lorsqu'elles sont soumises à des températures supérieures à 80 °C. Pour cette raison, il y a un effort grandissant au développement de membranes plus stables à haute température et avec une conductivité protonique acceptable. Le présent travail consiste au développement de membrane sans Nafion pour pile à combustible PEM à hydrocarbure direct contenant des phosphates de zircon en tant que conducteur protonique. Des membranes composites à base de phosphates de zircon (ZrP), un conducteur solide, précipités dans les pores d'une matrice de polytétrafluoroéthylène (PTFE) ont été synthétisées.

Pour ce travail, une poudre amorphe de phosphate de zirconium (ZrP) a été synthétisée en précipitant à température ambiante le produit de la réaction entre le $ZrOCl_2$ et H_3PO_4 en solution aqueuse. La conductivité protonique des poudres de ZrP a été étudiée aux mêmes conditions d'opération qu'une pile à combustible à hydrocarbure direct. Les résultats expérimentaux démontrent que la conductivité protonique du ZrP à 200°C est supérieure à celle des échantillons séchés au four à 70°C par un ordre de grandeur. Il est ainsi possible d'éviter la décroissance usuelle de la conductivité lors d'une augmentation de température en assurant une quantité de vapeur d'eau suffisante.

Cette thèse démontre les premières synthèses de membranes composites à base de ZrP, de PTFE et de glycérol (GLY). Le glycérol (GLY) a été introduit dans les pores de la matrice de PTFE avec le matériel conducteur de proton (ZrP) en utilisant une technique de mouillage/séchage successifs. Ces membranes ont démontré une conductivité protonique raisonnable et similaire à celle du Nafion à température ambiante (0.1 S cm^{-1}). La conductivité protonique s'éleve à 0.045 S cm^{-1}. Des échantillons de ces membranes composites ont été testés aux conditions d'opération d'une pile à combustible à base de

propane à 200 °C. Les résultats expérimentaux ont démontré que leur conductivité protonique est restée pratiquement inchangée.

Enfin, cette thèse décrit aussi les premières synthèses de membranes composites de phosphate de zircon (ZrP), de polytétrafluoroéthylène (PTFE) et de glycérol (GLY) modifiées avec du souffre ou du silicium. L'objectif était de remplacer une fraction du phosphore dans le ZrP par du souffre ou du silicium afin de modifier la conductivité protonique des membranes composites. La modification a été effectuée en mélangeant une petite quantité d'acide silicique ou sulfurique à l'acide phosphorique suivie d'une précipitation in-situ. Une haute conductivité protonique, 0.073 S cm^{-1}, c'est à dire 73% de celle du Nafion, a été démontrée pour la membrane composite de Si-ZrP/PTFE/GLY.

"Glory to You (O Lord), knowledge we have none, except what You have taught us. Verily, it is You are, the all-knower and the all-wise"

Quraan, 2:32.

ACKNOWLEDGMENTS

To begin with, I would like to express my sincere gratitude to my thesis supervisors Dr. Marten Ternan and Dr. André Tremblay for their guidance and endless support during my work on this research project. Their positive feedback, enthusiasm, innovative ideas and constructive criticism had a remarkable influence on me during the past five years of my life.

I would like to thank my mentor and my friend, Dr. Chris Gardner, for the time he spent in teaching me how to use the various electrochemical devices in the laboratory and, for sharing me with some of his broad experience in the field of fuel cells research. I also wish to thank Dr. Wendy Pell, Dr. Sadok Latief and Dr. Hamid Khakdaman for the useful discussions and feedback.

I would like to express my gratitude to the technical staff in the department of chemical and biological engineering: Louis Tremblay, Gerard Nina, and, Franco Ziroldo for the enormous effort provided in building the experimental setup, the prompt assistance whenever I needed throughout my experimental coursework and for being such good friends.

I wish to thank my friends in the department of chemical engineering for the constructive discussions, good company and the friendly environment created, that made the research process much more enjoyable to me. Special thanks to my dear friend Joanne for her impeccable sense of humor. Many thanks to Patrick Plouffe, for the time and effort he put in translating the abstract of this thesis into French.

I want to say thank you very much to my dear husband, Muhammad, for his endless support, patience and love in the past 10 years, and to my children Omar Alfarooq and Farah for lighting up my life. I also wish to thank my sisters and my brothers for their love, support and their sense of humor. Very warm thanks to my childhood friends, Neda, and Noor who were always with me, during my frustrating and wonderful times.

I would like to take this opportunity to express my heartfelt gratitude and appreciation to all those who have touched and contributed to my life in the past years.

Last and foremost, I wish to thank my parents for their nonstop love and support as a child and as a grown-up woman to become what I am now. I wish to thank them for their never-ending encouragement during this journey of learning, and to you father and mother, I dedicate this thesis.

TABLE OF CONTENTS

LIST OF FIGURES

Chapter One

Chapter Three

Chapter Four

Chapter Five

LIST OF TABLES

Chapter Three

Chapter Four

LIST OF UNITS, CHEMICAL FORMULAS AND ABBREVIATIONS

A	Ampere
R	Resistance (Ohm)
S cm^{-1}	Siemens per centimeter
σ	Proton conductivity (S cm^{-1})
……..	
DPFC	Direct propane fuel cells
GLY	Glycerol
H_3PO_4	Phosphoric acid
H_2SO_4	Sulphuric acid
PEMFC	Polymer electrolyte fuel cells
PTFE	Polytetrafluoroethylene
$SiO_2.H_2O$	Silicic acid
$Zr(HPO_4)_2$	ZrP or Zirconium phosphate
$ZrOCl_2.8H_2O$	Zirconium oxychloride octahydrate
……	
EIS	Electrochemical impedance spectroscopy
FTIR	Fourier transform infrared spectroscopy
SEM	Scanning electron microscopy
TGA	Thermo–gravimetric analysis
XRD	X-Ray diffraction

CHAPTER ONE - INTRODUCTION

Chapter 1- Introduction

Fuel cells were first described in 1839 by an English judge and a physicist, William Grove [1]. They are electro-chemical devices that convert the chemical energy stored in a fuel into electrical energy. Fuel cells are considered to be one of the promising technologies for efficient power generation. Although several types of fuel cells have been developed over the past 170 years of research, polymer electrolyte membrane fuel cells (PEMFC's) are currently receiving the most interest. Fuel cells are similar to the battery in that they produce electrical energy. They are unlike batteries in that, the reactants are continuously supplied and products are continuously removed. The most common types of fuels being used in PEM fuel cells are either methanol or hydrogen (derived from hydrocarbons). The fuels can be supplied continuously at the anode, whereas the oxidant (such as oxygen in air) can be continuously supplied at the cathode.

PEM fuel cells consist of two compartments, anodic and cathodic, separated by a proton exchange membrane. A schematic diagram of a PEM fuel cell is shown in Fig.1. The fuel (e.g. hydrogen) is fed to the anode, where it is oxidized to generate protons and electrons. Electrons flow in an external circuit to the cathode, resulting in direct electrical current. Protons diffuse through the proton exchange membrane to reach the cathode. The membrane is a proton conducting material. It only allows the passage of protons from the anode to the cathode. The combination of, diffusion of protons to the cathode and, the electron flow completes the electric circuit. The oxidant (air or pure oxygen) is fed to the cathode. Oxygen is reduced by the electrons flowing externally from the anode, to form O^{2-}. Then, O^{2-} combines with protons to form water.

Nafion is, by far, the most widely used membrane in PEMFC. Nafion was initially developed by Dupont in the 1960's [2]. This membrane performs quite well below 90 °C and under fully hydrated conditions, thus, PEMFC are usually operated at temperatures below 90 °C with pressures between 1 and 5 bar. Nafion consists of a fluorinated backbone and a sulfonated polyether chain. Hence, Nafion's good chemical and mechanical stability properties are due to the perfluorinated main chain [3]. The proton conductivity of this membrane is strongly dependent on the water content that is needed to solvate the proton of

the sulfonic acid groups. Dehydration of Nafion membranes limits the operation of a PEM fuel cell to temperatures below 100 °C at ambient pressure.

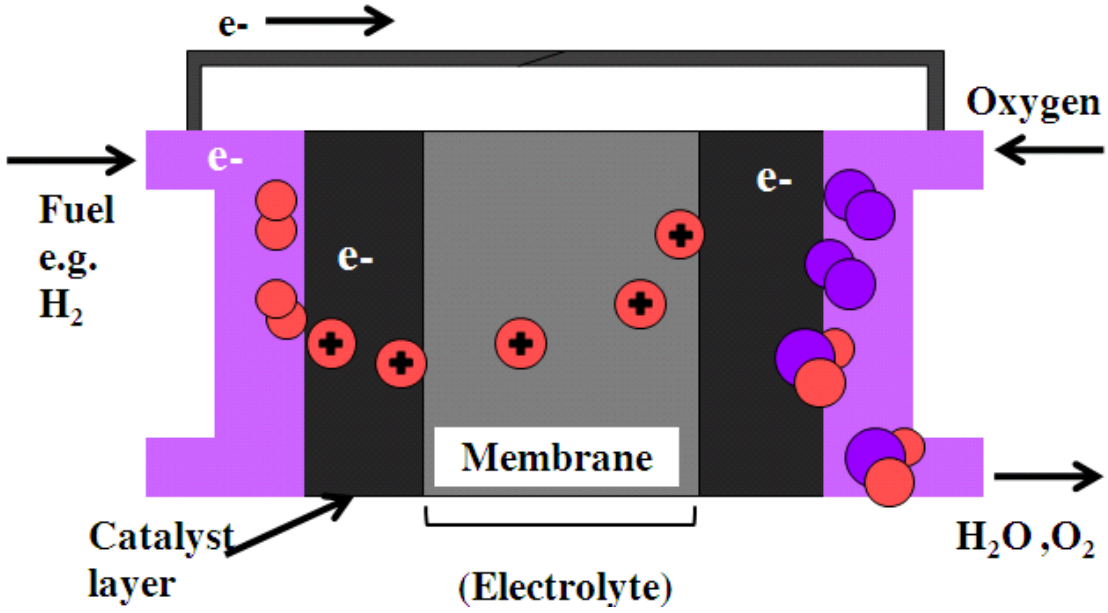

Fig. 1. Schematic Diagram of a PEM Fuel Cell.

High temperature operation is preferred in PEM fuel cells for several reasons. The reaction kinetics and the catalytic activity for both electrodes are enhanced at higher temperatures. High temperature operation also reduces the poisoning effect of the expensive catalyst (platinum) by fuel impurities such as carbon monoxide (CO), permitting a wider range of fuels to be used in addition to pure hydrogen. Extensive research efforts have been made to develop new membrane materials that can operate well at elevated temperatures and low hydration levels. For a membrane to be good for high temperature operation, it should have the characteristics of reasonable and/or high proton conductivity (preferably > 0.1 S/cm), good thermal and chemical stability and a low cost.

Hydrocarbons are desirable fuels for PEM fuel cells despite the fact that most PEM fuel cells currently operate using hydrogen or methanol. Hydrocarbons have several advantages including: higher energy storage density, global availability and, ease of transportation. The well established infrastructure made it possible to use hydrocarbons

(propane for rural areas and methane for urban areas) as fuel. Hydrocarbon fuel cells have been proposed for the application in rural locations where electricity is needed in modest quantities to meet residential demands. Liquefied petroleum gas (LPG or propane) is distributed via trucks to rural locations in North America and natural gas is distributed by pipelines in urban locations. If hydrocarbons are directly fed to the anode of the fuel cell, then the capital cost of using a PEM fuel cell will be lowered by 30% due to the elimination of the fuel processor unit used to make hydrogen or methanol. Although the advantages of hydrocarbons are substantial, they do have one major disadvantage. Reaction rates (fuel cell current densities) are extremely small. This work is an attempt to improve reaction rates by high temperature operation. As a result, the development of high temperature membranes is the subject of this thesis.

Despite all the breakthroughs achieved in the field of PEM fuel cells research, their penetration into the market is still limited. PEM fuel cells that operate on hydrogen or methanol are very expensive and this originates from the contribution of different components, mainly the cost of the membrane and the cost of the catalyst (a precious metal, platinum). Consequently, there is an immense effort on the development of both membranes and catalysts. These efforts have so far, achieved moderate success. In particular, improvements were achieved by: 1) the reduction of the precious metal catalyst (Pt) loading and, 2) by the development of alternative materials for Nafion.

1. 1 Research objectives

The principal objective of this research project was to study, develop and synthesize a Nafion–free high temperature composite membrane composed of porous polytetrafluoroethylene (PTFE) support and zirconium phosphate (ZrP), a solid proton conductor.

A fuel cell membrane should possess the mechanical integrity in addition to the reasonable proton conductivity. A composite membrane was synthesized, made of zirconium phosphate (ZrP), the proton conducting material, incorporated within the porous

polytetrafluoroethylene (PTFE) support material by an in-situ precipitation reaction. Thus, the composite membrane had the dual characteristics of (1) ZrP as a proton conductor and (2) the thermal stability of PTFE up 260 °C as a support. This type of high temperature membrane was synthesized and evaluated for its proton conduction properties at conditions representative of a direct hydrocarbon PEM fuel cell, operating at temperatures ~ 200 °C. A process flow sheet for the electro-oxidation of propane was prepared and a complete fuel cell test station was built for the purpose of preparing and testing membrane electrode assemblies (MEA's). Testing and diagnosis have been performed and a detailed description of the process flow sheet and fuel cell test station development are provided in appendix A of this thesis.

A sub–objective of this research project was to study and evaluate the proton conducting properties of zirconium phosphate as a possible high temperature electrolyte material for PEM fuel cells.

Experiments were performed to prepare ZrP powder via the precipitation reaction of zirconium oxychloride and phosphoric acid at room temperature. The ZrP powder was then dried / processed at different conditions. The ZrP samples were then analyzed and studied using various techniques such as X-Ray diffraction (XRD), Thermogravimetric Analysis (TGA) and evaluated for their proton conducting properties using a four probe electrochemical impedance spectroscopy (EIS) technique.

Another sub–objective of this research project was to synthesize the composite ZrP/PTFE membrane and improve its proton conductivity.

Once the characteristics of ZrP as a proton conducting material were studied and evaluated, experiments were performed to synthesize the ZrP/PTFE composite membrane. Nafion-free ZrP/PTFE/GLY composite membranes were synthesized and investigated as proton conductors for the first time in this research project. The proton conductor powder, ZrP, needed the support from a mechanically integrated membrane. Porous PTFE provided

the mechanical support. Therefore, ZrP was precipitated in such a way that completely filled the pores of PTFE. Thus, completing the path for protons to hop and reach the cathode. The early experimental attempts performed to synthesize the composite membrane along with the preliminary experimental results are shown in Appendix B of this thesis.

Zirconium oxychloride and glycerol (GLY) were introduced into the pores of PTFE first, followed by the addition of phosphoric acid to perform the precipitation reaction, and, forming ZrP in-situ. After the ZrP/PTFE/GLY composite membranes were synthesized, they were evaluated using several techniques such as XRD, EIS, Fourier Transform Infrared spectroscopy (FTIR) and Scanning Electron Microscopy (SEM). Most importantly, composite membranes were evaluated for proton conductivity and for the coverage of PTFE by the ZrP material.

A third sub–objective of this research project was to form S and Si–modified ZrP/PTFE/GLY membranes. Then, the proton conducting properties of these modified composite membranes were evaluated.

Modified sulphur "S" or silicon "Si", Si–ZrP/PTFE/GLY composite membranes were synthesized and investigated for the first time in this thesis. Composite membranes were modified using silicic acid or sulphuric acid that was added to phosphoric acid prior to the in-situ precipitation reaction. The S or Si-ZrP/PTFE/GLY composite membranes were synthesized and evaluated using several techniques such as XRD, EIS, Fourier Transform Infrared spectroscopy (FTIR) and Scanning Electron Microscopy (SEM). Most importantly, composite membranes were evaluated for their proton conductivity and the coverage of PTFE by the ZrP material.

1.2. Thesis structure and organization

This thesis is composed of eight chapters. The current one is the thesis introduction. Chapter two presents the background to this research project. Chapters three and four are independent scientific articles that were published in a refereed scientific journal. Therefore, each one of them can be read independently. Chapter five is to be submitted as a scientific article in a refereed scientific journal. Therefore, throughout these chapters, the common ideas, experimental procedures and the project core problem has been reiterated where applicable. Chapter six contains a general discussion that summarizes the ideas and integrates the results of chapters three, four and, five. The contributions, conclusions, and recommendations that resulted from the entire thesis are presented in chapters seven and eight. The development of a direct hydrocarbon fuel cell test station and the preliminary experimental investigations on the synthesis of the composite membrane are shown in Appendix A and B of this thesis.

1.3. References

1. G. Hoogers, "Fuel cell technology handbook" , CRC press LLC, USA 2003, p. 2-37.
2. P. Costamagna, S. Srinivasan, J. Power Sources, 102, 2001, p.242.
3. S. Banerjee, D. E. Curtin, J. Flour. Chem., 125, 2004, p.1211.

CHAPTER TWO – LITERATURE REVIEW

Chapter 2- Polymer electrolyte membrane fuel cells (PEM) and direct hydrocarbon fuel cells

Fuel cells are classified by their electrolyte material. Hence, they are divided into the following categories: alkaline, phosphoric acid, solid oxide, molten carbonate, and proton exchange membrane or polymer electrolyte membrane (PEM) fuel cells. PEM fuel cells show good performance as power generators for both stationary and transportation applications. Their all-solid construction (solid electrolyte) makes them perfect for many applications.

PEM fuel cells can be further categorized based on the fuel that is used, hydrogen fuel cells, direct methanol fuel cells, or hydrocarbon fuel cells. Both hydrogen and methanol fuels provide excellent fuel cell performance. The performance of hydrocarbons was investigated in the 1960's. Although their performance is poor, direct hydrocarbon fuel cells have a theoretically higher efficiency, potentially lower initial cost and lower maintenance cost. These characteristics are motivations for more research.

The direct oxidation of hydrocarbons was addressed in several studies during the 1960's and early 1970's [1-4]. The direct anodic oxidation of the hydrocarbon fuel can occur without the need for a fuel processor unit which accounts for one third of the fuel cell capital cost. In particular, the direct oxidation of hydrocarbon fuels in the presence of aqueous electrolytes and at temperatures less than 200 °C [5] was studied. More experiments were conducted to study the anodic oxidation of saturated hydrocarbon fuel cells using strong acids [6]. These studies concluded that no economical construction could be achieved due to the hydrocarbons limited anodic performance and the use of aqueous electrolytes.

The investigations using solid polymer electrolytes also began in 1960's. Niedrach for instance [7] investigated the oxidation behavior of hydrocarbons, such as propane and methane using a solid acid electrolyte based on reinforced sulfonated phenol formaldehyde resin. Neidrach used black platinum (Pt) or palladium (Pd) electrodes. The results

compared the performances of the two catalysts Pt and Pd, and Pt showed better performance at an oxidation current density of (less than 2 mA/cm^2) at 0.2 V.

Recently, a few computational fluid dynamics (CFD) studies were reported in literature to model the direct hydrocarbon fuel cell performance. Psofogiannakis et.al. [8] showed in a CFD model of a direct propane fuel cell that the over potential at the anode catalyst was the largest resistance. Khakdaman et.al [9] developed a two–dimensional CFD model for a direct propane fuel cell anode. The modeling results showed an improved anodic over–potential (one third less resistance obtained) at 150 ºC with zirconium phosphate (ZrP) as an electrolyte and platinum (Pt) as a catalyst. Khakdaman et.al [10] have also developed a two–dimensional CFD model to describe the performance of a complete direct propane fuel cell. The model prediction results showed that the performance of a direct propane fuel cell with a ZrP-PTFE composite membrane, at 150 ºC, was comparable to that obtained with Nafion and aqueous phosphoric acid electrolytes.

The electro-oxidation reactions taking place in a direct hydrocarbon fuel cell are described below, using propane as an example. Propane (C_3H_8) reacts at the anode as follows [9]:

$$C_3H_8 + 6\ H_2O = 3\ CO_2 + 20\ H^+ + 20\ e^{-1} \quad (1)$$

It can be seen that six moles of water are consumed per one mole of propane reacted.

Oxygen or air enters the cathode, and the following reaction takes place:

$$5\ O_2 + 20\ H^+ + 20\ e^{-1} = 10\ H_2O \quad (2)$$

The overall reaction is: $C_3H_8 + 5\ O_2 = 3\ CO_2 + 4\ H_2O$ (3)

The experimental performance of a direct hydrocarbon fuel cell was addressed in several studies. Savadogo et. el., [11] for example, studied the low temperature performance of a direct propane fuel cell (DPFC) using different membranes including Nafion 117, H_2SO_4 doped PBI, STA (silicotungstic acid), and modified Nafion 117. The study compared the performance of these membranes to an H_2/O_2 fuel cell with a Nafion 117 membrane. Savadogo's results showed that DPFC produced small current densities, and,

compared to the H_2/O_2 fuel cell, DPFC with Nafion 117 showed the poorest performance. Savadogo et. al. [12], also studied the electro-oxidation of acetals for the purpose of hydrocarbon fuel cell applications using different electrodes. The results showed that the highest rate of reaction (current density) was obtained with the platinum based electrodes.

Studies on hydrocarbon oxidation behavior reported the problems associated with using hydrocarbon fuels in PEM fuel cells at temperatures less than 120 °C. These problems included their poor electro-catalytic activity, the poisoning effect due to the adsorption of carbon monoxide (CO) on the precious metal (Pt) catalyst, and, the high degree of hydrocarbons cross over through the Nafion membrane [12]. It is therefore expected that high temperature operation (~200°C) should be beneficial for the hydrocarbon fuel cell performance in several ways. It will improve the reaction rate (current density) of the electro-catalytic process, and suppress the carbon monoxide, CO, adsorption on the catalyst. Furthermore, liquid phase water will be eliminated, thus, more rapid diffusion of reactants should be achieved.

2.1 Fuel cell performance

The performance of a PEM fuel cell can be evaluated by obtaining a polarization curve [13]. In this curve the cell potential (V) is plotted versus the cell current density (A/cm^2). The polarization curve shows the current densities at which polarizations (losses) cause a drop in potential. The actual cell potential decreases from its equilibrium potential due to physical and chemical phenomena taking place inside the fuel cell. These phenomena cause a loss of performance and can be attributed to, 1) kinetic losses (region of activation polarization), 2) ohmic losses (region of ohmic polarization) and, 3) mass transport losses (concentration polarization).

The activation polarization is the result of the electrode surface processes including adsorption, surface diffusion, reaction and, desorption. The ohmic polarization is caused by the resistance to the flow of electrons in the cell components including the flow in the graphite plates and external wires as well as the flow of protons in the electrolyte. The largest ohmic polarization is caused by the resistance of proton transport in the membrane.

The concentration polarization is attributed to the reactants diffusion into, and product diffusion from the anode and the cathode. This resistance can be very large at high current densities when liquid water floods the pore structure of the cathode.

2.2 High temperature membranes

The membrane in a fuel cell serves many purposes. It is the electrolyte material that provides the ionic (proton conduction) between the anode and the cathode. The membrane is also the selective conductor for protons and an insulator for electrons. The fuel cell membrane acts as a separator between the anode fuel and the cathode oxidant to prevent their cross over and mixing thus, preventing any resulting combustion reaction.

Nafion and perfluorosulfonic acid (PFSA) proton exchange membranes have been widely used due to their excellent proton conductivity and electrochemical stability. They were developed in the late 1960s by Walther Grot of DuPont [14]. Nafion membranes are durable under fully hydrated conditions and at temperatures ~ 80 º C. However, their conductivity and stability dramatically decrease at higher temperatures and the high temperature operation of PEM fuel cells is a desired target.

2.2.1 Motivation for higher temperature operation of PEM fuel cells

High temperature operation allows the generation and the recovery of useful heat and reduces the problems associated with liquid water accumulation at the cathode. The reduction of liquid phase water assists in increasing the exposed surface area of the catalyst allowing more molecules to diffuse into the reaction sites. It also diminishes corrosion rates. Higher temperature operation also improves cell tolerance for impurities such as carbon monoxide (CO), which permits the use of a wider range of fuels. Small amounts of CO as low as 10 ppm can poison the catalyst [15]. It was previously shown that the CO coverage on the catalyst surface can be reduced by increasing the temperature [16]. A study performed using platinum based catalysts showed that these catalysts can tolerate up to 1000 ppm CO at 130°C [17].

All the previous reasons are incentives for working at higher temperatures. Nafion and similar PEM's are unlikely to fulfill this target because proton conduction in these membranes is dependent on their hydration levels. Nafion loses its conductivity due to water loss (dehydration). For example, Nafion conductivity decreases from 0.066 to 0.00014 S/cm at 30°C when the relative humidity (RH) decreases from 100% to 34% [15]. Furthermore, the low glass transition temperature of Nafion (110 °C) is problematic because above this point the polymer loses its mechanical stability and degradation ultimately occurs [18].

2.3 Approaches to higher temperature membranes

Several approaches have been followed to develop membranes that permit the operation at higher temperatures. These approaches can be summarized in three major categories: (1) the development of PFSA membranes in which hygroscopic oxides and solid proton conductors are incorporated; (2) the development of sulfonated polyaromatic polymers and composite membranes, such as polyetheretherketone (PEEK) [15], and (3) the development of acid base polymer membranes such as sulphuric and phosphoric acid doped polybenzimidazole (PBI). The following review articles on the recent developments of high temperature membranes are available in literature [15, 19-22].

As for the first approach, considerable efforts have been made to modify the existing PFSA membranes. Weng et. al. [23] investigated a membrane, in which phosphoric acid was incorporated in Nafion. A conductivity of 0.05 S/cm at 150 °C was reported. The incorporation of oxides such as SiO_2, TiO_2 and tungsten oxide (WO_3), in Nafion was also studied [24]. The results showed higher water uptake properties with slightly better performance in contrast to Nafion at 110 °C. Composite membranes were also prepared by the incorporation of solid inorganic proton conductors [25] such as zirconium phosphates, and heteropolyacids. Zirconium phosphates (ZrP) in particular are the topic of this thesis. The synthesis of Nafion-zirconium phosphate composite membranes was addressed in several studies [26-31].

The second approach toward the development of high temperature membranes is the sulfonation of thermally resistant polymers such as polysulfones, fluoropolymers, and polyetheretherketone. The sulfonation of certain polymers such as polystyrenes was investigated in the 1960's [25]. However, it was shown that this type of polymer suffers from a short life time because the tertiary C–H bonds are sensitive to oxidation. The sulfonation of polysulfones (PSF) or polyethersulfone (PES), polyetheretherketone (PEEK), polybenzimidazoles (PBI), polyimides (PI), polyphenylenes (PP), and polyphenylene oxide (PPO) was also investigated in the presence of inorganic components [15]. Although reasonable and promising proton conductivities were obtained, the sulfonated organic compounds still require more study and evaluation for their applications in higher temperature operation.

The third approach involves maintaining reasonable proton conductivity at elevated temperatures by replacing water with another proton transport assisting solvent. This solvent is characterized by having a high boiling point such as phosphoric acid and imidazoles. One example is the preparation of poly (2, 5-benizimidazole) (PBI) membranes. The thermal stability of the PBI membranes doped with phosphoric acid at different temperatures was studied [32]. Samms et al. [32] indicated that that these membranes possess promising conductivity at 200 °C. Despite the promising conductivities reported for the PBI membranes, the poor mechanical properties and the adsorption of phosphate ion on the catalyst are still the major drawbacks.

2.4 Zirconium hydrogen phosphate $Zr(HPO_4)_2$ (ZrP) and ZrP- PTFE composite membranes

The interest in zirconium hydrogen phosphate $Zr(HPO_4)_2$ (abbreviated as ZrP) compound goes back to the 1950's when its behavior as a cation exchanger was discovered [33-35]. Inorganic ion exchangers were expected to be more stable at high temperatures and were investigated for their ion exchange properties. The ion exchange properties were explained by their layered structure, hence, the presence of passageways that provide a sufficiently free volume to allow un-hydrated cations to exchange [36]. Work on the electrical conductance of ZrP was reported in by Alberti et al. [37, 38]. It was shown that

the conductance of ZrP decreased as the degree of crystallanity increased. The fraction of the surface protons is small but their mobility is greater than the internal ones, and they cause high proton conductivity. Hence, there has been an increasing interest not only in the preparation of these inorganic proton conductors but also in their use in sensors, water electrolysis units and other electrochemical devices, e.g. fuel cells. The reported conductivity of amorphous ZrP in water at 80 °C approached 0.01 S/cm [39]. This has triggered several studies to evaluate the proton conductivity of ZrP after its incorporation within non conductive materials such as polymers [40].

A chemical procedure for the precipitation of inorganic fillers, (selected from the oxides and phosphates of the group consisting of Sn, Sb, Mo, W, Ti and Zr) was proposed [41]. The resultant membranes were expected to posses the proton conductivity of the inorganic material and the mechanical strength of the polymer. Following the procedure of Grot [41], composite membranes were prepared by the precipitation of zirconium phosphate in situ, within Nafion and porous supports such as polytetrafluoroethylene (PTFE) membranes. Yong et. al. [42] prepared composite membranes by mixing a PTFE emulsion and ZrP powder then drying, followed by pressing. Grot [41], described a process for the incorporation of ZrP into a Nafion membrane by the in situ precipitation of ZrP using phosphoric acid. Membranes were also prepared by the impregnation of Nafion films in a solution of zirconyl chloride and phosphoric acid [43]. ZrP was deposited into polyethylene oxides (PEO), PBI, Nafion, sulfonated polysulfone (SPSF), and sulfonated polyetheretherketone (SPEEK) [25]. For example, the sulfonated polyetheretherketone (SPEEK) – zirconium hydrogen phosphate (ZrP) composite membranes were prepared by Tripathi et al. [44]. ZrP precipitated in polytetramethylene oxide PTMO [45] was investigated in a PEM fuel cell at a temperature up to 130 °C. Zirconium phosphate (ZrP) was also deposited in polybenzimedizole (PBI) membranes [46]. Liu et. al. [47] used porous polytetrafluoroethylene (PTFE) membranes as support material for the preparation of Nafion/PTFE composite membranes by the impregnation of PTFE with Nafion solution. Nafion–Teflon–$Zr(HPO_4)_2$ (NTZP) composite membranes were also prepared for the purpose of operation at high temperatures [48]. The inorganic/organic composite membranes appear to be promising for the high temperature operation in fuel cells. These composite membranes are characterized by, 1) their reasonable proton conductivities due to

their water retention properties and, 2) their ability to reduce the undesired fuel cross over as a result of the pore- filling technique.

2.5 References

1. E.J. Cairns, Adv. Eletrochem. Electrochem. Eng., 8, (1971), p. 337.

2. W.T. Grubb, C.J. Michalske, Nature, 201, (1964), p.287.

3. E.J. Cairns, Nature, 210, (1966), p.161.

4. W. T. Grubb, L. W. Niedrach, J. Electrochem. Soc., 110, Issue 10, (1963), p. 1086.

5. Hydrocarbon Fuel Cell technology, Fuel Chem. Am. Chem. Soc. Symp., 150th National meeting, edited by S. Baker, Atlantic city, 1965, P. 429.

6. L.W. Neidrach , J. Electrochem. Soc. 113, (1966), p. 645.

7. L.W. Niedrach , J. Electrochem. Soc. 109, (1962), p. 1092.

8. G. Psofogiannakis , Y. Bourgault , B.E. Conway ,M. Ternan , J. Appl. Electrochem., 36 (2006), p.115.

9. H. Khakdaman, Y. Bourgault, M. Ternan, Ind. Eng. Chem. Res.,49, (2010), 49, p. 1079.

10. H. Khakdaman, Y. Bourgault, M. Ternan, J. Power Sources, 196 , (2011), p.3186.

11. O. Savadogo, F.J. Varela , J. New Mat. Electrochem. Sys., 4, (2001), p. 93.

12. O. Savadogo, X. Yang, J. Appl. Electrochem., 33 , (2001), p. 787

13. Fuel Cell Handbook (7th Edition), U.S. Department of Energy Office of Fossil Energy National Energy Technology Laboratory, 2004, (http://www.brennstoffzellen.rwth-aachen.de/Links/FCHandbook7.pdf).

14. D.J. Harper, "Fuel Cell Projects for Evil Genius", McGraw Hill, 2008, P.81.

15. J.L. Zhang ,Z. Xie ,J. Zhang , Y. Tang , C. Song , T. Navessin , Z. Shi, D. Song , H. Wang, D. Wilkinson , Z. Liu , S. Holdcroft , J. Power Sources 160, (2006), p.872.

16. C. Yang , p. Costamagna , S. Srinivasan, J. Benziger , A. Bocarsly, J. Power Sources, 103 (2001), p.1.

17. G. Xiao , Q.F. Li, A. Hans, N.J. Bjerrum , J. Electrochem. Soc. 142, (1995),p. 2890.

18. C. Yang , S. Srinivasan , A. Bocarsly , S. Tulyani , J.B. Benziger , J. Membrane Sci., 237,(2004), p.145.

19. O. Savadogo, J. Power Sources, 127, (2004), p.135.

20. V. Neburchilov, J. Martin, H. Wang , J. Zhang, Journal of Power Sources 169 ,(2007) p. 221.

21. S.M. Javaid Zaidi, Mat. Sci. Forum, 657, (2010), p.88.

22. S. Bose, T. Kuila, T. Xuan H. Nguyen, N. Hoon Kim, K. Lau,, J.H. Lee, Progress in Polym. Sci., 36, (2011), p. 813.

23. D. Weng. ,J.S. Wainright , U. Landau, R Savinell , J. Electrochem. Soc., 143, (1996),p. 1260.
24. Z.G. Shao , Solid State Ionics, 177, (2006),p.779.

25. Q. Li , R. He , J. Jensen , N.J. Bjerrum , Chem. Mater., 15, (2003), p. 4896

26. F. Bauer, M. Willert-Porada, J. Membr. Sci., 233 , (2004), p.141.

27. H. C. Kuan, C. S. Wu, C.Y. Chen, , Z.Z. Yu, A. Dasari, Y.W. Mai, Electrochem. Solid State Lett. , 9, (2006), p. A76.

28. E. Chalkov, M. V. Fedkin, S. Komarneni, S. N. Lvov, J. Electrochem. Soc., 154, (2997), p. B288.

29. D. Truffier-Boutry, A. De Geyer, L. Guetaz, O. Diat, G. Gebel, Macromolecules, 40, (2007), p. 8259.

30. C. Yang, S. Srinivasan, A. S. Arico, P. Cretı, V. Baglio, V. Antonucci,, Electrochem. Solid-State Lett., 4, (2001), p. A31.

31. G. Alberti, M. Casciola, A. Donnadio, R. Narducci, M. Pica, M. Sganappa, Desalination 199, (2006), p.280.

32. S.R. Samms , S. Wasmus , R.F. Savinell, J. Electrochem. Soc. 143,(1996), p. 1225.

33. C.B. Amphelett , L.A. McDonald., M.J. Redman , J. lnorg. Nucl. Chem. 6, (1958), p.220.

34. A. Clearfield, J.A. Stynes, J. Inorg. Nucl. Chem., 26, (1964), p. 117.

35. R. P. Hamlen , J. Electrochem. Soc., 109, (1962), p.746.

36. A. Clearfield , Ann. Rev. Mater. Sci. ,14 (1984), p. 205.

37. G. Alberti ,E. Torracca , J. lnorg. Nucl. Chem. 30, (1968),p.1093.

38. G. Alberti , M. Casciola,U. Costantino , G. Levi, G. Ricciardi , J. Inorg, Nucl. Chem., 40, (1978), p. 533

39. K. Peinemann , S.p. Nunes Eds, "Membranes for Energy Conversion", Vol. 2, P. 97.

40. M. Casciola, D. Capitani, A. Donnadio, V. Frittella, M. Pica, Fuel Cells, 9, (2009), p.381.

41. W.G. Grot , G. Rajendran, US Patent 5,919,583, 1999.

42. P.I. Yong , K. Jae-Dong , M. Nagai , J. Mat. Sci. Letters, 19, (2000), p.1735.

43. P. Costamagna , C. Yang, A. Bocarsly , S. Srinivasan , Electrochimica Acta ,47, (2002),p.1023

44. P. Tripathi , V.K. Shahi , J. Colloid Interface Sci., 316, (2007),p. 612.

45. J.K. Kim , T. Mori , J. Honma , J. Electrochem. Soc., 153, (2006), A508.

46. R. He , Q. Li , G. Xiao , N.J. Bjerrum , J. Membr. Sci., 226, (2003) p. 169.

47. F.Q. Liu, B.L. Yi, D.M. Xing, J.R. Yu, H.M. Zhang, J. Membr. Sci. 212, (2003) p. 213.

48. R. Jiang , H.R. Kunz , J. Fenton., Electrochim. Acta 51, (2006),p.5596.

CHAPTER THREE

Zirconium phosphate as the proton conducting material in direct hydrocarbon PEM fuel cells operating above the boiling point of water

Amani Al-Othman[a,b], André Y. Tremblay[a], Wendy Pell[b], Sadok Letaief[,b], Tara J. Burchell[c] , Brant A. Peppley[d], and Marten Ternan[e]

(a) Chemical and Biological Engineering,

(b) Catalysis Centre for Research and Innovation,

(c) Department of Physics, University of Ottawa, 161 Louis Pasteur, Ottawa, ON, K1N 6N5, Canada.

(d) Chemical Engineering, Queens University, Dupuis Hall, Kingston, ON, K7L 3N6, Canada.

(e) EnPross Inc., 147 Banning Road, Ottawa, ON, K2L 1C5, Canada

In: Journal of Power Sources 195 (2010) 2520–2525.

Chapter 3- Zirconium phosphate as the proton conducting material in direct hydrocarbon PEM fuel cells operating above the boiling point of water

ABSTRACT

Zirconium phosphate (ZrP) was investigated as a possible proton conductor material in direct hydrocarbon polymer electrolyte membrane (PEM) fuel cells that operate at greater temperatures than conventional PEM fuel cells. Amorphous zirconium phosphate was synthesized in this work by precipitation at room temperature via reaction of $ZrOCl_2$ with H_3PO_4 aqueous solutions. The conductivity of the synthesized ZrP materials was 7.04×10^{-5} S cm^{-1} for ZrP oven dried in laboratory air at 70 °C and 3.57×10^{-4} S cm^{-1} for ZrP powder dried first at 70 °C in laboratory air and then processed at 200 °C with continuous H_2O injection at an H_2O/N_2 molar ratio of 6. This work showed that by maintaining appropriate water content in the vapour phase at processing conditions, it was possible to alter the composition of zirconium phosphate to a sufficiently hydrated state, and thereby avoid the normal decrease in conductivity with increasing temperature.

3.1. Introduction

Work in our laboratory is being directed toward the development of direct hydrocarbon fuel cells having an electrolyte membrane containing zirconium phosphate as its proton conductor component. Hydrogen is the fuel used in most fuel cells. Methanol is the second most common fuel. The reason that hydrocarbons are normally not fed directly to the anode of a fuel cell is that fuel cell performance with hydrocarbon fuels is much worse than with hydrogen or methanol.

Increasing the fuel cell operating temperature is expected to improve the reaction kinetics and therefore, improve hydrocarbon fuel cell performance. Nafion, the polymer electrolyte membrane (PEM) used in many hydrogen fuel cells, becomes dehydrated as the temperature increases and is not suitable at temperatures greater than 85°C. In

contrast, composite electrolytes composed of zirconium phosphate, Nafion, and polytetrafluoroethylene (PTFE) have been used in hydrogen fuel cells at temperatures up to 120°C [1]. Although functional, the performance does decrease as the temperature rises above 80°C. The target temperature for this work is 200°C.

For a direct propane fuel cell, the overall reaction at the anode is:

$$C_3H_8 + 6\,H_2O = 3\,CO_2 + 20\,H^+ + 20\,e^- \quad (1)$$

Therefore, for a steady-state reaction, the feedstock must contain 6 moles of water for every mole of propane. In contrast, when hydrogen is the fuel there is no stoichiometric requirement to include water in the feedstock. Although the hydrogen feedstock to a hydrogen fuel cell is often humidified, the saturated water vapour pressure at the anode of hydrogen fuel cells is small compared to the stoichiometric quantity in Eq (1), above.

Zirconium hydrogen phosphate $Zr(HPO_4)_2$ (abbreviated as ZrP), is a solid protonic conductor. ZrP has a layered structure that allows the intercalation of guest molecules. It has cationic exchange properties, proton-conducting properties, and is a highly hydroscopic insoluble solid. The interest in this compound goes back to the 1950's since its behavior as a cation exchanger [2-4] was discovered. The cationic exchange behavior was explained by the layered structure and the presence of passageways that provide a sufficiently free volume to allow un-hydrated cations to exchange [5].

Work on the conductance properties of ZrP was reported by Alberti et al. [6,7]. It was shown that the conductance of ZrP decreased with an increase in the degree of crystallinity. The fraction of the surface protons is small but their mobility is greater than the internal ones. Their combination results in a large proton conductivity. Alberti et al.[7] found that the mobility of surface ions in α-ZrP are 10^4 times higher than interlayer ions. Therefore, high proton conductivity is the result of the high proton mobility on the surface of ZrP.

There has been an increasing interest, not only in the preparation of inorganic proton conductors, such as zirconium phosphate, but also in their use for the operation in sensors, water electrolysis units and electrochemical devices such as fuel cells. The conductivity of amorphous ZrP in water at 80 °C approaches 0.01 S cm^{-1} [8]. This has triggered several

studies in literature to evaluate the proton conductivity of ZrP after its incorporation within non-conductive materials such as polymers [9]. Examples are composite membranes prepared by the precipitation of zirconium phosphate in-situ, in polytetraflouroethylene (PTFE) [10], in Nafion [1,10], and in the composites prepared by Park et al. [11] by mixing the PTFE emulsion and the ZrP powder followed by drying and pressing.

The objective of this work is to investigate ZrP as an electrolyte material for hydrocarbon fuel cells: specifically, to 1) investigate the degree of ZrP hydration at high temperatures and to 2) investigate the effect of hydration on conductivity.

3.2. Experimental

3.2.1 Preparation and characterization of zirconium phosphate powder (ZrP)

Zirconium phosphate powder (ZrP) was prepared by the reaction of aqueous solutions of zirconium oxychloride ($ZrOCl_2$) and phosphoric acid (H_3PO_4). A 100 mL (0.5 M) solution of $ZrOCl_2$ was prepared using $ZrOCl_2.8H_2O$ purchased from Aldrich. The ZrP powder was precipitated at room temperature upon the addition of 1 M of H_3PO_4 in three stages. The precipitation reaction proceeded according to the following equation:

$$ZrOCl_2 + 2\ H_3PO_4 \rightarrow Zr(HPO_4)_2 + 2\ HCl + H_2O \qquad (2)$$

The gel, formed by the reaction, was then filtered and washed 5 times with de-ionized water. The samples obtained were heated to different temperatures. These samples were subjected to various characterization methods.

The various ZrP samples were subjected to one of two different sets of environmental conditions. The first set of environmental conditions involved heat treatment in laboratory air for 24 hours, as follows: a) ZrP powder oven dried at 70°C in laboratory air, i.e. at a relative humidity of 20 %); b) ZrP powder oven dried at 110°C in laboratory air; c) ZrP powder oven dried first at 70°C and then at 200 °C both in laboratory air. The second set of environmental conditions was a combination of heat treatment and elevated water vapour pressure, specifically: d) ZrP powder dried first at 70 °C in laboratory air and then processed at 200 °C in a tube furnace, for 3 hours with continuous H_2O injection at an

H_2O/N_2 molar ratio of 6, the stoichiometric ratio in the direct propane fuel cell reaction, as shown in Fig. 1. After this processing, each sample was placed in a closed bag made of non-porous PTFE and sent for analysis.

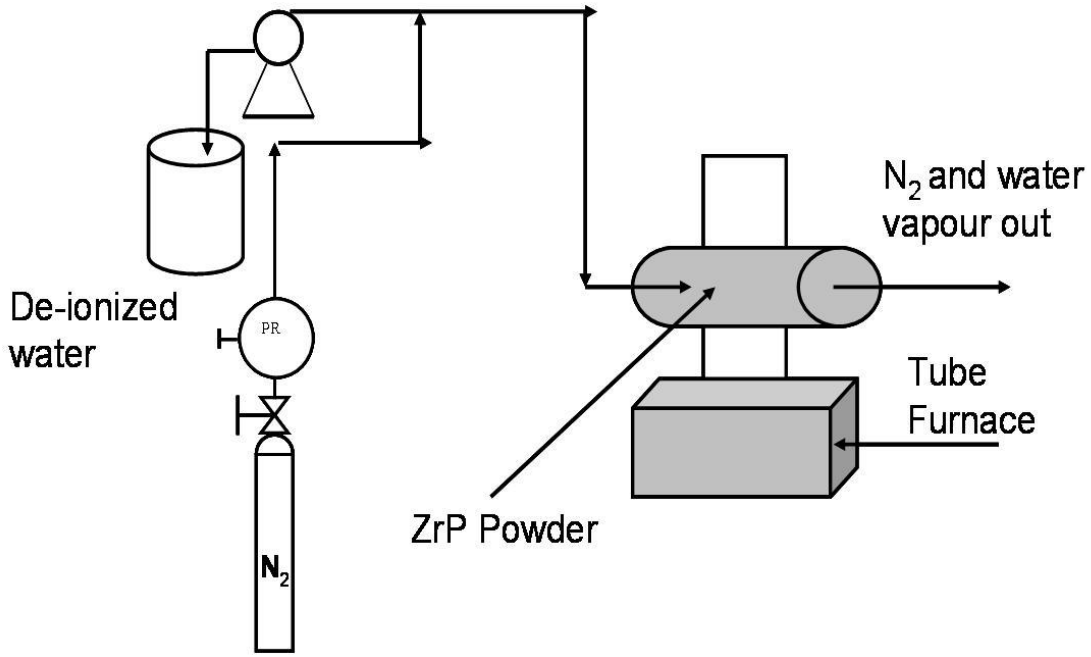

Fig. 1. H_2O partial pressure experiment equipment

3.2.2 Conductivity measurements (electrochemical impedance spectroscopy EIS)

The Electrochemical Impedance of ZrP electrolyte was measured using a common electrochemical cell that is shown in Fig. 2. 304 stainless-steel was used to construct the cell electrodes. The design of the cell was taken from Wang et al. [12]. It was a one end closed cell, cylindrical in shape with a diameter of 7.08 mm and a length of 25.91 mm. A 304 stainless steel bolt (24 threads per inch, or pitch = 1.058 mm per thread) could be screwed into one end of the ceramic cylinder. The other end of the ceramic cylinder was also threaded and was connected to a 304 stainless steel base. A typical pellet would have a diameter of 7 mm and a thickness of 0.7 mm.

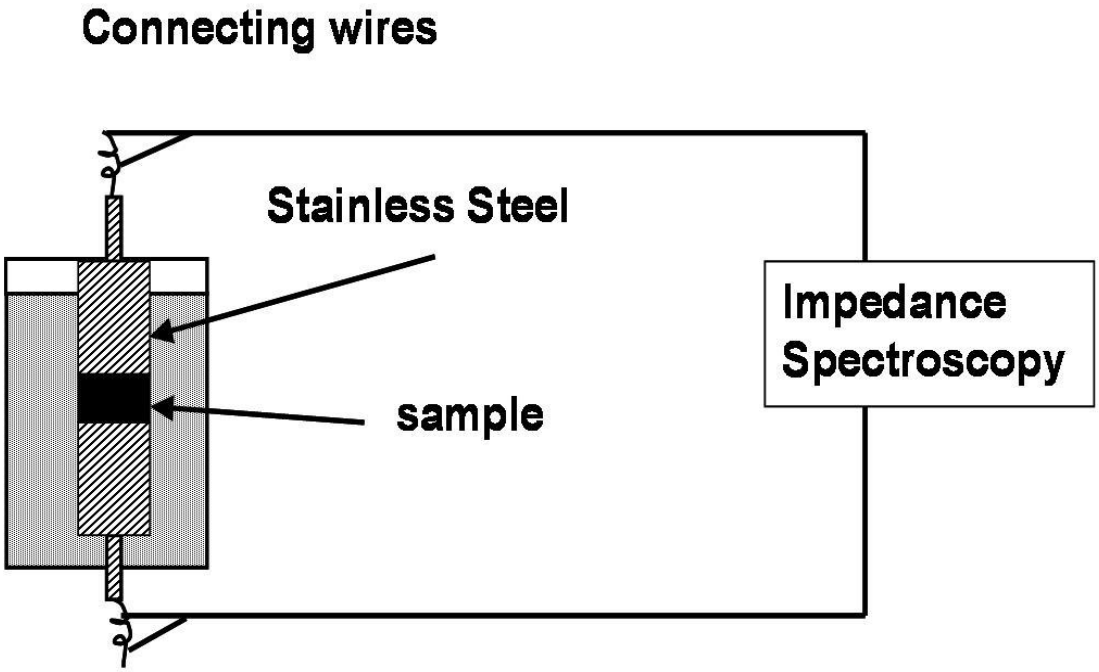

Fig. 2. Impedance spectroscopy cell.

The resultant ZrP samples were crushed to form a fine powder. The powder was placed in the cell and compressed until a constant torque was obtained. The resulting pellet was used for the conductivity measurements. The torque applied to the cell was measured with a torque wrench and had a value of 40 lb_F in (4.5 N m). The load, F, used to compress the powder was calculated from the torque, T, using an empirical engineering formula, F = 0.2 *D *T, where D is the nominal bolt diameter and 0.2 is the "nut" factor. The pressure, P = F/A, where A is the cross-sectional area of the flat end of the bolt was determined to be 300 kPa.

The four probe EIS (Electrochemical Impedance Spectroscopy) measurements were made using a Parstat 2273 electrochemical measurement system running electrochemical Power Suite software over a frequency range of 1 – 100 kHz with an applied voltage of +/- 10 mV. For each sample tested, a value for the electrolyte resistance was derived from the impedance experiments. Nyquist plots were obtained from impedance data. A typical

Nyquist plot obtained during this work was composed of a small portion of a semicircle at high frequencies followed by a Warburg tail that approaches a straight line, at low frequencies. The data at the very highest frequencies in Fig. 3 show a short line that is almost vertical. It is one end of the semi-circle. Data obtained with less compacted ZrP material, not shown in this work, formed a complete semi-circle. The straight line in the Nyquist plot can be extrapolated to its intersection with the x-axis to obtain a value of resistance. The conductivity (σ) in S cm^{-1} was then calculated [12] according to the equation:

$$\sigma = d / RA \qquad (3)$$

where d and A are the thickness and the area for the sample respectively. Values of the electrolyte resistances, R, were obtained from Nyquist plots.

3.2.3 Samples characterization

The samples were analysed by XRD (X-ray diffraction) using Philips PW 1830 generator machine and TGA (Thermo Gravimetric Analysis) using a 2960 SDT analyser from TA instruments. Thermal analysis was performed under N_2 and at a heating rate of 15 °C min^{-1} and 1 °C min^{-1}.

3.3. Results and Discussion

3.3.1 Conductivity measurement

The ZrP powders were analyzed using Electrochemical Impedance Spectroscopy (EIS) after being dried at various temperatures. The samples tested were 1) ZrP powder dried at 70°C in laboratory air 2) ZrP powder dried at 200 °C in laboratory air 3) ZrP powder dried first at 70 °C in laboratory air and then processed at 200 °C in a tube furnace with continuous H_2O injection at an H_2O/N_2 molar ratio of 6, which is the stoichiometric ratio in the direct propane fuel cell reaction. The objective was to evaluate their conductivities. The conductivity results, measured at room temperature, are presented as Nyquist plots in Fig. 3. The frequencies are shown as a separate line in Fig. 3. In general,

the conductivity plots are composed of a Warburg line at frequencies less than 100 kHz and a partial semi-circle (not visible in Fig. 3) at frequencies greater than 100 kHz [12]. The electrolyte resistance was then determined by extrapolating the Warburg portion of the plot to the x-axis. The intercept at the x-axis is the real part of the ZrP impedance.

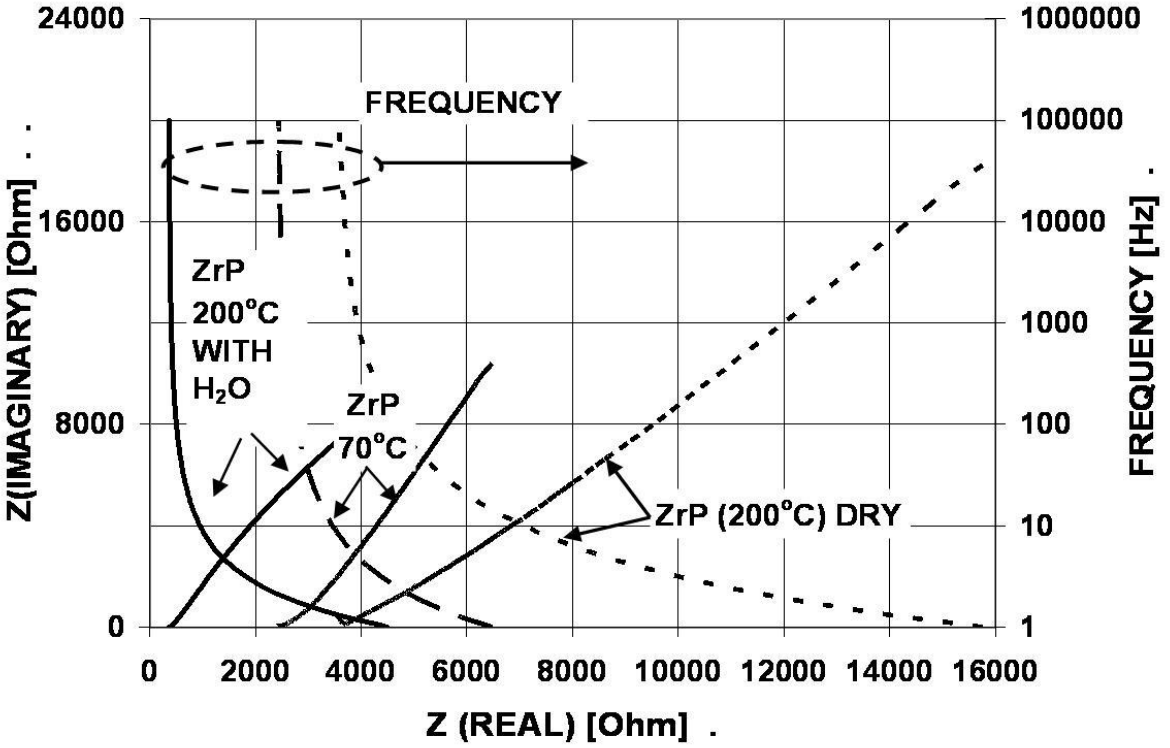

Fig. 3. Nyquist plot for ZrP samples (ZrP powder dried at 70 ◦C in laboratory air; ZrP powder dried at 200 ◦C in laboratory air; and ZrP powder dried first at 70 ◦C in laboratory air and then processed at 200 ◦C in a tube furnace with continuous H_2O injection at anH_2O/N_2 molar ratio of 6, the stoichiometric ratio in the direct propane fuel cell reaction).

The Nyquist plots, in Fig. 3, provided values of ohmic resistances that were 2400 Ohms after 70°C final air drying temperature, 3500 Ohms after 200°C final air drying temperature and 375 Ohms after 200°C final processing temperature with a H_2O/N_2 molar ratio of 6. These resistance values along with the thickness and the area of the sample were

used in Eq. (3) to calculate the conductivity,σ, in S cm $^{-1}$. The results are shown in Table 1. It can be seen that the conductivity decreased from 7.04×10^{-5} to 5.79×10^{-5} S cm^{-1} with the increase in the final drying temperature (in laboratory air) from 70 to 200 °C. This is typical behavior. As the temperature increases, water evaporates and condensation of the hydroxyl groups in ZrP occurs. Loss of protons as a result causes the conductivity to decrease considerably [13]. The above results are also in agreement with previous conclusions that the transport of ions in ZrP is protonic via the Grothuss mechanism [14] as the conductivity decreases with the loss of protons. More importantly our experimental data in Table 1 show that by maintaining the ZrP material in an atmosphere that is predominantly water, the proton conductivity (3.57×10^{-4} S cm^{-1}) is almost an order of magnitude greater than when it is in a relatively dry atmosphere (5.79×10^{-5} S cm^{-1}).

Table1: Experimental conductivity values as a function of processing conditions

Processing Conditions	**Proton Conductivity [S cm^{-1}]**
70°C Air Drying	7.04×10^{-5}
200°C Air Drying	5.79×10^{-5}
200°C Processing at an H_2O/N_2 molar ratio of 6	3.57×10^{-4}

ZrP proton conductivities have been reported in previous studies. For instance, the proton conductivities of the crystalline phase α-ZrP, $Zr(HPO_4)_2.H_2O$, were 9.4, 3.7 and 3×10^{-5} S cm^{-1} [5,15]. These results are consistent with the conclusion that the conductivity decreases with the degree of crystallinity. Patel et al. [13] and Thakkar et al. [16] have

reported that amorphous ZrP pellets had protonic conductivity values of 4.2×10^{-6} to 1.9×10^{-6} S cm^{-1} over the temperature range of 30 to 120 °C respectively. Casciola et al. [17] have also reported a value of 3.2×10^{-6} S cm^{-1} at 30°C for ZrP conductivity. These values have been summarized in Table 2 where it can be seen that the conductivity of ZrP decreases with temperature.

Table 2: Conductivity values reported in the literature [S cm^{-1}]

Material	Literature values of Conductivity [S cm^{-1}]	Reference
$Zr(HPO_4)_2.H_2O$	9.4×10^{-5}	5
↓ increasing	3.7×10^{-5}	5
↓ crystallinity	3×10^{-5}	5, 15
amorphous ZrP at 30°C	3.2×10^{-6}	17
amorphous ZrP at 30°C	4.2×10^{-6}	13
amorphous ZrP at 120°C	1.9×10^{-6}	13, 16

Our experimental results showed that a conductivity of 3.57×10^{-4} S cm^{-1} was obtained with water injection. This water-injection technique was successful in maintaining a reasonable conductivity value. In comparison, 1.9×10^{-6} S cm^{-1} was reported at 120°C under dry conditions [13]. Our own relatively dry value at 200°C, in Table 1, was 5.79×10^{-5} S cm^{-1}. The conductivity result measured in a predominantly water atmosphere, results from two factors acting against each other: 1) water injection which provides the necessary hydration to ensure proton conductivity and 2) the condensation of hydroxyl groups that

occur at temperatures ~180°C and causes a loss of proton groups [18]. The experimental results in Table 1 suggest that the first factor had the most influence.

3.3.2 Thermo-gravimetric analysis

In this work, the thermal stability of amorphous ZrP was investigated by performing thermo-gravimetric analyses (TGA) for the same samples described above. The TGA analyses were performed at a heating rate of 15 °C min^{-1} in a N_2 atmosphere. The TGA results for the sample that produced the best impedance analysis performance (200°C – wet) are shown in Fig. 4.

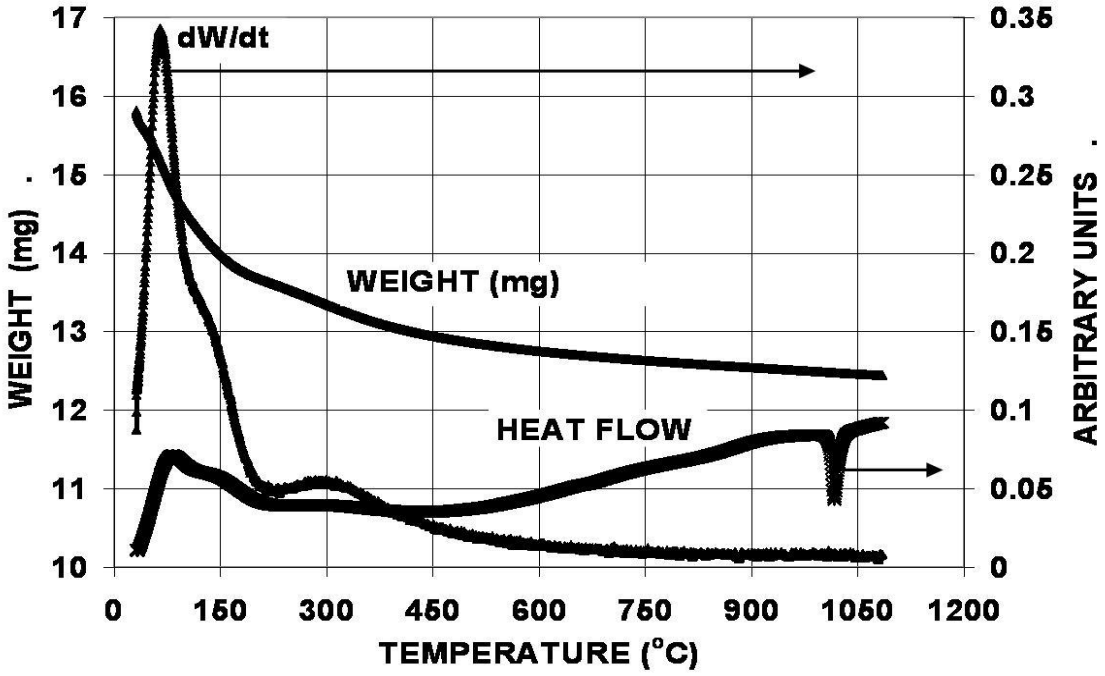

Fig. 4. TGA data for the ZrP sample that was previously dried at 70 °C and was subjected to water injection at 200 °C. [Heat flow values (Wg^{-1}) were divided by −1000 to match the scale of the other two plots: (a) dW/dt (mg min^{-1}) and (b) weight (mg).]

The TGA analysis showed a weight loss of 2.14 mg in the temperature range (25 – 210 °C) with a maximum in the rates of weight loss at 65 and an inflection point at 141°C. The weight loss (1.15 mg) in the temperature range (210 – 1100 °C) had a maximum in the rate of weight loss at 304 °C. The thermal behaviour of ZrP as ion exchangers has been the subject of several previous studies. The studies concluded that: 1) the TGA results are a function of heating rate, preparation method and properties of the starting materials, 2) there is a condensation reaction that takes place between P–OH groups and leads to a mixture of phosphate – pyrophosphate phases [19].

3.3.3 X-Ray diffraction results

A ZrP sample was examined by X-ray diffraction (XRD) after calcinations at 1100 °C for 1 hour. The spectrum is shown in the lower part of Fig. 5. The spectrum was identified as the crystalline structure of zirconium pyrophosphate (ZrP_2O_7). One interesting observation in Fig. 4 was the occurrence of a sharp exothermic peak in the heat flow at 1015 °C indicating a phase change. This is explained by the transformation of layered pyrophosphate to cubic pyrophosphate that occurs at this temperature range [19-22]. Since there was no accompanying change in weight, the change in heat flow was not caused by a loss of material. These results indicate that heating to a sufficient temperature ultimately converts hydrated zirconium phosphate to zirconium pyrophosphate.

The XRD patterns for the hydrated ZrP samples that were air-dried at various temperatures are also shown in Fig. 5. Although they do not have nice crystalline patterns, like the zirconium pyrophosphate, they do have some less intensive peaks indicating that they are not completely amorphous and that they do have some structure. These patterns are characteristic of the ZrP formed from the precipitation reaction of $ZrOCl_2$ and H_3PO_4 solutions at room temperature [3,13].

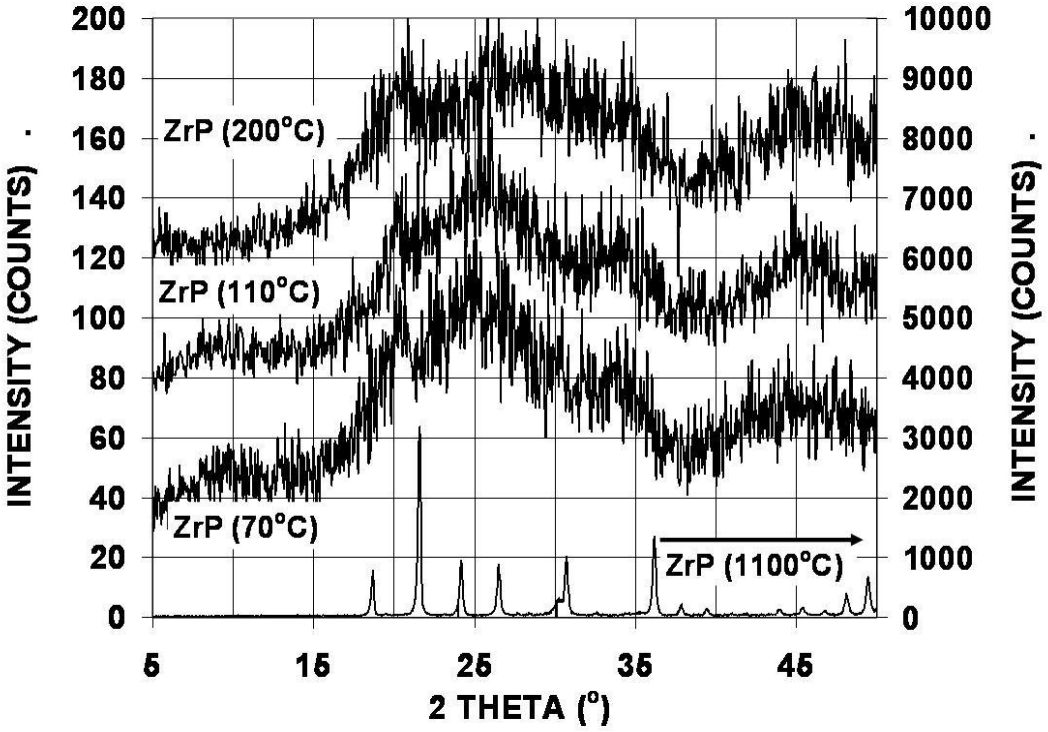

Fig. 5. XRD pattern for ZrP samples dried in laboratory air at 70, 110 and 200 ˚C respectively plus a ZrP sample that was calcined at 1100 ˚C for 1 h.

3.3.4 Analysis of the TGA data

The combination of the XRD data in Fig. 5 showing that zirconium pyrophosphate is formed above 1015°C, and the TGA data in Fig. 4 showing that the weight at temperatures above 1015°C is approaching a constant value, suggests a basis for analyzing the TGA data. Specifically, it suggests that all samples when heated sufficiently will approach a constant weight in the form of zirconium pyrophosphate. Therefore the TGA weight data above 500°C were fitted to the following empirical equation:

$$y = A + B / \exp [(T - 500) / C] \quad (4)$$

where T = Temperature (°C), y is the weight of the ZrP pellet (mg), A = weight of the ZrP sample at T = ∞, in (mg), B = y (T_{500}) – y (T_{∞}) in (mg), and C is an arbitrary parameter. The values of the parameters are shown in Table 3.

Table 3: Experimental conductivity values as a function of the material's processing conditions

Processing Conditions	**A**	**B**	**C**
70°C Air Drying	83.34	3.72	367.98
200°C Air Drying	77.09	2.39	367.97
200°C Processing at an H_2O/N_2 molar ratio of 6	77.19	4.09	594.62

Fitting using Eq. 4, resulted in an excellent agreement between the calculated line and the TGA experimental data (shown as diamonds in Fig. 6). The insert in Fig. 6 shows both the diamond experimental data points and the calculated straight line. The data points are so close together in the main plot in Fig. 6 that it is impossible to distinguish between the trajectory of diamond data points and the line calculated from Eq. 4. Eq. 4 was used to calculate the weight of zirconium pyrophosphate that would be produced from all ZrP samples when their temperatures approached T = ∞.

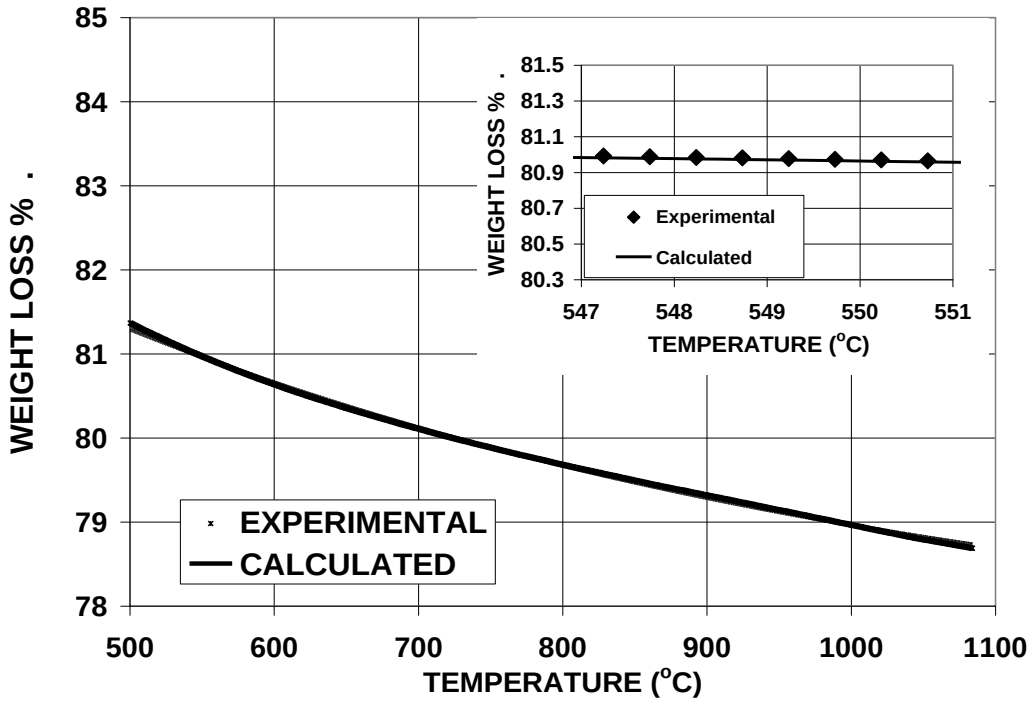

Fig. 6. The agreement between the TGA experimental data (solid diamonds) and the values calculated using Eq. (4).

ZrP_2O_7 is formed according to the following series of reactions, each of which eliminates a water molecule:

$$ZrPO_4(H_2PO_4)\bullet xH_2O\ (x > 2) \rightarrow ZrPO_4(H_2PO_4)\bullet 2H_2O \rightarrow$$

$$\rightarrow Zr(HPO_4)_2\bullet H_2O \rightarrow Zr(HPO_4)_2 \rightarrow ZrP_2O_7 \qquad (5)$$

When all the water of hydration that is bound to the ZrP chemical structure has been removed, then only anhydrous zirconium hydrogen phosphate [$Zr(HPO_4)_2$] remains. It is subsequently converted to zirconium pyrophosphate in the final reaction.

3.3.5 Quantitative water content of ZrP

With the knowledge of the zirconium pyrophosphate (ZrP_2O_7) weight and by ascribing the TGA weight loss to water, the ratio (mols H_2O / mol ZrP_2O_7) at any temperature was calculated. The results are shown in Fig. 7 as moles of H_2O per mole of ZrP_2O_7.

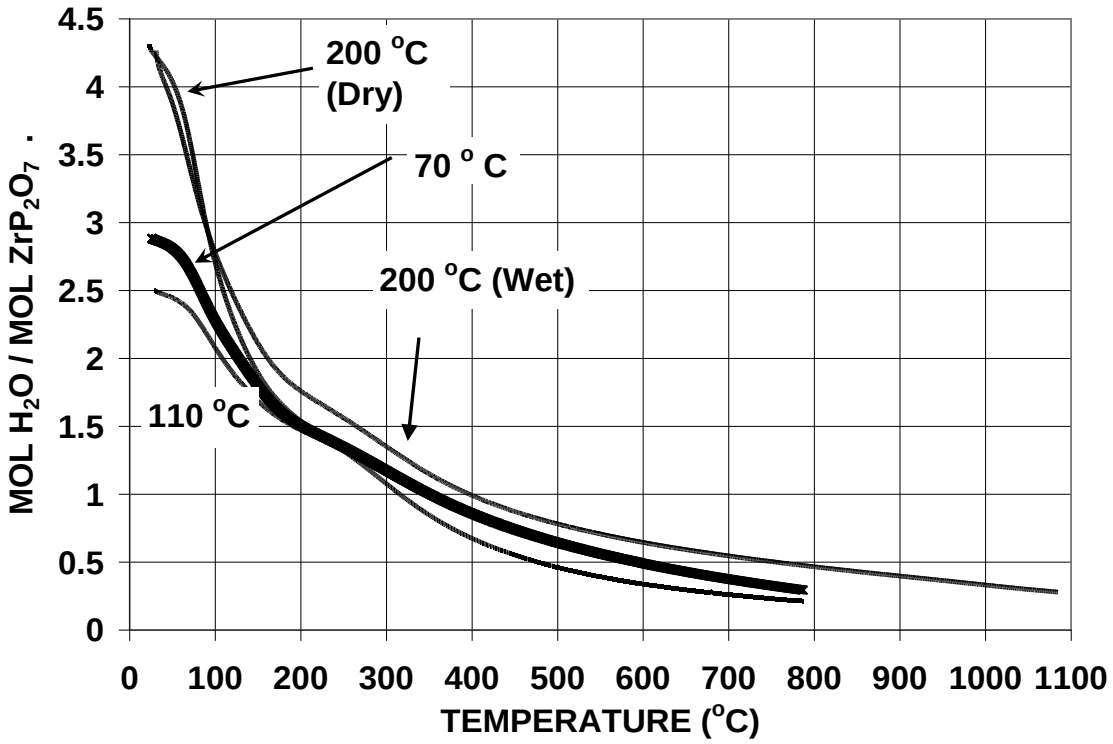

Fig. 7. TGA data fitting for ZrP samples dried at 70, 110 and 200 ˚C in the oven plus ZrP at 200 ˚C with H_2O injection (200 ˚C–wet).

The states of hydration in the various zirconium phosphate compounds can be identified in terms of the H_2O / ZrP_2O_7 molar ratio shown in Fig. 7. A value of "0" H_2O / ZrP_2O_7 ratio in Fig. 7 represents ZrP_2O_7. A value of "1" in Fig. 7 represents $Zr(HPO_4)_2$. A

value of "2" in Fig. 7 represents $Zr(HPO_4)_2 \bullet H_2O$. A value of "3" in Fig. 7 represents $ZrPO_4(H_2PO_4) \bullet 2H_2O$.

Any value greater than 3 represents $ZrPO_4(H_2PO_4) \bullet xH_2O$ where $x > 2$. That is the formula that is used to represent the starting material, prior to drying at any temperature. Results similar to those in Fig. 7 were obtained in previous studies such as Constantino et al. [19] and Patel et al. [21]. The sample dried in laboratory air at 70°C had a value slightly less than "3" indicating that the statistically average extent of hydration was slightly less than that of γ zirconium phosphate. The sample dried in laboratory air at 110°C had a value of approximately "2.5" indicating that its statistically average extent of hydration was between that of γ zirconium phosphate and α zirconium phosphate. Based on the above observations, it was expected that the sample dried in laboratory air at 200 °C would have a value less than "2.5". It was found to be greater than "2.5". This sample may have picked the additional moisture by being exposed to the atmosphere for an extended period of time prior to its thermogravimetric measurement. This is consistent with the results obtained by Amphlett [20] who reported that it was possible to reconvert pyrophosphates back into phosphates upon immersion in aqueous solutions at 300 °C. Finally the sample processed at a H_2O / N_2 molar ratio of 6 was expected to have a greater value than the others since it was processed in an environment with large water content.

The water content of all the samples in Fig. 7 decreased as the temperature increased. At all temperatures, the solid sample processed at 200 °C with a H_2O / N_2 molar ratio of 6 had a greater water content than any of all the other solid samples. This observation indicates that the presence of a water rich vapour phase produced a zirconium phosphate solid that was hydrated to a greater extent than the zirconium phosphate solids that were prepared in laboratory air. The two samples dried at 200°C, one in the presence of a water rich vapour and the other in laboratory, air provide a direct comparison showing that the water rich vapour caused the solid to be hydrated to a greater extent.

Finally the sample processed with an H_2O/N_2 molar ratio of 6 at 200°C had both the greatest conductivity and the largest hydrated water content compared to all other samples.

This is consistent with the concept that: by maintaining an appropriate water content in the vapour phase at processing conditions, it was possible to maintain the zirconium phosphate in a sufficiently hydrated state, so that the conductivity values could also be maintained.

3.4. Conclusions

Two conclusions can be made related to the operation of zirconium phosphate fuel cell membranes at elevated temperatures (200°C). (1) The decrease in proton conductivity that has sometimes been attributed to a loss in water content is consistent with our measurements of conductivity and water content that are reported here in relatively dry laboratory air from 70 – 200°C. (2) Furthermore, it was shown that an adjustment of the vapour phase water content during processing (so that the gas phase in contact with the zirconium phosphate membrane contained an H_2O / N_2 molar ratio of 6, the stoichiometric feed ratio in a direct propane fuel cell), enhanced the hydrated water content of the zirconium phosphate material compared to when it was in the presence of a relatively dry atmosphere. In addition, our experiments showed that the conductivity of this 200°C material having the enhanced hydrate water content was even greater than that of material that had only been at 70°C in a relatively dry atmosphere. This finding indicates that it should be possible to operate direct hydrocarbon fuel cells at elevated temperatures, without encountering degradation in the proton conductivity of the membrane and thereby take advantage of more rapid kinetics and greater current densities.

3.5. Acknowledgments

The authors gratefully acknowledge the financial support from the Canadian federal government's Natural Sciences and Engineering Research Council and from the Ontario provincial government's Ministry of Research and Innovation (Ontario Fuel Cell Research and Innovation Network).

3.6. References

1. Y. Si, R. Jiang, J.C. Lin, H.R. Kunz, J.M. Fenton, J. Electrochem. Soc. 151 (2004) A1820.
2. C.B. Amphelett, L.A. McDonald, M.J. Redman, J. lnorg. Nucl. Chem. 6 (1958) 220.
3. A. Clearfield, J.A. Stynes, J. Inorg. Nucl. Chem. 26 (1964) 117.
4. R.P. Hamlen, J. Electrochem. Soc. 109 (1962) 746.
5. A. Clearfield, Ann. Rev. Mater. Sci. 14 (1984) 205.
6. G. Alberti, E. Torracca, J. lnorg. Nucl. Chem. 30 (1968) 1093.
7. G. Alberti, M. Casciola, U. Costantino, G. Levi, G. Ricciardi, J. Inorg, Nucl. Chem. 40 (1978) 533.
8. K. Peinemann, S.P. Nunes, (Eds.) Membranes for Energy Conversion, Vol. 2, p.97.
9. O. Savadogo, J. Power Sources 127 (2004)135.
10. W.G. Grot, G. Rajendran, US Patent 5,919,583, 1999.
11. Y.I. Park, K. Jae-Dong, M. Nagai, J. Mat. Sci. Letters 19 (2000)1735.
12. Y.J. Wang, Y. Pan, L. Chen, Mat. Chem. and Physics 92 (2005) 354.

13. H. Patel, U. Chudasama, J. Chem. Sci. 119 (2007) 35.

14. A. Clearfield, Chem. Rev. 88 (1988)125.

15. Y.I. Park, J.D. Kim. M. Nagai, Mat. Res. Soc. Symp. Proc. 600 (2000) 305.

16. R. Thakkar, H. Patel, U. Chudasama, Bull. Mater. Sci. 30 (2007) 205.

17. M. Casciola, D. Bianchi, Solid State Ionics **17** (1985) 287.

18. G. Alberti, A. Conte, E. Torracca, J. Inorg. Nucl. Chem. 28 (1966) 225.

19. U. Constantino, A.L. Ginestra, Thermochimica Acta 58 (1982) 179.

20. C.B. Amphlett, Inorganic Ion Exchangers, Elsevier; London; (1964) 107.

21. H.K. Patel, R.S. Joshi, U. Chudasama, Indian J. Chem. 47 A (2008) 348.

22. U. Constantino, R. Vivani, V. Zima, E. Cernoskova, J. Solid State Chem. 132 (1997) 17.

CHAPTER FOUR

The effect of glycerol on the conductivity of Nafion-free ZrP/PTFE composite membrane electrolytes for direct hydrocarbon fuel cells

Amani Al-Othman [a,b], André Y. Tremblay[a], Wendy Pell [b], Yun Liu [b], Brant A. Peppley [c], Marten Ternan [d]

(a) Chemical and Biological Engineering,

(b) Catalysis Centre for Research and Innovation,

(c) Chemical Engineering, Queens University, Dupuis Hall, Kingston, ON, K7L 3N6, Canada.

(d) EnPross Inc., 147 Banning Road, Ottawa, ON, K2L 1C5, Canada

In : Journal of Power Sources 199 (2012) 14– 21

Chapter 4-The effect of glycerol on the conductivity of Nafion-free ZrP/PTFE composite membrane electrolytes for direct hydrocarbon fuel cells

ABSTRACT

Composite membranes composed of zirconium phosphate (ZrP, a proton conductor), and porous polytetrafluoethylene (PTFE, a mechanical support for ZrP), have been studied as electrolytes for direct hydrocarbon fuel cells that might operate at temperatures approaching 200°C. The previous literature describes membranes formed by compressing PTFE particles and ZrP particles (conductivity = 10^{-3} S cm^{-1}). The results reported here show that adding glycerol (GLY) to a reaction mixture of $ZrOCl_2 \bullet 8H_2O$ and H_3PO_4 to form ZrP in-situ within the pores of PTFE, produced a membrane (conductivity = 0.02 – 0.045 S cm^{-1}) that approached the performance of Nafion (conductivity = 0.1 S cm^{-1}). The conductivity remained unchanged when one of the membranes (conductivity = 0.02 S cm^{-1}) was processed at the inlet conditions to a direct propane fuel cell (200°C and steam mole fraction y_{H2O} = 0.86). The composite membrane, prepared with glycerol, contained ZrP spheres (100 – 500 nm) that were smaller than the PTFE pore diameters (1000 – 2000 nm). The enhanced conductivity may have been caused by a combination of proton transport on the exterior surfaces of the ZrP solid spheres, proton hopping through the bulk of the ZrP, and proton hopping via the OH groups in glycerol.

4.1. Introduction

High temperature operation (~ 200°C) is desired in polymer electrolyte membrane (PEM) fuel cells for several reasons. It enhances reaction kinetics, improves the cell tolerance for impurities, permits the use of fuels that produce carbon monoxide, and, increases the temperature at which heat is generated, thereby allowing the recovery of useful heat.

Current PEM fuel cell technology relies on perfluorosulfonic acid (PFSA) polymer membranes (e.g. Nafion) as the proton conductive material. Nafion is the leading and the

most successful electrolyte used in PEM fuel cells. Dupont developed it in the 1960's. It consists of a linear perfluorinated backbone with perfluoro side chains containing sulfonic acid groups [1].

Nafion membranes perform quite well below 90 °C under fully hydrated conditions. They also possess good chemical and mechanical stability due to the perfluorinated main chain. However, proton conductivity of this membrane is strongly dependent on its water content. Water is required to solvate the proton of the sulfonic acid groups. The substantial decrease in Nafion's proton conductivity at low hydration levels is one of the motivations toward the development of new membrane materials. For example, Nafion conductivity decreases from 0.066 to 0.00014 S/cm at 30°C when the relative humidity (RH) decreases from 100% to 34% [2]. This is why the high temperature operation of a PEM fuel cell with Nafion is limited to temperatures below 100 °C at ambient pressure. Also, Nafion starts to lose its mechanical stability above its glass transition temperature of 110 °C [3]. This is problematic because above this temperature, degradation eventually occurs. A membrane suitable for high temperature operation should have reasonable and/or high proton conductivity, good thermal and chemical stability, and low cost.

The development of high temperature membranes can be categorized into three major groups: (1) the modification of the current Nafion or PFSA membranes by the addition of hydroscopic oxides and solid proton conductors such as zirconium hydrogen phosphate $Zr(HPO_4)_2 \bullet H_2O$, (ZrP); (2) the development of sulfonated polyaromatic polymers and composite membranes, such as polyetheretherketone (PEEK) [2], and (3) the development of acid base polymer membranes such as sulphuric and phosphoric acid doped polybenzimidazole (PBI).

Considerable effort has been made to modify the existing PFSA membranes (e.g. Nafion) by the incorporation zirconium hydrogen phosphate $Zr(HPO_4)_2 \bullet H_2O$. ZrP was one of the inorganic compounds suggested by Grot [4]. Grot proposed that inorganic fillers, such as, the oxides and phosphates of Sn, Sb, Mo, W, Ti and Zr metals be precipitated in membranes.

Zirconium hydrogen phosphate, $Zr(HPO_4)_2 \bullet H_2O$, belongs to the class of solid protonic conductors that has a layered structure allowing the intercalation of guest molecules. It is a highly hydroscopic insoluble solid and the interest in this compound goes back to the 1950's when it was discovered to have cation exchange properties [5 –7]. Examples of composite membranes with ZrP incorporated into Nafion have been reported by: Savadogo et al. [8] who casted a membrane using a Nafion® solution that contained zirconium (Zr^{+4}) ions, Houa et al., [9] who incorporated zirconium phosphates into Nafion 115, Bauer et. al. [10] who incorporated zirconium phosphates into Nafion 1135 and 117, and Casciola et. al. [11], who prepared Nafion 117 – zirconium phosphate membranes.

Composite membranes using ZrP and polytetrafluoroethlyne (PTFE) have been also reported. Park et al. [12] prepared a composite membrane by mixing the particles of a PTFE emulsion with a ZrP crystalline powder, then drying, followed by pressing. The addition of zirconium phosphate in Park's work caused the proton conductivity to increase to 2.2×10^{-3} S cm^{-1} compared to 10^{-13} S cm^{-1} for PTFE alone. Liu et al. [13] impregnated a porous polytetrafluoroethylene (PTFE) with Nafion solution to prepare Nafion/PTFE composite membranes. Jiang et al. [14] prepared Nafion–Teflon®–$Zr(HPO_4)_2$ (NTZP) composite membranes via a direct impregnation method.

Research in our laboratory is directed toward the use of ZrP without using Nafion, since our target temperature is 200°C. Our earlier work on ZrP powders [15] investigated the effect of hydration on the proton conductivity of ZrP. It showed that the water to hydrocarbon stoichiometric ratio required for direct propane fuel cells caused a substantial enhancement in ZrP proton conductivity compared to the conductivity at dry conditions. In this work ZrP particles were precipitated during an in-situ reaction of $ZrOCl_2.8H_2O$ with H_3PO_4 inside the pores of a porous PTFE membrane. The resulting composite membrane has, (1) proton conducting properties, (2) thermal stability limited by PTFE (260°C) and, (3) mechanical support for the ZrP particles, provided by the PTFE. It was anticipated that this composite ZrP-PTFE membrane would be particularly suitable for direct hydrocarbon fuel cells. In this work, the effect of glycerol addition on the morphology and conductivity of the composite membrane was investigated. We were unable to find any previous experimental

work specifically describing the effect of glycerol on proton conductivity in fuel cell membranes.

4.2. Experimental

4.2.1. Synthesis of a ZrP – PTFE composite membrane

There were several component materials used to make the composite membrane. The porous film was unlaminated Sterlitech PTFE (with a nominal thickness of 50 μm and a nominal pore size of 0.22 μm). $ZrOCl_2 \cdot 8H_2O$ from Sigma Aldrich was the source of the zirconium for ZrP. 85% o-phosphoric acid from Fischer Scientific was the source of phosphorous for ZrP. Ethanol (Anhydrous ethyl alcohol from Commerical Alcohols Inc.), glycerol (certified ACS, assay 99.7% from Fisher Scientific) and iso-propanol (HPLC grade, assay 99.8% from EMD Chemicals Inc.) were obtained.

The first step of the procedure was to prepare a suspension containing the $ZrOCl_2 \cdot 8H_2O$ salt having a liquid phase that would wet the surface of the porous PTFE film. Although $ZrOCl_2 \cdot 8H_2O$ dissolved readily in water, the interfacial tension between water and PTFE prevented the water from spreading on the surface of the PTFE. In contrast, both isopropanol and ethanol have lower surface tension than water, hence they wetted the PTFE surface. These alcohols were observed to penetrate through the PTFE film. In addition, fine particles of $ZrOCl_2 \cdot 8H_2O$ could be suspended in alcohol.

Suspensions were prepared using several methods. Two different liquid phase compositions were used: (a) 50 mL ethanol and 350 mL iso-propanol, and (b) 2 mL of water plus 50 mL of ethanol and 150 mL of iso-propanol. The water dissolved much of the $ZrOCl_2 \cdot 8H_2O$. The proportion of water in the liquid was sufficiently small that the liquid mixture would wet the PTFE. As a result the total volume of the suspensions prepared with water was substantially diminished compared to the suspensions prepared without water. For some of the suspensions a small amount of glycerol (GLY) was added in order to vary the GLY/ZrP mass ratio. The suspension was placed on a stirring hot plate and vigorously mixed using a magnetic stirrer. The quantity of $ZrOCl_2 \cdot 8H_2O$ in the suspension was sufficient for the void volume of pores in the PTFE film to be filled with ZrP,

$Zr(HPO_4)_2 \cdot H_2O$. That stoichiometric amount of $ZrOCl_2.8H_2O$ was determined from the chemical reaction [16] in Equation 1.

$$ZrOCl_2 \cdot 8H_2O + 2\ H_3PO_4 \rightarrow Zr(HPO_4)_2 \cdot H_2O + 2\ HCl + 8\ H_2O \quad (1)$$

The suspension was introduced into the pores of the PTFE film as follows: A piece of porous PTFE was weighed, then placed between two Teflon™ hoops (concentric Teflon™ rings). The hoops were attached to a mixer shaft and rotated. As shown in Fig.1, the stirred alcoholic suspension of $ZrOCl_2.8H_2O$ was heated to 70°C, pumped at a rate of 3 mL/min and, dripped onto the top side of the PTFE porous film so that it was well distributed. Periodically, dripping was stopped to allow the alcohol in the suspension to evaporate while the membrane continued to rotate. Once the membrane appeared to be dry, dripping began again. This procedure was repeated until the total amount of the alcoholic suspension had been used.

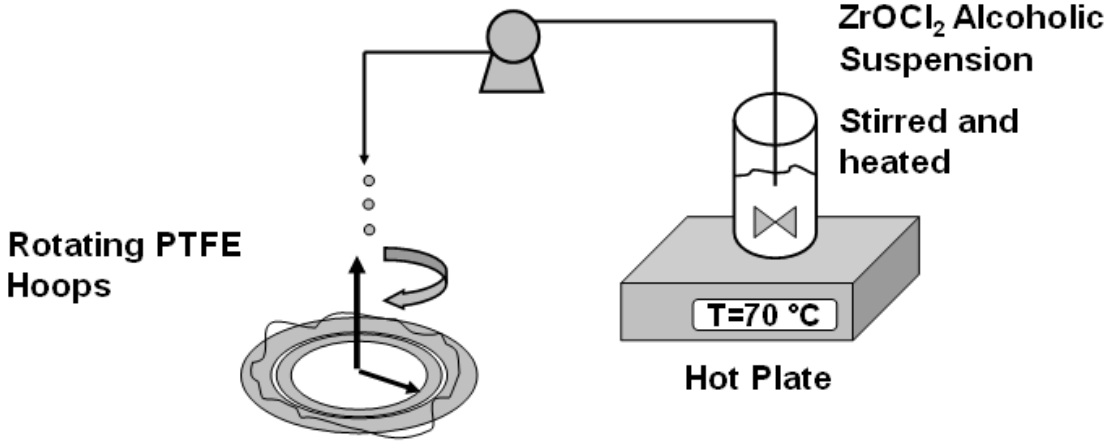

Fig . 1. Membrane synthesis set-up.

The membranes containing $ZrOCl_2.8H_2O$ were then immersed in H_3PO_4 for 72 hours. This caused the reaction in Eq. 1 to occur. Subsequently the membrane was rinsed gently with de-ionized water and isopropanol (ratio of 50:50 by volume) twice and oven

dried for 24 hours at 120 °C. The boiling point of glycerol is 290 °C [17]. Therefore, the majority of the glycerol was not expected to evaporate under the 120 °C maximum temperature membrane drying conditions.

A sample of the membrane prepared as described above was cut, weighed, and then further processed in a tube furnace (wet test) at 200 °C for 1.5 hours with continuous H_2O injection under Argon (Ar) at an H_2O/Ar molar ratio of 6, $y_{H2O} = 0.86$. This condition was chosen because it is the stoichiometric ratio in the direct propane fuel cell reaction where H_2O is a reactant. After processing, the membrane sample was re-weighed and placed in a sealed non-porous Teflon bag and then examined by electrochemical impedance spectroscopy (EIS).

4.2.2. Synthesis of a glycerol / PTFE membrane

The membranes that were composed only of PTFE and glycerol, without $ZrOCl_2.8H_2O$, were prepared as follows. The Sterlitech PTFE unlaminated film was cut and weighed. A specified amount of glycerol was added drop-wise while the weight was recorded on a digital balance scale. The film was then folded and cold pressed at 96.7 psig using a Carver press, model 3856.

4.2.3. Investigation of the composite membranes proton conductivity

Electrochemical impedance spectroscopy (EIS) measurements were made on the various membranes. A four probe measurement method was performed using a Parstat 2273 instrument and PowerSuite 2.58, 2003 electrochemical software, over a frequency range of 1 – 100 kHz. The resulting impedance data were used to make Nyquist plots. The value of the real electrolyte resistance, R, was obtained from the intersection of the line on the Nyquist plot with the x-axis. After measuring the membrane thickness, d, and area, A, the proton conductivity,σ was obtained from Eq. 2 [18]:

$$\sigma = d / (R \times A) \qquad (2)$$

4.2.4. Characterization techniques: scanning electron microscopy (SEM) and energy dispersive X-ray spectroscopy

Scanning Electron Microscopy (SEM) was performed using a JEOL JSM-7500F Field Emission Scanning Microscope. Prior to examination of membrane cross-sections, the membranes were immersed in liquid nitrogen and freeze–fractured. The freeze-fractured samples were further studied using the COMPO (composition analysis) feature in SEM. i.e. the use of back scattered electrons in order to detect the contrast between areas of different compositions (atomic numbers) at the membrane cross section. Energy-dispersive X-ray spectroscopy (EDS) was used to identify the elemental composition of some samples.

4.3. Experimental results

4.3.1 Membrane morphology studies

The composite membranes prepared in this study have two solid phase components, zirconium phosphate (ZrP) and a porous polytetrafluoethylene (PTFE) film, plus in some cases a liquid phase component, glycerol (GLY). Previously we investigated ZrP powder without the PTFE film [15]. A scanning electron micrograph (SEM) of the PTFE film used in the composite membranes is shown in Fig. 2(a) in its as received condition. The spaces between the strands of PTFE form pores that appear to be oblong in shape with a typical narrow dimension near 1 μm and a typical long dimension near 2 μm. These dimensions are somewhat different than the 0.22 μm pore size provided by the manufacturer. The 0.22 μm pore size is the absolute pore size value that was determined by the manufacturer using the bubble point test with isopropanol.

The SEM image in Fig. 2(b) shows a ZrP composite membrane after the PTFE pores had been filled with ZrP using a preparation method that did not use glycerol. The surface is composed of flakes of zirconium phosphate material (ZrP) that cover the PTFE surface. A

typical flake size is greater than 1 μm. Conductivity, in the order of 10^{-5} S cm^{-1} was reported for this membrane.

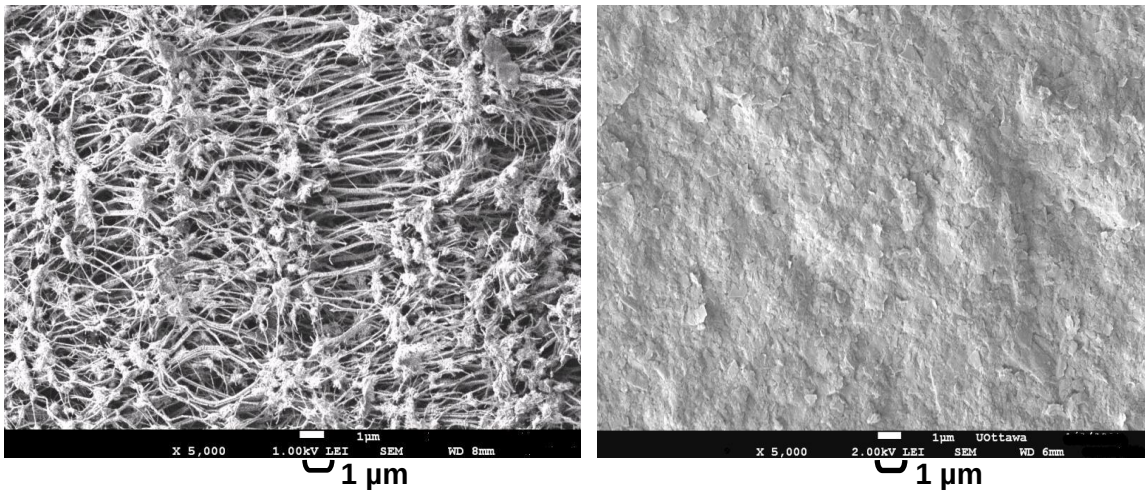

(a) **(b)**

Fig . 2. Scanning electron microscopy (SEM) images for; (a) top view of the Sterlitech PTFE (Teflon) film as received and (b) top view of a ZrP-PTFE composite membrane prepared without the use of glycerol**.**

The top view of a ZrP– PTFE composite membrane prepared using a GLY/ZrP mass ratio, $MR_{GLY/ZrP}$, of 0.4 is shown in Fig. 3. Fig. 3(a) and 3(b) are for the same film but at different magnifications, 1900 for (a) and 5000 in (b). The comparison between Fig. 2 and 3 reveals a difference in morphology. The presence of glycerol has changed the ZrP particles morphology from the flakes larger than 1 μm in Fig. 2(b) into nearly spherical particles in the range of 100 nm to 500 nm that have formed aggregates in some regions. In addition, it is apparent that the spherical particles in Fig. 3(b) are definitely smaller than the pore dimensions in Fig. 2(a).

One possible explanation for the spherical shape of the particles is that the glycerol molecules, $HOCH_2$-CHOH-CH_2OH, might have occupied positions near the $ZrOCl_2.8H_2O$ solid. Specifically the OH groups might have been adjacent to the $ZrOCl_2.8H_2O$ solid and

the CH or CH_2 groups might have been adjacent to the PTFE. Such positioning would be consistent with the values of solubility parameters that can be used to assess the compatibility of materials. One common use of solubility parameters is to describe miscibility of two liquid phase components (like dissolves like). In this case PTFE has a solubility parameter of 14 $MPa^{1/2}$. Examples of solubility parameters of alkanes are pentane = 14.4 $MPa^{1/2}$ and hexane = 14.9 $MPa^{1/2}$. The solubility parameters for the CH and CH_2 groups (alkane structures) in glycerol might be similar to the solubility parameter for PTFE. Similarly $ZrOCl_2 \bullet 8H_2O$ has many OH groups that would be compatible with the OH groups in glycerol. Specifically, the solubility parameter for water is 47.8 $MPa^{1/2}$ and the value for glycerol (OH groups plus CH groups) is 36.2 $MPa^{1/2}$. These numbers suggest that glycerol would be a suitable molecule to be located at the interface between a hydrophobic region, PTFE, and a hydrophilic region $Zr(HPO_4)_2 \bullet H_2O$. Nafion, one of the best fuel cell membranes, also has hydrophobic and hydrophilic regions.

Furthermore, the small spherical shape of the ZrP particles/aggregates seen in the SEM images might have resulted from the presence of glycerol that has a high surface tension, combined with successive wetting and drying cycles inside the confined PTFE hydrophobic pores.

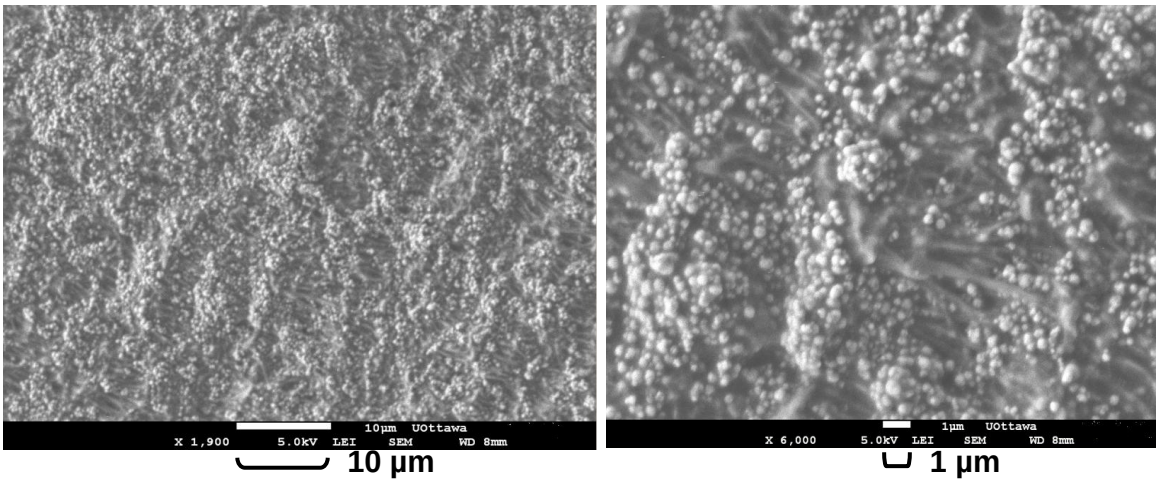

(a) **(b)**

Fig . 3. Scanning electron microscopy (SEM) images for: Top view of a ZrP – PTFE membrane prepared with a GLY/ZrP mass ratio of 0.4, having magnifications of (a) 1900 and (b) 5000.

A cross-sectional view of the same ZrP-PTFE composite membrane shown in Fig. 3 (top view) is shown after freeze-fracturing in Fig. 4 at two magnifications. At the higher magnification several features of the composite membrane morphology can be seen: individual ZrP particles, agglomerates of ZrP particles, some strands of the PTFE polymer, and some void spaces. The void spaces are undesirable since if they were connected, they would provide a path for species to cross over the membrane from one electrode to the other. The SEM image of the membrane cross-section in Fig. 4 at the higher magnification confirms the individual particle size range of 100 to 500 nm.

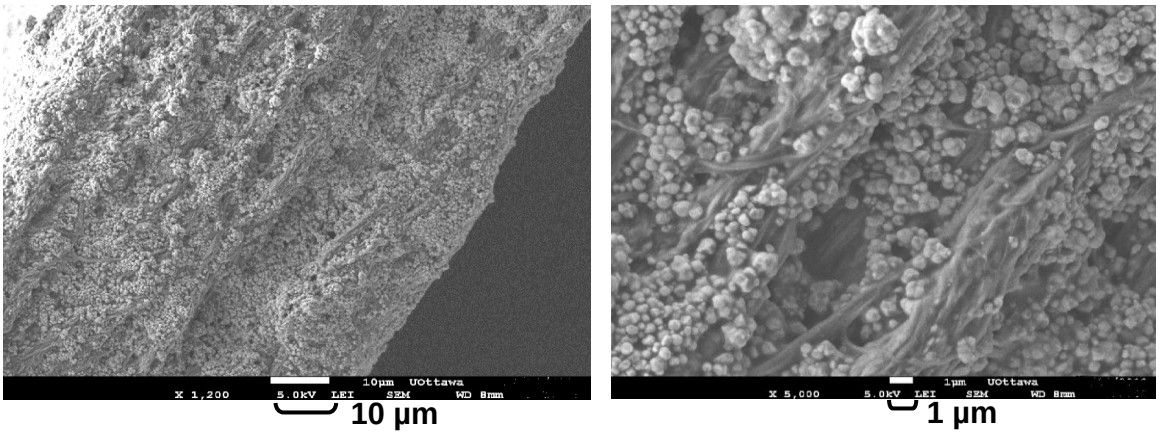

Fig . 4. SEM image for a cross sectional view of ZrP – PTFE membrane prepared with a GLY/ZrP mass ratio of 0.4 at different magnifications.

A cross sectional view after freeze-fracturing of a different composite membrane, having a GLY/ZrP mass ratio, $MR_{GLY/ZrP}$, of 0.4 is shown in Fig. 5a. The composition of the cross-section was measured by the COMPO feature in SEM which reveals a contrast based on the atomic number of each component, i.e., ZrP appears in a whiter shade. The results are shown in Fig. 5(b). At this scale of observation it appears that the ZrP particles were deposited almost uniformly across the thickness of the composite membrane, indicating that the pores were filled with ZrP.

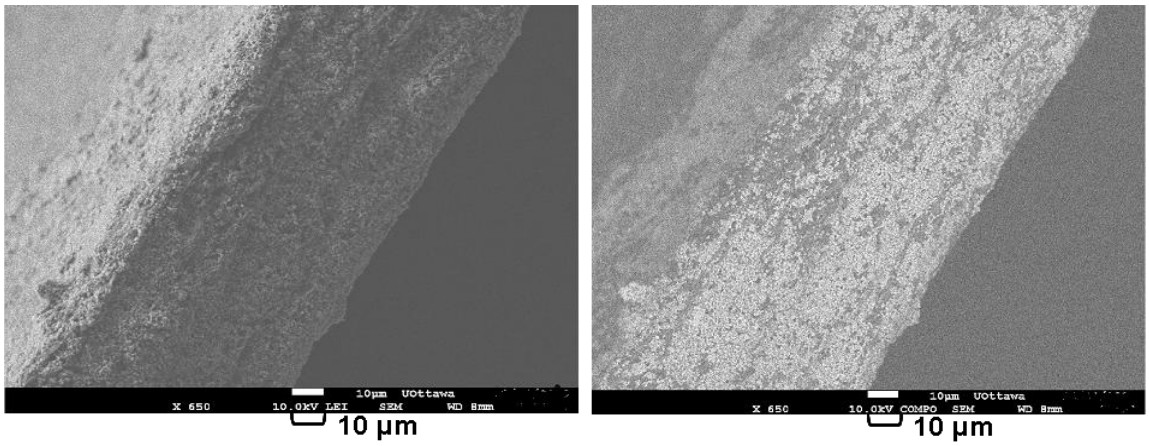

(a) **(b)**

Fig . 5. SEM image for; (a) cross sectional view of ZrP – PTFE membrane prepared with a GLY/ZrP mass ratio of 0.4 and (b) same image but using the composition analysis (COMPO feature) in SEM.

SEM images for a ZrP – PTFE composite membrane with a GLY/ZrP mass ratio, $MR_{GLY/ZrP}$, of 0.8 are shown in Fig. 6. Two different regions are apparent in Fig. 6(a). The dominant feature in the upper region is the ZrP particles, indicating that the pores in that region have been filled with ZrP particles. The particle diameters in Fig. 6(b) and 6(f) appear to be distributed over a larger range, 100 to 1000 nm, than those shown in Fig. 3 and 4. In Fig. 6(e) a large agglomerate of ZrP is seen to be on top of ZrP particles. The lower region in Fig. 6(a) appears to consist of empty pores. However, at higher magnifications, Fig. 6(c) and particularly 6(d) suggest that the pores are partially filled with a fluid like material (glycerol) in which isolated ZrP particles with diameters slightly greater than 100 nm appear to be embedded.

The observations of (a) empty pores within the membrane and (b) ZrP plates on the exterior of the membrane are consistent with the preparation method. At a GLY/ZrP mass ratio of 0.8, the volume of glycerol plus $ZrOCl_2.8H_2O$ in the suspension exceeds the pore volume of the PTFE. Therefore during the dripping step of the membrane synthesis there will be a point at which all the pores have been filled with glycerol plus $ZrOCl_2.8H_2O$, but

not all of the $ZrOCl_2.8H_2O$ necessary to fill the pores (Fig. 6(c)) will have been dripped onto the PTFE. As the dripping step continues the additional glycerol and at least some of the additional $ZrOCl_2.8H_2O$, [and as a result eventually some of the ZrP] will be located on the exterior of the PTFE, Fig. 6(f). The presence of glycerol inside the pores without the corresponding quantity of $ZrOCl_2.8H_2O$ would support the suggestion that there would be some pores that do not contain ZrP. In addition the deposition of glycerol plus $ZrOCl_2.8H_2O$ on the membrane exterior after all the pores had been filled with glycerol would suggest that ZrP deposits (flakes) would be formed on the membrane exterior.

EDS measurements (not shown here) were performed on the agglomerated region that appeared in in Fig. 6(e). The results for the agglomerate were compared with other EDS analyses for $ZrOCl_2.8H_2O$ and for ZrP powder. The composition of the agglomerated region resembled that of ZrP with a minor shift in some peaks, plus large oxygen peaks. High oxygen content was attributed to the presence of glycerol. This suggested that the agglomerated region in Fig. 6(e) is ZrP material associated with glycerol.

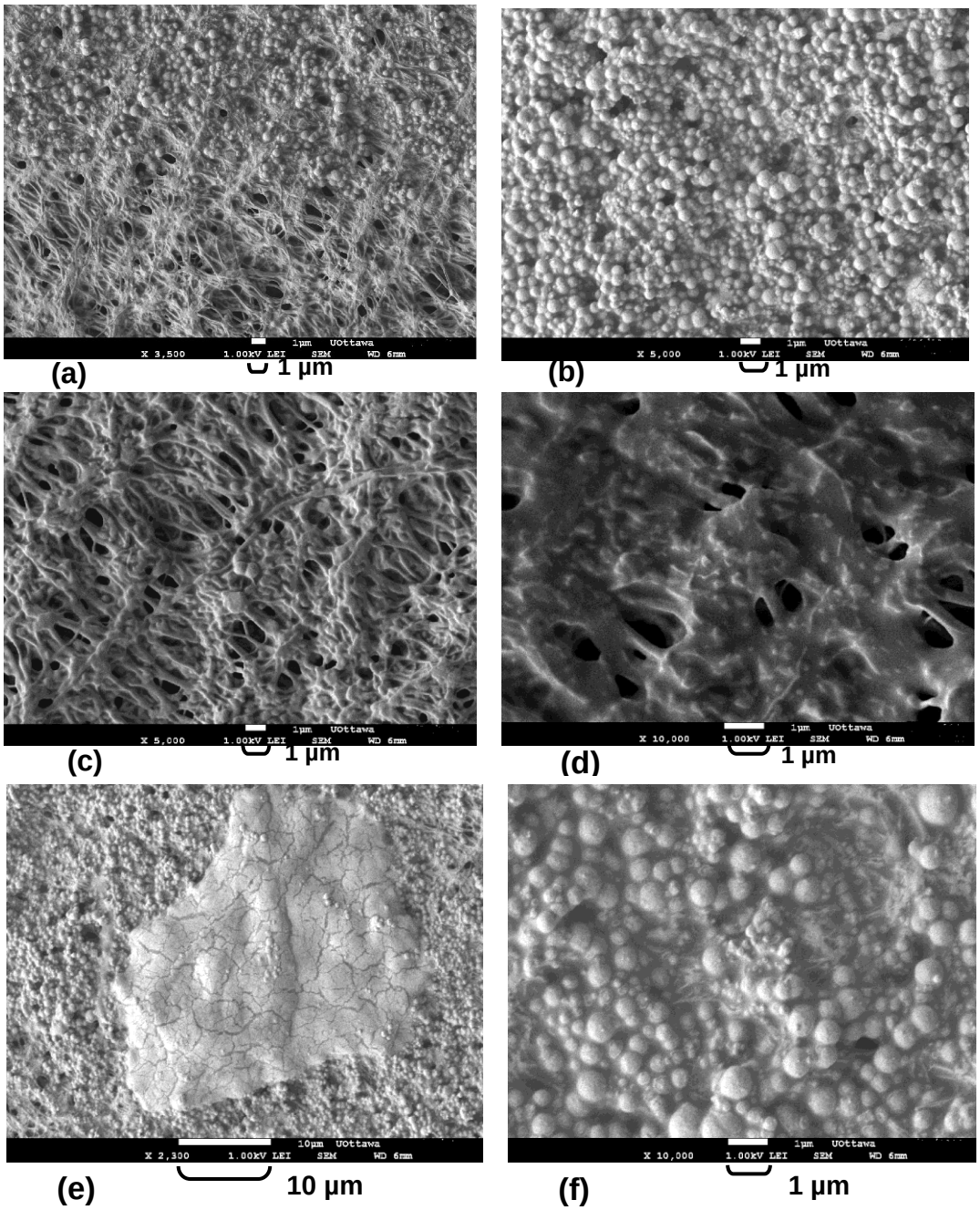

Fig . 6. A top view SEM image of a ZrP – PTFE composite membrane prepared with a GLY/ZrP mass ratio of 0.8. (a) two distinct regions in the same range, an upper region of ZrP particles and a lower region of empty pores, (b) and (f) ZrP particles at greater magnifications, (e) a large agglomerate of ZrP on top of the ZrP particles, (c) and (d) empty pores at greater magnifications showing the presence of a fluid-like material (glycerol) adhering to the strands of PTFE.

4.3.2. Effect of glycerol on conductivity in films of PTFE

The conductivity of the porous PTFE film (Sterlitech unlaminated film) used in these composite membranes was measured by EIS as received with no additives. An erratic or irregular pattern was apparent. Such a pattern might be expected for a material that does not posses proton conducting properties. Conductivities for PTFE as low as 10^{-13} S cm^{-1} have been reported in literature [12].

Different amounts of glycerol were added to a set of porous Sterlitech PTFE films. Their impedance plots are shown in Fig. 7 as a function of the GLY/ PTFE mass ratio $(MR)_{GLY/PTFE}$. The presence of glycerol caused the PTFE film to change from being an insulator material to being a conductor. Specifically, the resistance of the PTFE film decreased as its glycerol content increased. Overall, glycerol in the PTFE film caused the conductivity to increase by several orders of magnitude, from 10^{-13} S cm^{-1} to 10^{-4} S cm^{-1}. In the Nyquist plot, the imaginary component of the impedance is a linear function of the real component of the impedance. That linear relationship is typically associated with proton conduction being related to a diffusion phenomenon that results from a gradient in the concentration.

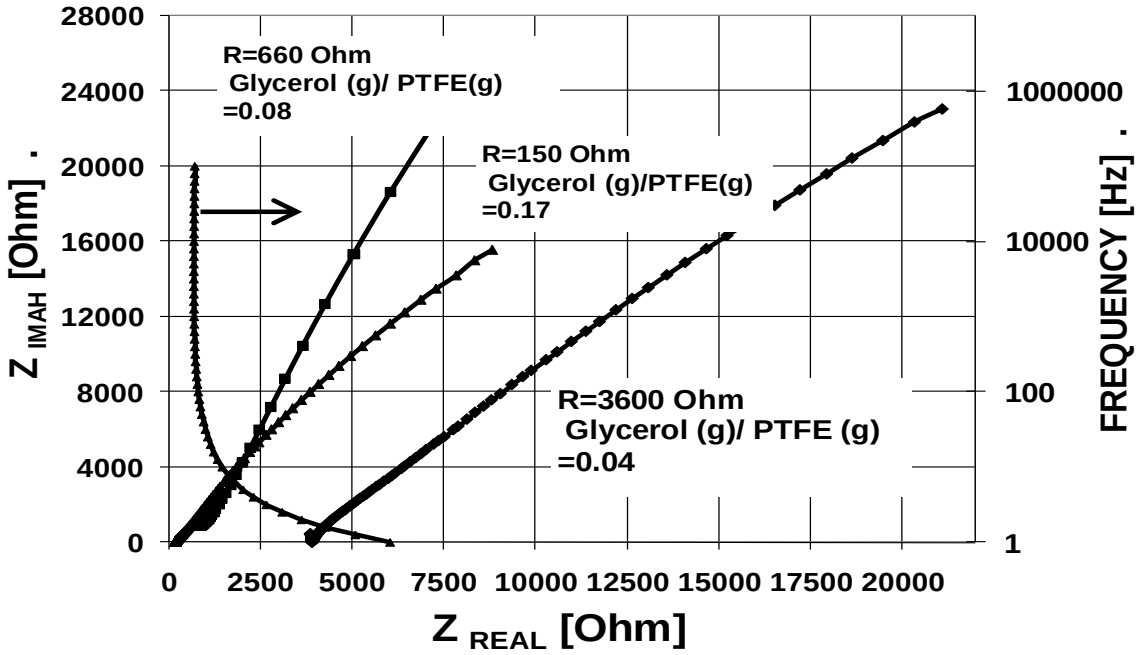

Fig . 7. Electrochemical impedance spectroscopy pattern for a porous Sterlitech PTFE films containing specified GLY/ PTFE mass ratios.

The resistances obtained in Fig. 7 are shown in Table 1. The conductivities were calculated from the resistances using Eq. 2, and are also shown in Table 1. It is seen that there is a linear relationship between the GLY/PTFE ratio and the conductivity.

Table 1: Resistances of PTFE films containing glycerol.

Mass Ratio [GLY/ PTFE] $MR_{GLY/PTFE}$	Resistance [Ohms]	Conductivity [S cm^{-1}]
0.04	3600	$6.49*10^{-6}$
0.08	660	$3.50*10^{-5}$
0.17	150	$1.56*10^{-4}$

EIS measurements were also made on the composite membranes that had been prepared by filling the pores of the PTFE film with solid particles of zirconium phosphate. A Nyquist plot obtained by EIS for a ZrP–PTFE composite membrane that did not contain any glycerol is shown in Fig. 8. The semi-circular shape on the left-hand (high frequency) side of the Nyquist plot in Fig. 8 is typically associated with a combination of (a) a double layer and (b) charge transfer reaction kinetics, resulting from a gradient in the electrical potential. The linear portion at the low frequency end of Fig. 8 is typically associated with diffusion resulting from a concentration gradient. It is similar in shape to those reported in the literature for crystalline ZrP [19] but different than some of our previous results for amorphous ZrP [15]. Its resistance (R= 1000Ω) and conductivity (1.7×10^{-5} S cm^{-1}) were of the same order of magnitude as the values for PTFE films that contained glycerol. That observation suggests that the addition of ZrP to PTFE has an influence on the magnitude of the conductivity that is somewhat similar to the addition of glycerol.

A Nyquist plot is shown in Fig. 9 for a ZrP – PTFE composite membrane to which glycerol had been added. Its glycerol to ZrP mass ratio, $MR_{GLY/ZrP}$ was 0.4. The resistance of the glycerol containing composite membrane in Fig. 9 was orders of magnitude less than that of the glycerol-free composite membrane in Fig. 8. While the conductivities of the two component materials, 6.9×10^{-5} – 1.5×10^{-4} S cm^{-1} for the GLY/PTFE membrane in Fig. 7, and 1.7×10^{-5} S cm^{-1} for the ZrP/PTFE membrane in Fig. 8, were much greater than PTFE alone, the combination of the three components, in Fig. 9, had a conductivity, 2×10^{-2} S cm^{-1}, that was vastly superior to either of the two component materials. The shape of the Nyquist plot in Fig. 9 is indicative of diffusion.

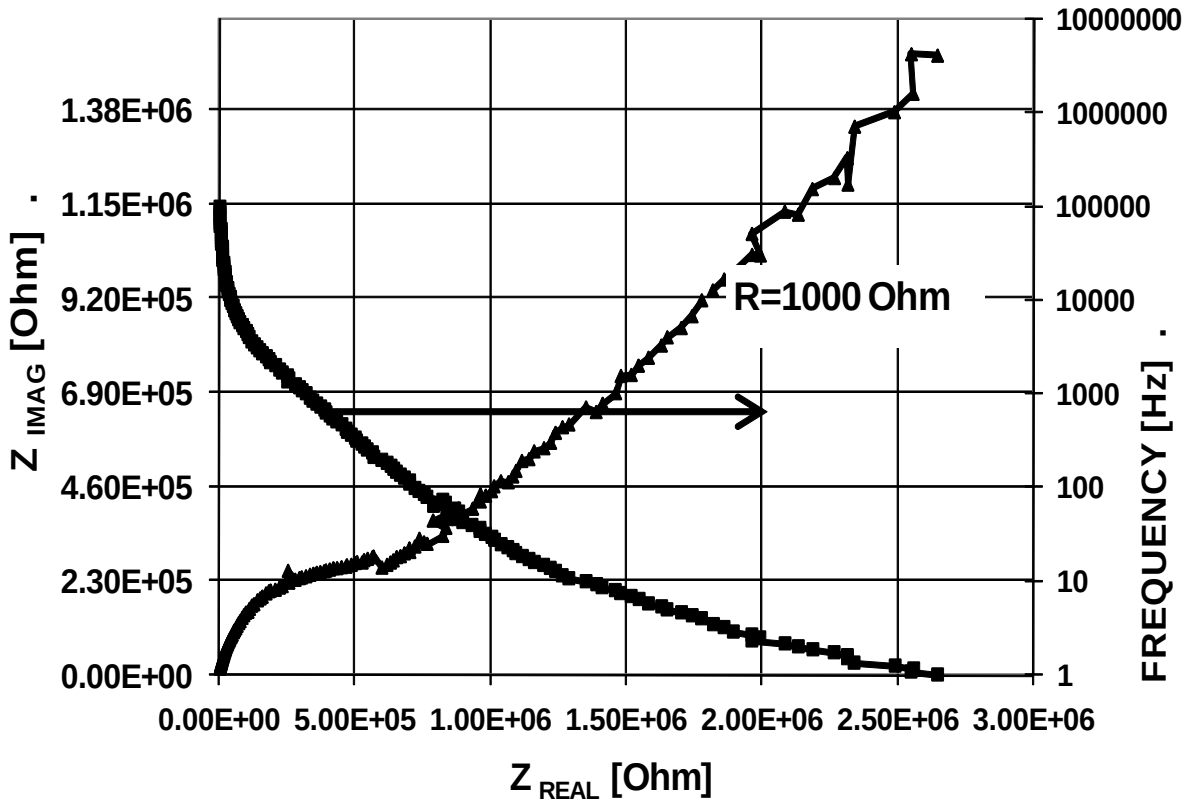

Fig . 8. Electrochemical impedance spectroscopy pattern for a ZrP –PTFE composite membrane that did not contain glycerol.

A Nyquist plot for a ZrP composite membrane having an $MR_{GLY/ZrP}$ of 0.8 is shown in Fig. 10. In general its shape was similar to that in Fig. 9. However, its resistance, 3 Ohms, was slightly larger and its conductivity, 6.5×10^{-3} S cm^{-1}, was slightly smaller than the corresponding values derived from Fig. 9. The poorer performance with an $MR_{GLY/ZrP}$ value of 0.8 is consistent with the morphology seen in Fig. 6, where some of the pores did not contain ZrP particles and the external membrane surface contained comparatively large ZrP agglomerates.

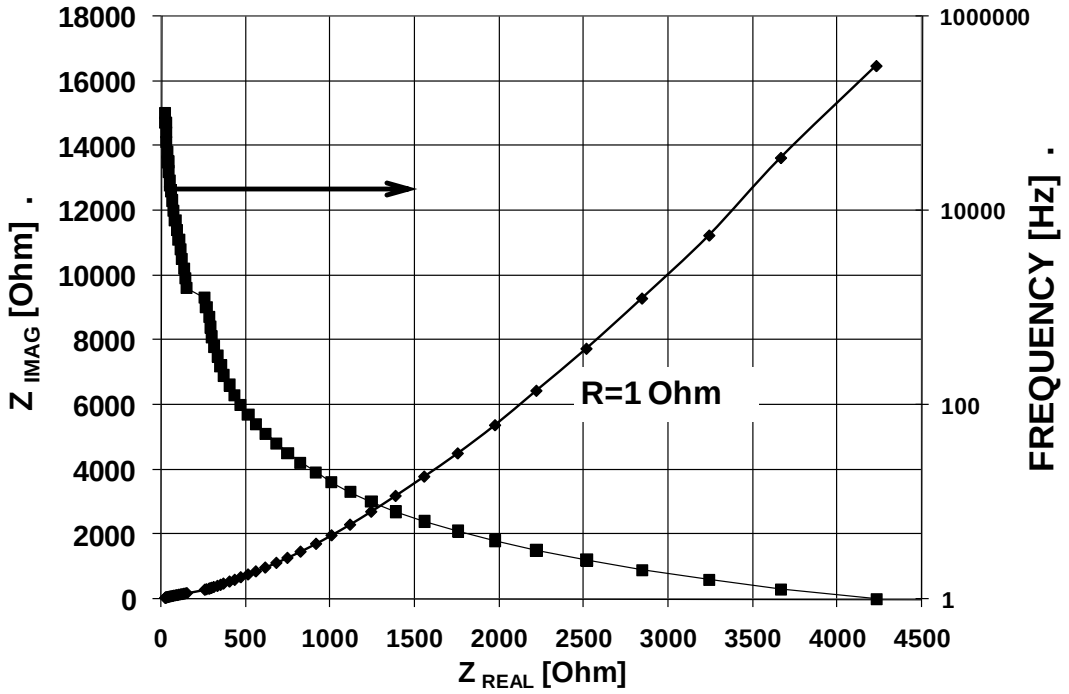

Fig . 9. Electrochemical impedance spectroscopy pattern for a ZrP –PTFE composite membrane having a Glycerol / ZrP mass ratio of 0.4.

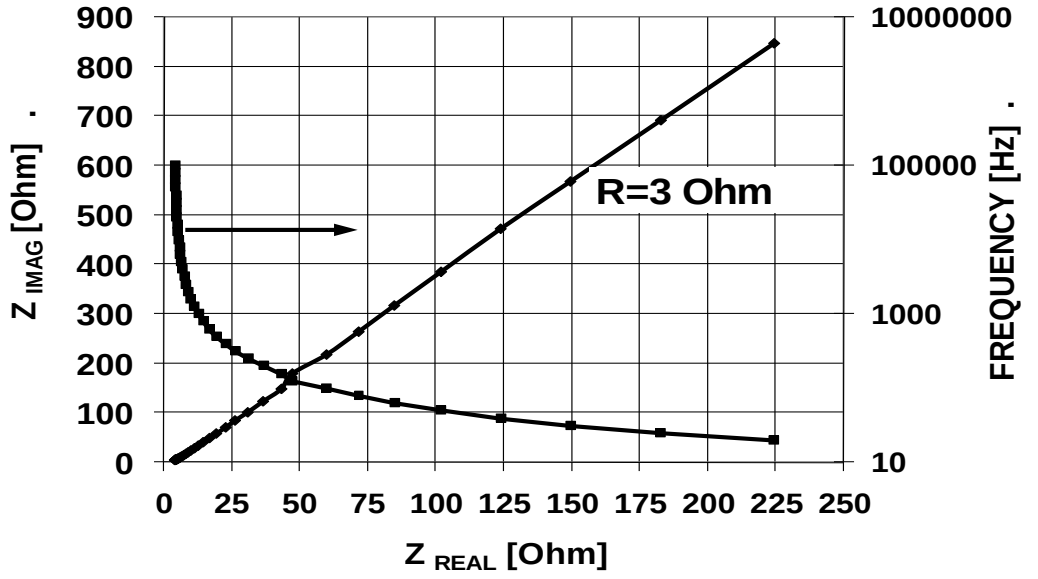

Fig . 10. Electrochemical impedance spectroscopy pattern for a ZrP –PTFE composite membrane having a Glycerol / ZrP mass ratio of 0.8.

The conductivity results for the GLY/ZrP/PTFE composite membranes are shown in Fig. 11 as a function of the GLY/ ZrP mass ratio, $MR_{GLY/ZrP}$. The proton conductivity increased by several orders of magnitude when glycerol was introduced to the ZrP/PTFE composite membranes. The proton conductivity reached a maximum value (0.02 – 0.045 S cm^{-1}) when the GLY/ ZrP mass ratio was in the region of 0.2 to 0.4. It is also evident from Fig. 11 that the proton conductivity decreased by almost an order of magnitude when the $MR_{GLY/ZrP}$ was increased to 0.8. This result is consistent with what was presented earlier by the SEM images showing that larger spherical particles were formed at this $MR_{GLY/ZrP}$ ratio, i.e., a decrease in the total surface area of ZrP particles leads to a decrease in the proton conductivity. Furthermore, the non-uniform distribution of ZrP and the appearance of two distinctive regions of ZrP and glycerol (referring to Fig. 6 (a) and (e) might have contributed to the decrease in proton conductivity.

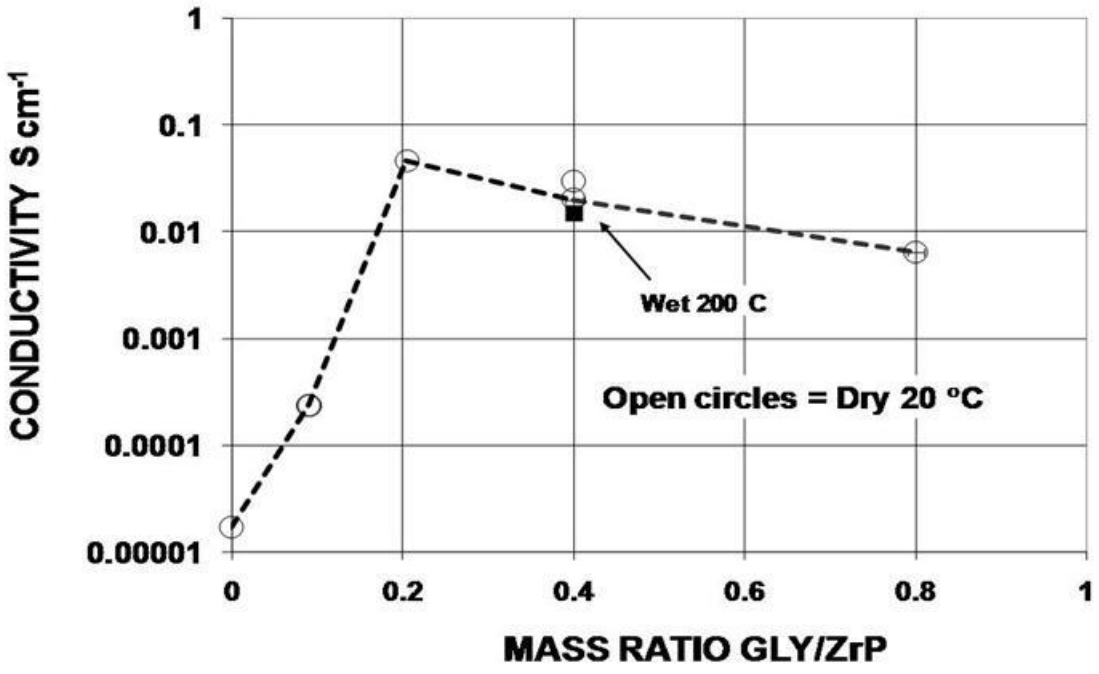

Fig . 11. Change of proton conductivity (σ) S cm^{-1} with glycerol /ZrP mass ratio in the composite membrane.

Proton hopping is generally considered to be the mechanism that is responsible for proton conductivity. For example, proton hopping in water has been extensively reviewed [20]. Similarly, protons could be expected to hop between the oxygen atoms in the OH groups in glycerol, $HOCH_2$-CHOH-CH_2OH. That might be an explanation for the conductivity observed in GLY/PTFE membranes. In ZrP, each zirconium atom is associated with a $Zr(HPO_4)_2 \bullet H_2O$ structure that has two OH groups and one H_2O molecule. Hopping between the oxygen atoms in the OH groups and the water of hydration within a $Zr(HPO_4)_2 \bullet H_2O$ structure molecule might be expected.

Proton conductivity on the external surfaces of ZrP particles has also been suggested as a phenomenon. Alberti et al. [21, 22] showed that the conductance of ZrP decreased with the increase in the degree of crystallinity and that although the fraction of the surface covered with protons is small, their mobility is 10^4 greater than the protons in the bulk. Thus, greater external ZrP surface area, results in greater proton conductivity.

The conductivity results obtained in this work have been compared with some literature values in Table 2. PTFE is an insulator. In contrast the conductivity of ZrP particles is orders of magnitude greater than that for PTFE. When the void volume of porous PTFE was filled with glycerol, the conductivity was as good as or better than that of ZrP particles. When a dry ZrP/PTFE membrane was composed of a combination of a porous PTFE film plus flakes of ZrP the conductivity was comparable to that of dry ZrP particles. However when the ZrP/PTFE membrane was composed of a combination of PTFE particles and ZrP particles compressed together, there was an order of magnitude increase in the conductivity compared to the combination of porous PTFE and ZrP flakes. Finally when ZrP was formed in-situ within the pores of a porous PTFE in the presence of glycerol, the conductivity increased by two orders of magnitude. The conductivity of the GLY/ZrP/PTFE composite membrane approached 40% of the value for Nafion. Furthermore, that value was maintained when the temperature was increased from 20 to 200°C provided the steam to feedstock ratio was typical of that required for a direct propane fuel cell.

Table 2 : Summary of conductivity results

Material	Proton Conductivity [Scm^{-1}] Literature Value	Proton Conductivity [$S\ cm^{-1}$] This work
PTFE [12]	10^{-13}	
ZrP (particles)		
Crystallites – dry [23,24]	$10^{-6} – 10^{-5}$	
Amorphous – dry [15]	10^{-5}	
Amorphous – wet [15]	10^{-4}	
GLY/PTFE (porous film)		$0.7 – 1.5 \times 10^{-4}$
ZrP(particles)-PTFE (particles)		
– dry [12]	$10^{-4} – 10^{-3}$	
ZrP(flakes)-PTFE (porous film)		
– dry [15]	10^{-5}	1.7×10^{-5}
GLY–ZrP(spheres)-PTFE(porous film)		
– dry		0.02– 0.045
– wet (y_{H2O} = 0.86 at 200°C)		0.015
Nafion – 20 °C and 95 % Relative Humidity [25]	0.12	
– 120°C and 90 % Relative Humidity [25]	0.013	

The inclusion of glycerol in the GLY/ZrP/PTFE membrane made two differences. The morphology of the ZrP changed from flakes to small spheres. Also the surfaces of the solid ZrP spheres were in contact with glycerol. It is possible that the enhancement in conductivity in the GLY/ZrP/PTFE membranes may have been caused by proton transport at the interface between the small solid ZrP spheres and their glycerol coating. In addition to two bulk phenomena, proton transport though ZrP and proton transport thorough glycerol, surface phenomena may have also contributed to the conductivity. Presumably two surface phenomena, proton transport on solid ZrP surfaces and proton hopping via the OH groups in glycerol, may have been operating simultaneously. Because the PTFE pores contained a large number of small spheres, together they would have a large surface area. The combination of the two proton surface transport mechanisms plus the large interfacial area may help to explain the two order of magnitude improvement in conductivity. Furthermore, the high surface tension of glycerol and the successive wetting and drying cycles inside the hydrophobic pores have favored the formation of small aggregates of $ZrOCl_2$. The presence of glycerol has prevented these aggregates from coalescing, hence, the formation of nano-scale particles within the confined environment existing in the PTFE pores. These particles were relatively spherical in shape resulting in a high total surface area and a highly conducting membrane.

4.4. Conclusions

Glycerol was found to enhance the proton conductivity when added to both a porous PTFE film and a ZrP/PTFE composite membrane. Small spheres of ZrP (100 – 500 nm) were observed in the GLY/ZrP/PTFE composite membrane. The enhanced conductivity may have been caused by a combination of proton transport on the increased surface area on the exterior of the small ZrP spheres plus proton hopping using both the OH groups in glycerol and the ZrP bulk. The conductivity of GLY/ZrP/PTFE composite membranes at 20°C approached 40 % of the conductivity of a Nafion membrane. This proton conductivity was maintained when the membrane was processed at 200°C in the presence of a steam partial pressure typical of a direct propane fuel cell. For fuel cell operations above the

boiling point of water, these membranes could be promising alternatives to Nafion membranes.

4.5 Acknowledgments

The authors are grateful for the financial support from the Canadian federal government's Natural Sciences and Engineering Research Council and from the Ontario provincial government's Ministry of Research and Innovation (Ontario Fuel Cell Research and Innovation Network). The authors wish to also thank Dr. Takeshi Matsuura for his assistance in providing some literature references.

4.6 References

1. P. J. James, J. A. Elliot, T. J. McMaster, J. M. Newton, A.M.S. Elliot, S. Hanna, M. Miles, , J. Mater. Sci. 35 (2000) 5111.

2. J.L. Zhang., Z. Xie , J. Zhang , Y. Tang, C. Song , T. Navessin, Z. Shi, D. Song, H. Wang, D. Wilkinson, Z. Liu, S. Holdcroft, J. Power Sources 160 (2006) 872.

3. C. Yang, S. Srinivasan, A. Bocarsly. , S. Tulyani, J.B. Benziger, J. Membr. Sci. 237 (2004) 145.

4. W. G. Grot, G. Rajendran, US Patent 5,919,583, 1999.

5. C.B. Amphelett, L.A. McDonald, M.J. Redman., J. lnorg. Nucl. Chem. 6 (1958) 220.

6. A. Clearfield, J.A. Stynes, J. Inorg. Nucl. Chem. 26 (1964) 117.

7. R.P. Hamlen, J. Electrochem. Soc. 109 (1962) 746.

8. O. Savadogo, J. Power Sources 127 (2004) 135.

9. H. Hou, G. Sun, Z. Wu, W. Jin,, Q. Xin, Inter. J. Hydrog. Energ. 33 (2008) 3402.

10. F. Bauer, M.Willert-Porada, Fuel Cells 6 (2006) 261.

11. M. Casciola, D. Capitani, A. Comite, A. Donnadio, V. Frittella, M. Pica, M. Sganappa, A. Varzi, Fuel Cells 8 (2008) 217.

12. Y. Park, K. Jae-Dong, M. Nagai, J. Mater. Sci. Lett. 19 (2000) 1735.

13. F. Liu, B. Yi, D. Xing, J. Yu, H. Zhang, J. Membr. Sci. 212 (2003) 213.

14. R. Jiang, H.R. Kunz, J. Fenton, Electrochim. Acta 51 (2006) 5596.

15. A. Al-Othman, A. Y. Tremblay, W. Pell , S. Letaief ,T.J. Burchell, B. A. Peppley, M. Ternan, J. Power Sources 195 (2010) 2520.

16. H.L. Lin , S.H. Yeh, T. L. Yu, L.C. Chen, J. Polym. Res. 16 (2009) 519.

17. M.C. Burshe, S.B. Sawant, V.G. Pangarkar, J. Am. Oil Chem. Soc. 76 (1999) 209.

18. Y.J. Wang, Y. Pan, L. Chen, Mater. Chem. Phys. 92 (2005) 354.

19. D. Bianchi, M. Casciola, Solid State Ionics 17 (1985) 7.

20. E. Gileadi, E. Kirowa-Eisner, Electrochim. Acta 51 (2006) 6003.

21. G. Alberti , E. Torracca, J. lnorg. Nucl. Chem. 30 (1968) 1093.

22. G. Alberti, M. Casciola, U. Costantino, G. Levi, G. Ricciardi, J. Inorg, Nucl. Chem. 40 (1978) 533.

23. H. Patel, U. Chudasam, J. Chem. Sci., 119 (2007) 35.

24. A. Clearfield, Annu. Rev. Mater. Sci. 14 (1984) 205.

25. M. Casciola, G. Alberti, M. Sganappa, R. Narducci, J. Power Sources 162 (2006) 141.

CHAPTER FIVE

A modified silicic acid (Si) and sulphuric acid (S) –ZrP/PTFE/Glycerol composite membrane for high temperature direct hydrocarbon fuel cells

Amani Al-Othman [a,b], André Y. Tremblay[a], Wendy Pell [b], Sadok Letaief, Yun Liu [b], Brant A. Peppley[c], Marten Ternan[d]

(a) Chemical and Biological Engineering, University of Ottawa, 161 Louis Pasteur, Ottawa, ON K1N 6N5, Canada

(b) Catalysis Centre for Research and Innovation, University of Ottawa, 30 Marie-Currie, Ottawa, ON K1N 6N5, Canada

(c) Chemical Engineering, Queens University, Dupuis Hall, Kingston, ON K7L 3N6, Canada

(d) EnPross Inc., 147 Banning Road, Ottawa, ON K2L 1C5, Canada

Chapter 5- A modified silicic acid (Si) and sulphuric acid (S) – ZrP/PTFE/Glycerol composite membrane for high temperature direct hydrocarbon fuel cells

ABSTRACT

Composite membranes composed of modified S or Si–zirconium phosphate (ZrP), porous polytetrafluoethylene (PTFE) and, glycerol (GLY) were synthesized in this work. ZrP was precipitated via the in-situ reaction of zirconium oxychloride ($ZrOCl_2$) with phosphoric acid (H_3PO_4). Silicic acid and sulphuric acid were introduced as additives to phosphoric acid with variable Si/P or S/P mass ratios in the acid solution/suspension. The modified membranes were investigated as electrolytes for direct hydrocarbon fuel cells operating at temperatures~200°C. Our previous work described a composite membrane (ZrP/PTFE/GLY) synthesis that possessed a proton conductivity of 0.045 S cm^{-1}. The present work shows that adding a small amount of silicic acid to phosphoric acid enhanced the proton conductivity, i.e. by having an Si/P mass ratio of (0.01) in the acid solution/suspension, the Si-ZrP/PTFE/GLY membrane conductivity was 0.073 S cm^{-1}. This value approached the conductivity of Nafion (0.1 S cm^{-1}). The results also showed that adding sulphuric acid to phosphoric acid led to a significant decrease in the membrane's proton conductivity. The enhancement of proton conductivity for the Si-ZrP/PTFE/GLY composite membrane might be attributed to the improvement in water retention properties and the possible formation of the Si–O–P bond.

5.1 Introduction

Proton exchange membrane fuel cells (PEMFC) currently operate at temperatures around 80 °C with pressures between 1 and 5 bars. PEMFC are attractive for their several advantages including the high power density, and all solid construction. By far, the conventional perfluorosulfonic acid (PFSA) membrane (Nafion) is the most commonly used membrane in PEMFC.

The incentives for high temperature operation in PEMFC are, 1) increasing the reaction kinetics, 2) reduction and /or the elimination of the liquid water accumulation inside the fuel cell, mainly at the cathode, and 3) heat generation at greater temperatures. The reduction of the liquid phase will diminish the diffusion resistance, thus, more molecules will have easier access to the reaction sites.

The proton conductivity of Nafion and similar PFSA membranes is known to be strongly dependent on the water content needed to solvate the proton of the sulfonic acid groups. Although increasing the temperature is beneficial in the operation of PEMFC, the membrane material is still one of the main obstacles. Higher temperatures cause the PFSA (Nafion) membranes to dehydrate, i.e. a dramatic decrease in proton conductivity. Therefore, alternative materials have been explored to replace the existing PFSA membranes. These membrane materials are made of sulfonated aromatic compounds, solution polymers membranes, inorganic-organic composite membranes, or acid base polymer materials [1].

Various studies have investigated the synthesis of sulfonated aromatic compounds for fuel cell applications. Examples are the work of Chikashige et.al. [2], in which sulfonated poly (arylene ether) ionomers were prepared and, the work of Kang et.al. [3], in which polybenzimidazole compounds were prepared. Other studies explored the synthesis of solution polymer membranes such as the work of Kim et.al. [4]. Extensive efforts aimed at modifying the existing PFSA membranes based on the procedure of Grot [5], to enhance their water retention properties. Grot proposed the incorporation of inorganic fillers in membranes. The result is an inorganic-organic composite membrane. The preparation methods for such membranes are variable. They include the in situ precipitation of the inorganic material within the polymer matrix, and the introduction of the inorganic material into the polymer dispersion.

Nafion membranes have been modified by the incorporation of metal hydrogen phosphates, such as zirconium phosphate (ZrP), a solid proton conductor [6,7], by the incorporation of silica [8], an inorganic compound, and by the incorporation of metal oxides particles [9]. In particular, the incorporation of silica in Nafion has received a considerable attention in the literature due to the hygroscopic nature of silica compounds. Examples are

the work of Pereira et.al.[10], in which a Nafion/mesoporous silica membrane was prepared, and the work of Ke et.al. [11], where nano-sized Nafion/ SiO_2 were formed in-situ by the sol-gel process.

Zirconium phosphate $Zr(HPO_4)_2.H_2O$, (ZrP), is one example of an inorganic material that has the attractive characteristics of: 1) possessing proton conductivity and, 2) a layered structure permitting the passage of guest molecules, 3) having weak acidic groups; thus, allowing the exchange of the protons in the POH group with other cations [12]. As a result, the admitted cations accommodated within the layers are expected to cause a change in the interlayer distance depending on the size of the guest molecule. Other examples of inorganic materials in composite membranes are ZrO_2 and TiO_2. These oxides have attracted attention of scientists due to their water uptake properties.

This work describes an improvement over our previous synthesis of Nafion–free ZrP/PTFE/Glycerol (GLY) composite membranes [13]. It is aimed at modifying the ZrP PTFE/GLY membranes using a second acid, either sulphuric acid (H_2SO_4) or silicic acid ($SiO_2.H_2O$). The modified S and Si–ZrP/PTFE/Glycerol composite membranes were investigated as potential electrolytes for high temperature PEMFC. To our knowledge, this type of composite membranes, with this combination of electrolyte materials, has not been reported in literature. Phosphoric acid solutions (H_3PO_4) containing small amounts of either sulphuric acid (H_2SO_4) or silicic acid ($SiO_2.H_2O$, or H_2O_3Si) were used to react with zirconium oxychloride ($ZrOCl_2.8H_2O$) to form modified ZrP. By having solutions, in which the acids are mutually soluble, it was expected that a small proportion of the "P" atoms in the resultant ZrP could be replaced by either "S" atoms or "Si" atoms. Therefore, it is expected that the incorporation of "Si" would result in zirconium phosphate ($Zr(HPO_4)_2.H_2O$) material, and a minor fraction of $Zr(H_2SiO_4)_2.H_2O$, thus, increasing the OH groups in the ZrP lattice. The incorporation of "S" on the other hand is anticipated to decrease the number of OH groups in the ZrP lattice by yielding a minor fraction of material that has the formula $Zr(SO_4)_2.H_2O$. Since the Grotthus mechanism of proton conduction [14], is proton hopping between either water molecules or OH groups, the proton conductivity was expected to increase with increasing the OH groups in the composite membranes. In this work, the following investigations were performed on the composite

membranes: 1) changes in the ZrP morphology upon the introduction of Si and S and, 2) the evaluation of the modified composite membranes for proton conductivity.

5.2. Experimental

5.2.1. Synthesis of S - ZrP /PTFE/Glycerol and Si-ZrP/PTFE/Glycerol composite membranes

Unlaminated Sterlitech PTFE films (with a nominal thickness of 50 μm and a nominal pore size of 0.22 μm) were used as the porous starting material in this work. Zirconium oxychloride, $ZrOCl_2 \cdot 8H_2O$ (Sigma Aldrich) was reacted with 85% o-phosphoric acid (Fisher Scientific) to produce zirconium phosphate, $Zr(HPO_4)_2 \cdot H_2O$, ZrP according to the chemical reaction described in equation (1) [15].

$$ZrOCl_2 \cdot 8H_2O + 2\ H_3PO_4 \rightarrow Zr(HPO_4)_2 \cdot H_2O + 2\ HCl + 8\ H_2O \quad (1)$$

Ethanol (anhydrous ethyl alcohol from Commercial Alcohols Inc.), glycerol (certified ACS, assay 99.7% from Fisher Scientific) and iso-propanol (HPLC grade, assay 99.8% from EMD) were obtained to prepare the alcoholic suspension of $ZrOCl_2 \cdot 8H_2O$. $ZrOCl_2 \cdot 8H_2O$ suspension was prepared using 50 mL of ethanol, 2 mL of water, 150 mL of isopropnaol and a specific amount of glycerol (GLY). GLY was added in order to vary the GLY/ZrP mass ratio in the composite membrane. The alcoholic suspension was placed on a stirring hot plate and vigorously mixed using a magnetic stirrer.

The PTFE film was first weighed, then placed between Teflon™ hoops. The Teflon™ hoops were attached to a mixer shaft. The stirred alcoholic suspension was heated at 70 °C, and then introduced into the pores of the PTFE film as the hoops rotated. It was dripped onto the top side of the PTFE porous film so that it was well distributed. Dripping was periodically stopped to allow the evaporation of alcohol while the membrane continued to rotate. The dripping was started again once the rotating membrane appeared to be dry. This procedure was repeated until the total amount of alcoholic suspension of $ZrOCl_2.8H_2O$ was consumed. The resulting membranes were then immersed in H_3PO_4 for 72 hours, allowing reaction in Eq. (1) to take place. In subsequent experiments, the zirconium

phosphates (ZrP) material was modified by adding either sulphuric acid or silicic acid to phosphoric acid. For example, $SiO_2.H_2O$ (- 80 mesh powder, from Sigma Aldrich) was added to phosphoric acid with variable quantities to study the effect of various Si/P mass ratios. At some Si/P mass ratios, silicic acid was in solution. However, the solubility of silicic acid in phosphoric acid is limited. The maximum amount observed to dissolve was 0.1 g $SiO_2.H_2O$ in 20 mL of 85% H_3PO_4. In some experiments, silicic acid was in solution, however, at higher Si/P ratios, when the solubility limit was exceeded, part of it was in solution while the other part appeared in suspension. Sulphuric acid (A.C.S reagent from Fisher Scientific) was also used to modify the membranes. Specified volumes of sulphuric acid were added to phosphoric acid in such a way to vary the S/P mass ratio in the acid solution. The membranes were then immersed in the acid solutions for 72 hours and then, were gently rinsed with de-ionized water and isopropanol (ratio of 50:50 by volume) followed by drying in the oven for 24 hours at 120 °C.

A high temperature processing test was performed at 200 °C for a sample of an Si-ZrP/PTFE/GLY membrane. The sample was first cut, weighed then put in a tube furnace under a combination of heat treatment and elevated water vapour pressure for 30 minutes. H_2O and argon were injected at an H_2O/Ar molar ratio of 6, and $y_{H2O} = 0.86$ (wet test). This H_2O/Ar molar ratio is identical to the H_2O/C_3H_8 ratio in the direct propane fuel cell reaction where H_2O is a reactant. The processed membrane sample was then re-weighed and placed in a sealed non–porous Teflon bag and sent for electrochemical impedance spectroscopy (EIS) analysis.

5.2.2. Characterization of the S- ZrP /PTFE/Glycerol and Si- ZrP/PTFE/Glycerol composite membranes

Proton conductivity measurements were performed using electrochemical impedance spectroscopy (EIS) by the four probe method. A Parstat, 2273 instrument and PowerSuite 2.58, 2003 electrochemical software were used. The measurement was done over a frequency range of 1 – 100 kHz. As explained in our earlier work [13], the value of the real electrolyte resistance, R, was obtained from the intersection of the line on the Nyquist plot

with the x-axis. The membrane thickness, d, was measured and the cross sectional area of the sample, A, was calculated. The proton conductivity (σ) was obtained from Eq. 2 [16]:

$$\sigma = d / (R \times A) \quad (2)$$

The surfaces of the composite membranes were examined by scanning electron microscopy (SEM). SEM was performed using a JEOL JSM-7500F Field Emission Scanning Microscope. Some composite membrane samples were freeze-fractured using liquid nitrogen prior to SEM analyses to examine their cross sections. Further analysis for the composite membranes was performed using Fourier transform infrared spectrometer, FT-IR analysis, using an FT-IR Nicole 6700 Spectrometer equipped with a ZnSe plate. The spectra for the samples were recorded in the range 3000 – 800 cm^{-1} at room temperature. Samples of composite membranes were also analyzed by XRD (X-ray diffraction) using a Philips PW 1830 generator machine.

5.3. Experimental results

5.3.1 SEM observations and morphology studies of composite membranes

Fig. 1., shows SEM images for the unmodified ZrP/PTFE/GLY, and the Si or S modified composite membranes, and, compares them based on their top view. The composite membranes were all synthesized at a GLY/ZrP mass ratio of 0.4. The Si/P and the S/P mass ratios were 0.004 in the phosphoric acid–silicic acid (solution) for the modified membranes. SEM images show the ZrP material covering most of the pores of PTFE with some strands of the PTFE polymer still observable. SEM image (a) presents an unmodified ZrP/PTFE/GLY composite membrane, whereas images (b) and (c) of the same figure show a modified, Si-ZrP/PTFE/GLY and S-ZrP/PTFE/GLY composite membranes respectively. Careful examination of image (a) in Fig. 1, reveals the formation of nearly spherical ZrP particles, in the size range of 250 – 500 nm. Further examination of images (b) and (c) shows a visible change in the formed ZrP material's morphology. It is apparent that the addition of silicic acid into phosphoric acid, caused a change in the produced ZrP particle size and shape. Plate-like ZrP particles of nearly 1 um in size were observed in image (b) for the Si- modified membranes. The particle size for the S–modified membranes also varied in

the range of 1 μm to 5 μm in some regions, as seen in image (c), with much less coverage observed than that appeared in images (a) and (b).

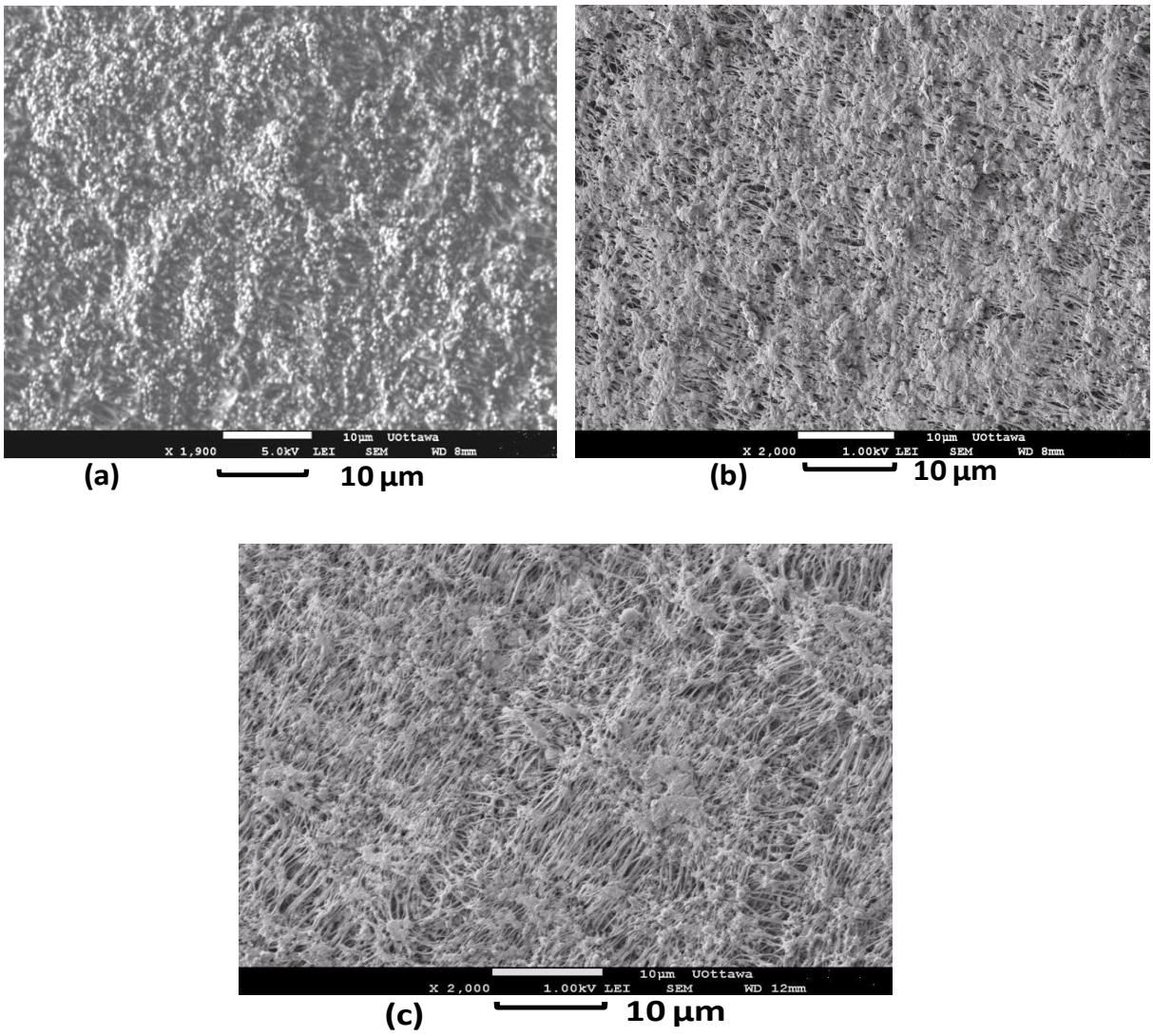

Fig . 1. SEM images for composite membranes, all at a GLY/ZrP mass ratio of 0.4. (a) an unmodified ZrP/PTFE/GLY membrane, (b) Si- ZrP/PTFE/GLY membrane with an Si/P mass ratio of 0.004 and (c) a S-ZrP/PTFE/GLY membrane at a S/P mass ratio of 0.004.

In general, the morphology of the Si–modified composite membranes changed from being nearly spherical in all regions, into an assortment of plate-like ZrP material of 1 um in size. The S-modification of ZrP also caused a change in morphology. This change in

morphology was also accompanied by a change in proton conductivity for both, the Si-modified ZrP/PTFE/GLY and the S-modified ZrP/PTFE/GLY membranes.

The effect of varying the Si/P mass ratios is shown in Fig.2. All ZrP/PTFE/GLY composite membranes were prepared, at a GLY/ZrP mass ratio of 0.2. The Si/P mass ratios were varied from 0.0 to 0.02. SEM images in Fig.2. show a top view for the composite membranes. Image (a) shows an unmodified ZrP/PTFE/GLY membrane (Si/P=0.0). The ZrP particles appear to be nearly spherical in shape, in the size range of 300-600 nm. Image (b) shows an Si-ZrP/PTFE/GLY at an Si/P = 0.004 in the phosphoric acid–silicic acid (solution). At this Si/P ratio, all the silicic acid was soluble in phosphoric acid. It can be seen that the shape and size of the Si-ZrP material has changed from nearly spherical particles into a plate-like particles of a 1 μm average size. Image (c) shows an Si-ZrP/PTFE/GLY membrane with an Si/P = 0.01 in the phosphoric acid – silicic acid suspension. At this Si/P ratio, some of the silicic acid was in solution, and some of it appeared in suspension. Additional changes in particles morphology were observed. Larger size ZrP material appeared, having a flaky shape with an average size of 2 μm. This noticeable change in size and morphology was accompanied by a change in the proton conductivity. Images (d) and (e) show an Si-ZrP/PTFE/GLY membrane with an Si/P = 0.02 in the phosphoric acid – silicic acid suspension. A plate like material continued to appear but it was evident that adding more silicic acid has resulted in much less coverage on top of the composite membrane. Further examination of image (d), shows strands of the polymer appeared to be entirely uncovered by the proton conducting material in some regions whereas the particles appear to agglomerate in other regions. It could be explained as a phase separation phenomenon as reported in literature for silica containing membranes. Lin et. al. [17] reported phase separation in Nafion®/–SO_3H functionalized mesoporous silica composite membranes. Changes in proton conductivities were also observed for these Si-modified composite membranes, as shall be discussed in section 3.2.

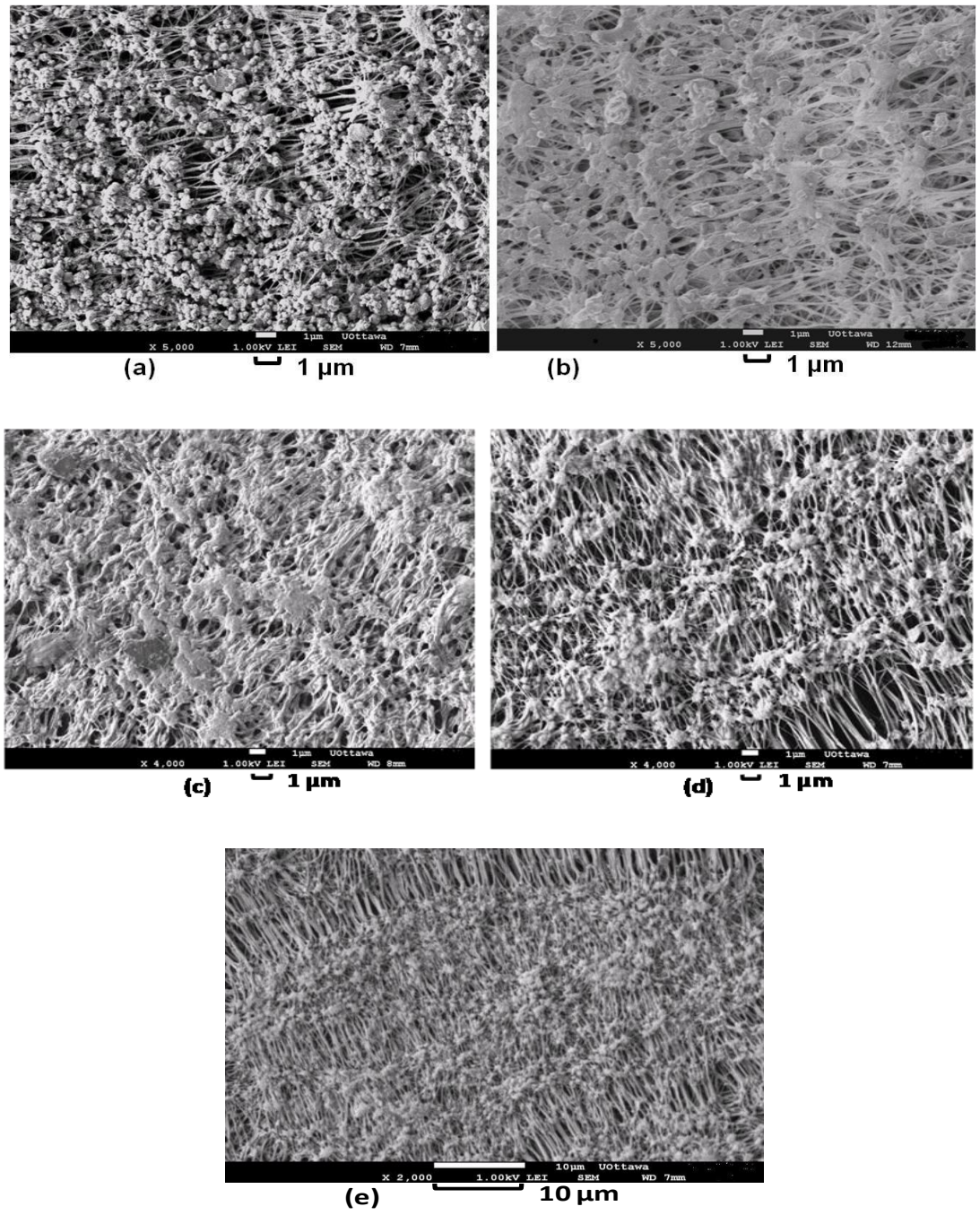

Fig . 2. SEM images for a ZrP/PTFE/GLY composite membranes, all at a GLY/ZrP mass ratio of 0.2., variable Si/P mass ratios, (a) ZrP/PTFE/GLY membrane (Si/P=0.0), (b) Si-ZrP/PTFE/GLY membrane Si/P = 0.004 (silicic acid is completely dissolved in phosphoric acid) ,(c) Si–ZrP/PTFE/GLY at Si/P = 0.01 some silicic acid is in suspension in phosphoric acid, (d) and (e) are for Si–ZrP/PTFE/GLY at an Si/P = 0.02, some silicic acid is in suspension in phosphoric acid

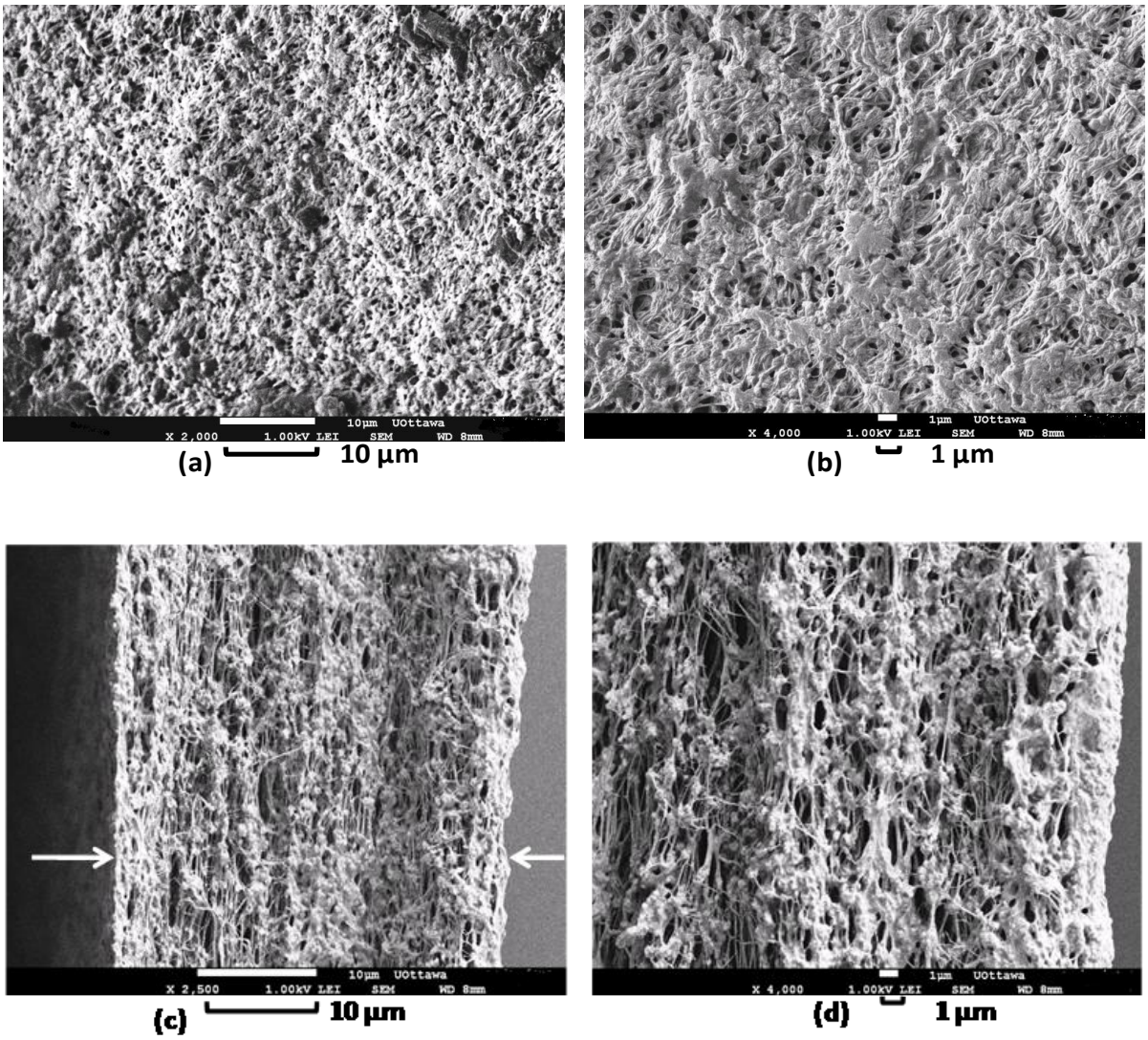

Fig . 3. SEM images for an Si– ZrP/PTFE/GLY composite membrane, at a GLY/ZrP mass ratio of 0.2. and an Si/P mass ratio of 0.01 (some silicic acid is in suspension in the phosphoric acid) (a) and (b) are top view images. (c) and (d) are cross-sectional view images obtained by freeze-fracture. Edges of the membrane are indicated by the arrows in image (c).

Fig.3. shows the SEM results for the Si– ZrP /PTFE/GLY membrane with an Si/P = 0.01, that had some silicic acid in suspension. Images (a) and (b) show top view for the membrane at a different location than that appeared in Fig.2 (c). This figure confirms the

changes in morphology and coverage observed in Fig.2. Images (c) and (d) of Fig. 3, are a cross-sectional view of this composite membrane and they show the following: 1) The ZrP material appears to be suspended along the cross section of the highly porous support (PTFE), 2) The ZrP morphology appears to be different within the cross section (nearly spherical particles of ~ 300 nm in diameter) compared to the (plate-like) particles observed on the top, and, 3) the intersections of the polymer strands appear to have been nucleation sites for the ZrP material with particles aggregation observed in some regions. A cross–sectional SEM view of the unmodified ZrP/PTFE/GLY composite membranes was shown in our previous work [13]. The cross section was quite different than the open structure shown in Fig.3. Instead, the cross section shown in our previous work appeared to be densely packed with the spherical nano-scale ZrP material.

5.3.2. Proton conductivity of the Si–ZrP /PTFE/GLY and S –ZrP /PTFE/GLY composite membranes

The proton conductivities of the S and Si–ZrP/PTFE/GLY composite membranes were measured by EIS. The Nyquist plot obtained for the Si–ZrP/PTFE/GLY is shown in Fig. 4. In the same figure, the resistances of the Si–ZrP/PTFE/GLY (Si/P =0.004) and the ZrP/PTFE/GLY composite membranes are compared. Both composite membranes were prepared having a GLY/ZrP mass ratio of 0.2. Both resistances obtained from the Nyquist plot, were used in Eq. 2 to calculate the proton conductivity. The results show that there is a decrease in the composite membrane resistance from 0.41 Ω to 0.37 Ω upon the addition of a small amount of silicic acid into phosphoric acid. The decrease in the composite membrane resistance led to an enhancement in proton conductivity. A conductivity of 0.056 S cm^{-1} value was obtained for the Si–ZrP/PTFE/GLY composite membrane, as opposed to a 0.045 S cm^{-1} for the ZrP/PTFE/GLY membranes, i.e., an enhancement of 24 % in proton conductivity.

The proton conductivity of the S–modified composite membrane (S–ZrP/PTFE/GLY) was also measured by EIS. The Nyquist plot in Fig. 5 compares the resistances of the ZrP/PTFE/GLY composite membrane and the S–ZrP/PTFE/GLY

composite membrane. Both membranes were prepared at a GLY/ZrP mass ratio of 0.4, and the composite membrane modified with sulphuric acid (H_2SO_4) had an S/P mass ratio of 0.004. It is evident that the addition of sulphuric acid caused an increase in the composite membrane resistance. The resistance increased from 1 Ω for the ZrP/PTFE/GLY membrane to 4.5 Ω for the S–ZrP/PTFE/GLY membrane. This increase in resistance resulted in a decrease in proton conductivity of one order of magnitude. The proton conductivity decreased from 0.02 S cm^{-1} to 0.0044 S cm^{-1} for the S–ZrP/PTFE/GLY membrane. The effect of sulphuric acid was also investigated at an S/P mass ratio of 0.54. The EIS measurements (not shown here) determined a resistance of 28 Ω, hence, a conductivity of 6.49×10^{-4} S cm^{-1},i.e. significant decrease in proton conductivity.

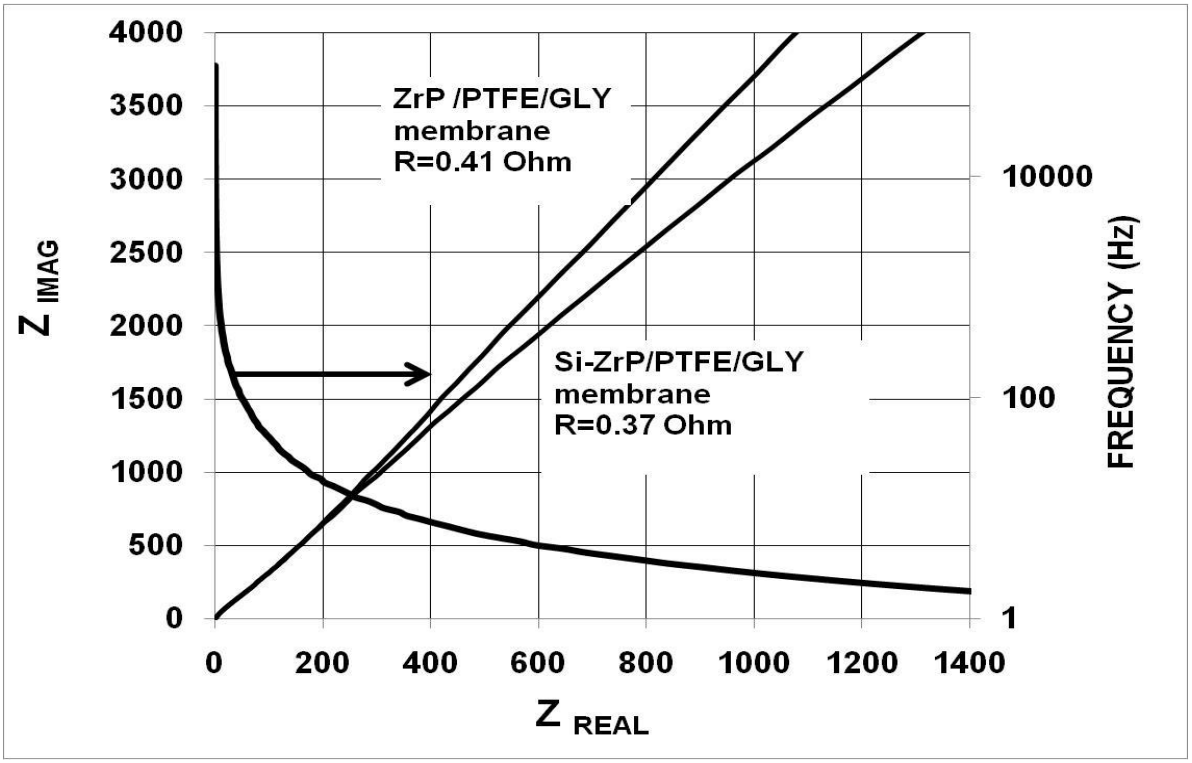

Fig . 4. Electrochemical impedance spectroscopy pattern for an unmodified ZrP/PTFE/GLY membrane and an Si–ZrP/PTFE/GLY composite membrane, both at a GLY/ZrP mass ratio of 0.2, and Si/P mass ratio of 0.004 in the phosphoric acid–silicic acid (solution).

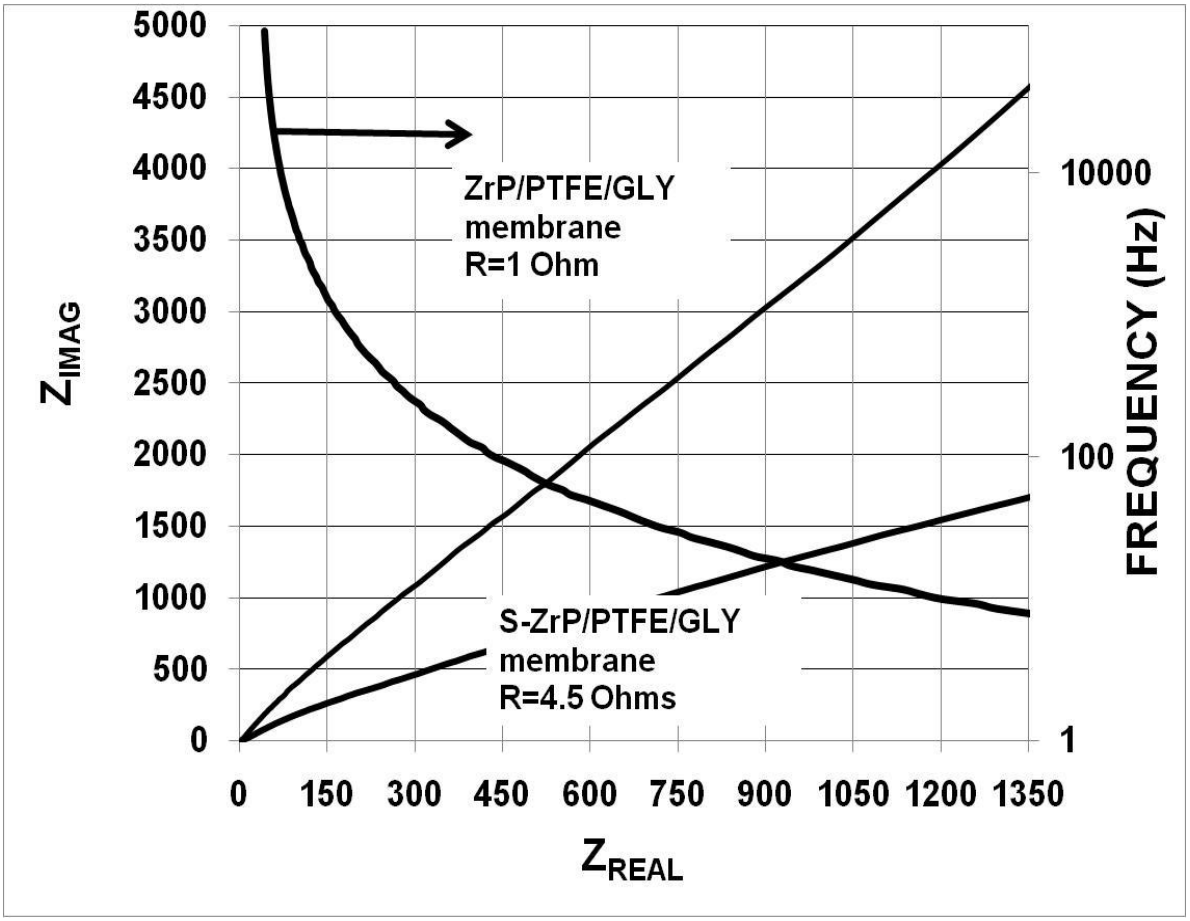

Fig . 5. Electrochemical impedance spectroscopy pattern for an unmodified ZrP/PTFE/GLY membrane and a S–ZrP/PTFE/GLY composite membrane, both at a GLY/ZrP mass ratio of 0.4, and S/P mass ratio of 0.004 in the phosphoric acid–silicic acid solution.

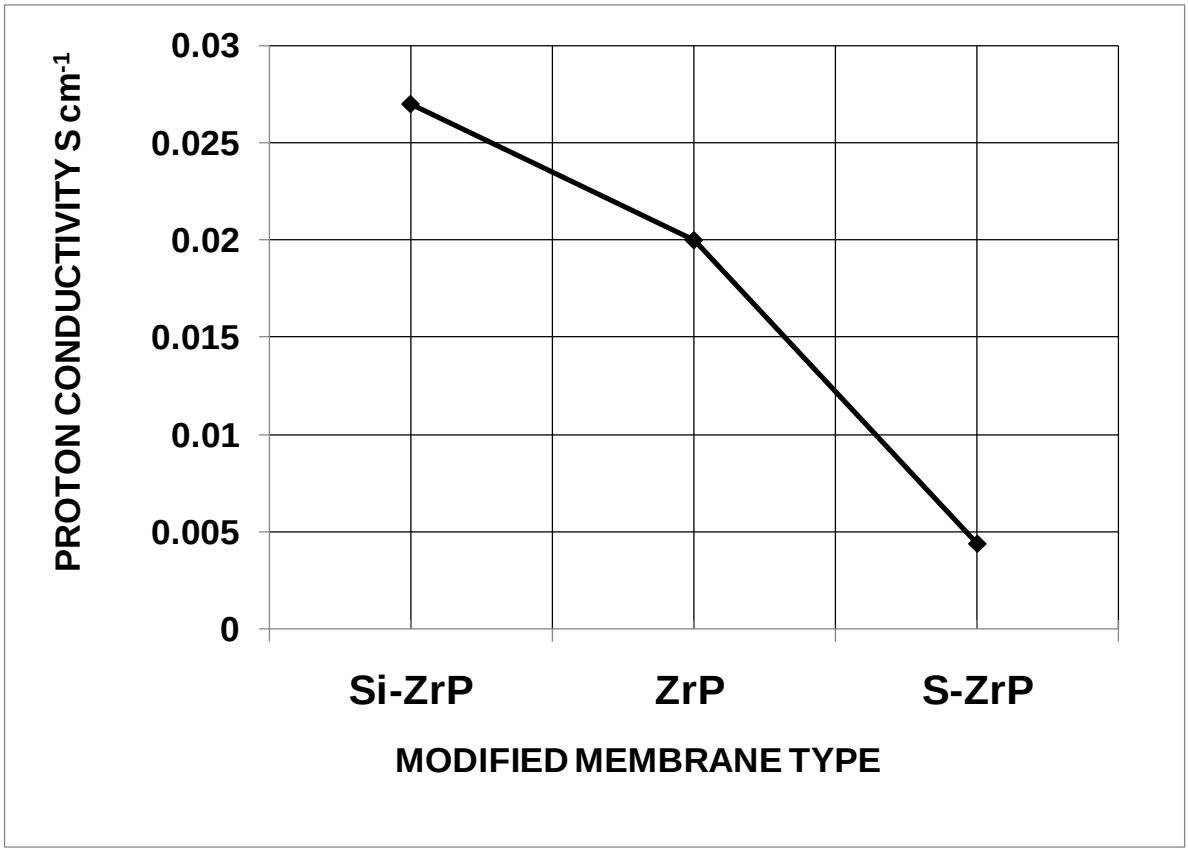

Fig . 6. A comparison between the three types of membranes, the ZrP/PTFE/GLY, the Si-ZrP/PTFE/GLY and the S-ZrP/PTFE/GLY in terms of proton conductivity. All were prepared at a GLY/ZrP mass ratio of 0.4 and Si/P, or S/P mass ratio of 0.004 in the acid solution.

A comparison of the proton conductivity for the three types of the composite membranes is shown in Fig.6. The GLY/ZrP mass ratio was 0.4 and the Si/P and, S/P mass ratios were 0.004, i.e. silicic acid was soluble at these conditions. The Si–ZrP/PTFE/GLY composite membrane showed the highest proton conductivity. The value of proton conductivity was improved from 0.02 S cm^{-1} (for the ZrP/PTFE/GLY membranes, at GLY/ZrP = 0.4) to 0.027 S cm^{-1} upon the modification with silicic acid. This increase in proton conductivity is anticipated to be due to the increase in the number of OH groups as previously discussed.

The effect of silicic acid addition at larger Si/P mass ratios was also investigated. As the Si/P ratio increased, the solubility limit of silicic acid in phosphoric acid was exceeded. At Si/P ratios larger than 0.004, a portion of silicic acid was soluble and some was still suspended in H_3PO_4. The results are shown in Fig. 7 and 8.

The new results for the Si–ZrP/PTFE/GLY composite membranes conductivity are shown in Fig.7 as a function of the GLY/ZrP mass ratios. The new results are compared with results that were previously published for the unmodified membranes [13]. The maximum proton conductivity was reported at a GLY/ZrP mass ratio of 0.2 for both sets of composite membranes. It can be seen that there was a noticeable enhancement in proton conductivity upon the addition of silicic acid at all GLY/ZrP mass ratios. For example, the ZrP/PTFE/GLY composite membrane of 0.2 GLY/ZrP ratio, possessed a proton conductivity of 0.045 S cm^{-1}, whereas the modified (Si-ZrP/PTFE/GLY) composite membrane (prepared at the same GLY/ZrP mass ratio 0.2) possessed a higher proton conductivity of 0.056 S cm^{-1}.

A sample of the Si–ZrP/PTFE/GLY composite membrane (soluble silicic acid, Si/P = 0.004, and GLY/ZrP = 0.2, open triangle symbol) was processed at 200 °C and an H_2O/Ar molar ratio of 6, and y_{H2O} = 0.86, (a wet test = the inlet conditions of a direct hydrocarbon fuel cell). EIS analysis for this sample showed a slight decrease in proton conductivity, from 0.056 S cm^{-1} to 0.046 S cm^{-1} (shown as the solid triangle),i.e., a decrease in conductivity of only 24%. In comparison, the conductivity of Nafion 117 membranes at 120 °C and relative humidity (RH) of 95% is 0.013 S cm^{-1} [18], and the conductivity of Nafion-silicate (NF-Si), and Nafion zirconium phosphates (NF-ZrP) at 130 °C and 28.8 % RH are 1.27 $\times 10^{-3}$ and 1.53 $\times 10^{-3}$ S cm^{-1} respectively [14]. After the 20% decrease in proton conductivity caused by the wet test, the proton conductivity for the Si–ZrP/PTFE/GLY composite membrane was still an order of magnitude larger than that of Nafion at comparable conditions.

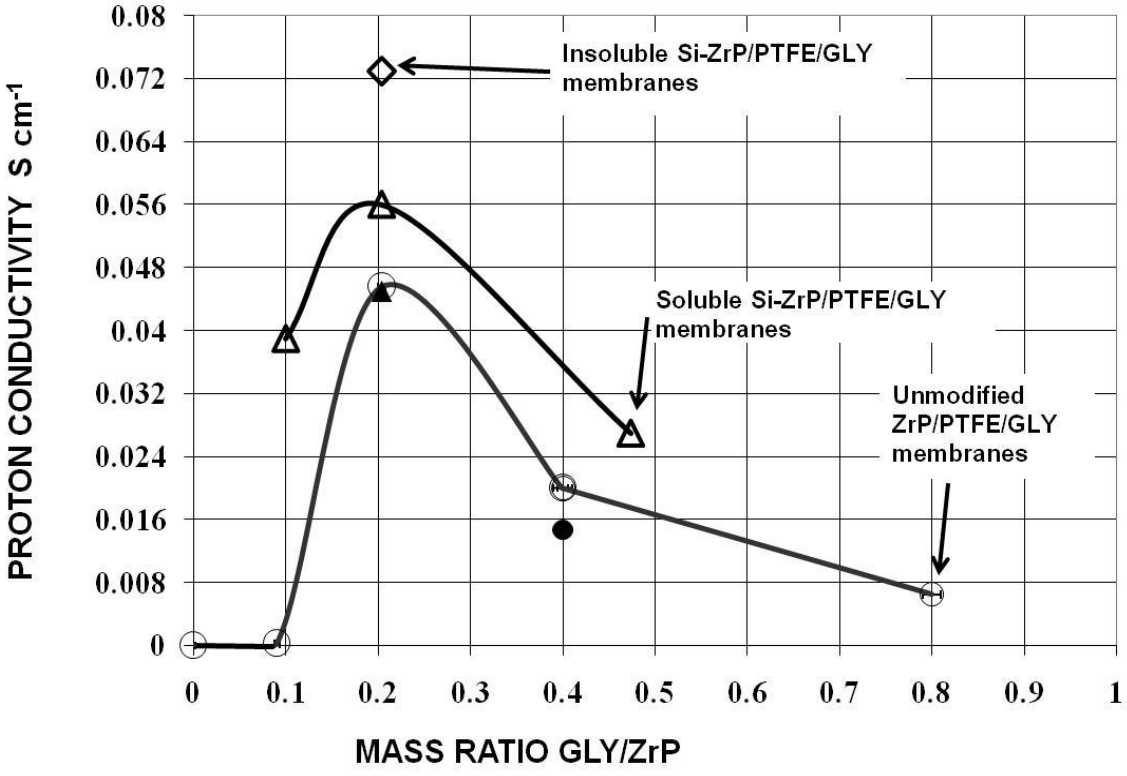

Fig . 7. Change of proton conductivity (σ) S cm^{-1} versus glycerol GLY) /ZrP mass ratio. Open circles present the unmodified ZrP/PTFE/GLY composite membranes. Triangles: represent the Si-ZrP/PTFE/GLY composite membranes, Si/P mass ratio = 0.004 (silicic acid was completely soluble). Solid symbols represent the 200 ºC wet test result of proton conductivity (σ) S cm^{-1}. Diamond symbol represents the Si-ZrP/PTFE/GLY composite membrane, Si/P mass ratio = 0.01 (some silicic acid was in the form of suspended particles).

The conductivities of the Si–ZrP/PTFE/GLY membranes were investigated as a function of their Si/P mass ratios. The results are shown in Fig. 8. The GLY/ZrP mass ratio was kept constant at 0.2, because the highest conductivity value obtained in Fig. 7 was obtained at this GLY/ZrP mass ratio. As the Si/P mass ratio increased, proton conductivity (σ) also increased. As previously stated, up to an Si/P mass ratio of 0.004, silicic acid was still in solution. The maximum proton conductivity 0.073 S cm^{-1} was obtained at an Si/P

mass ratio of 0.01. When some of the silicic acid was present as insoluble particles, at Si/P mass ratios in the range of ($0.004 < Si/P \leq 0.01$), additional proton hopping paths were provided by the surfaces of the hydrophilic $SiO_2.H_2O$ suspended particles. At Si/P mass ratios larger than 0.01, the conductivity decreased reaching a value of 0.051 S cm^{-1} at an Si/P mass ratio of 0.02. This decrease in conductivity can be explained by the morphology studies previously presented in Fig. 2 (d) and (e) for this membrane. Upon the addition of more silicic acid,(i.e. Si/P mass ratio = 0.02), poor coverage, more voids, and agglomeration of particles in some regions were obtained. Hence, it led to a decrease in proton conductivity.

The addition of silicic acid ($SiO_2.H_2O$) to phosphoric acid, i.e. at Si/P mass ratios larger than 0.004, resulted in both soluble $SiO_2.H_2O$ in H_3PO_4 and suspended particles of $SiO_2.H_2O$. The presence of $SiO_2.H_2O$ in solution improved water retention properties due to its hydrophilic nature. As previously discussed, by having $SiO_2.H_2O$ in solution, some of the "P" atoms in ZrP might have been replaced by some of the "Si" atoms. Hence, increasing the number of OH groups, and, providing more paths for the protons to hop. Therefore, the proton conductivity increased. The further enhancement in proton conductivity upon the addition of $SiO_2.H_2O$ in excess, (of Si/P mass ratios = 0.01) might have been caused by proton hopping in GLY, on the surface and in the bulk of Si-ZrP, and hopping on the surfaces of the hydrophilic insoluble silicic acid (Si `$O_2.H_2O$) particles.

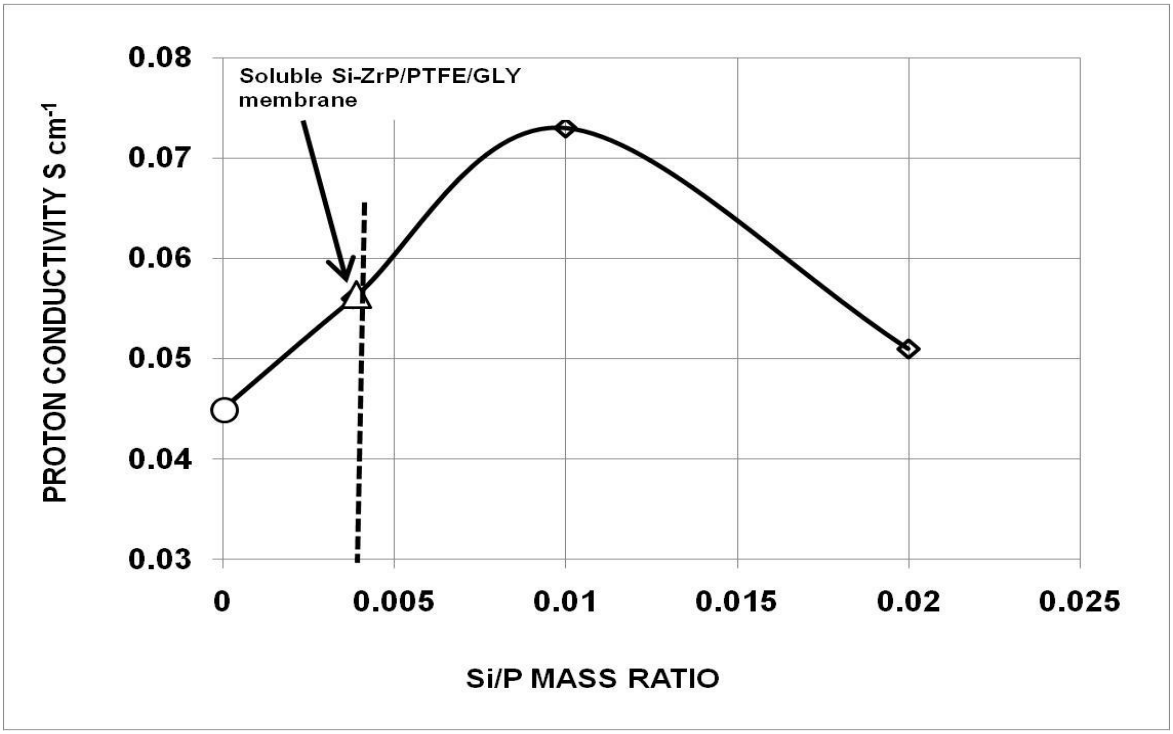

Fig . 8. Change of proton conductivity (σ) with the Si/P mass ratio for the Si-ZrP/PTFE/GLY membrane at constant GLY/ZrP mass ratio of 0.2. (Si/P mass ratios larger than 0.004 contained insoluble portion of silicic acid in H_3PO_4 as indicated by the dashed line).

5.3.3. FT-IR spectroscopy study

The FT-IR spectra obtained for the ZrP/PTFE/GLY, Si–ZrP /PTFE/GLY and S–ZrP/PTFE/GLY composite membranes are shown in Fig. 9. All composite membranes were prepared at a GLY/ZrP mass ratio of 0.4 and Si/P or S/P mass ratios of 0.004. The spectra of composite membranes revealed characteristic peaks (bands) and shoulders. The characteristic peaks for the phosphate group at 1150 and 1200 cm^{-1}, are attributed to the P-O asymmetric stretching in the PO_4 group [19]. The P-O asymmetric stretching peaks were sharp and observed in all samples spectra. The shoulder at 970 cm^{-1} for the ZrP/PTFE/GLY membrane sample is a characteristic of the P-OH stretching bond [19, 20]. The shoulder appeared at 1690 cm^{-1} in the unmodified ZrP/PTFE/GLY composite membrane is a

characteristic of bulk water [21]. In general, the FT–IR spectra suggest that no major changes observed on the basic chemical structure of the ZrP material when "S" or "Si" replaced a minor amount of "P" in the ZrP. One change is observed on the shoulder at 970 cm^{-1} in the unmodified ZrP/PTFE/GLY composite membranes. This shoulder becomes progressively less strong in the Si–ZrP/PTFE/GLY composite membrane and least evident in the S–ZrP/PTFE/GLY composite membrane. The appearance of the shoulder at 1030 cm^{-1} in the Si–ZrP /PTFE/GLY membrane sample might have resulted from a chemical interaction between the silicic acid ($SiO_2.H_2O$) and ZrP in the composite membrane, and explained as Le Van So reported [21] follows :

$$Si - OH + H \cdots O - P \longrightarrow Si - O - P + H_2O \qquad (3)$$

This interaction presented in Eq.(3), might have been taking place in our composite membranes that contained $SiO_2.H_2O$ and ZrP, ($Zr(HPO_4)_2$. Presumably, an Si–O–P bond might have been formed. Another possible explanation for the shoulder at 1030 cm^{-1} in the Si–ZrP /PTFE/GLY membrane, is that it could be due to the stretching vibrations of the Si–O–Si bond [21].

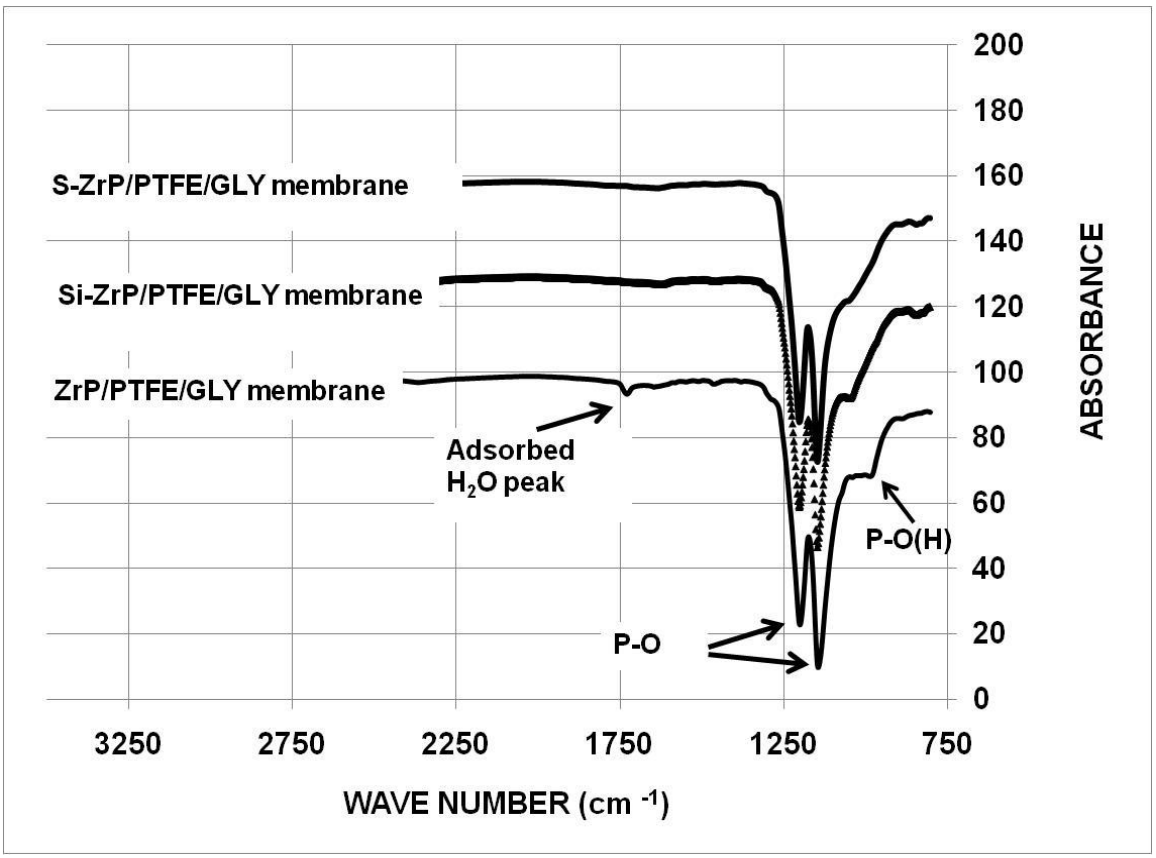

Fig . 9. FT-IR spectra of composite membranes, ZrP/PTFE/GLY, Si-ZrP/PTFE/GLY and S-ZrP/PTFE/GLY , all at GLY/ZrP mass ratio of 0.4, Si/P and S/P mass ratios of 0.004.

5.3.4. X-Ray diffraction (XRD) studies

The XRD patterns for different composite membranes are shown in Fig. 10, and 11. In Fig. 10, the composite membranes studied were the unmodified ZrP/PTFE/GLY and Si-ZrP/PTFE/GLY composites at variable GLY/ZrP and Si/P mass ratios as indicated on the graph. In the three samples, there is a highly intense peak appeared at 2θ ~ 18 °, in addition to two peaks appeared at 2θ ~ 31.5 °, and 2θ ~ 36.6 °. These peaks are all characteristics of PTFE [23]. However, the PTFE peaks that appeared at 2θ ~ 31.5 °, and 2θ ~ 36.6 ° in the Si–ZrP/PTFE/GLY membranes appear to be more intense than those appeared in the

unmodified membranes. One possible explanation for that is due to their morphology as previously seen in SEM analysis (Fig.2). More PTFE area was exposed in the Si–ZrP/PTFE/GLY membranes, hence, more intense peaks of PTFE were observed.

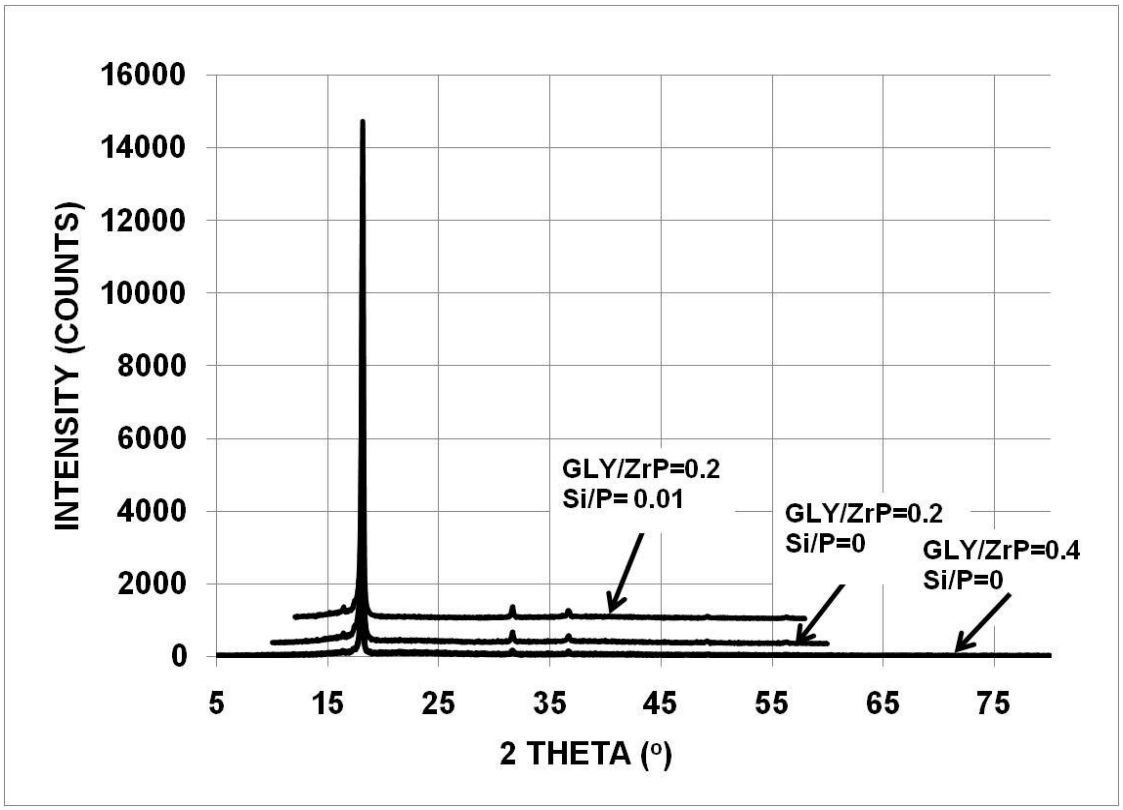

Fig . 10. XRD pattern for ZrP/PTFE/GLY and Si-ZrP/PTFE/GLY composite membranes at variable GLY/ZrP and Si/P mass ratios as labeled.

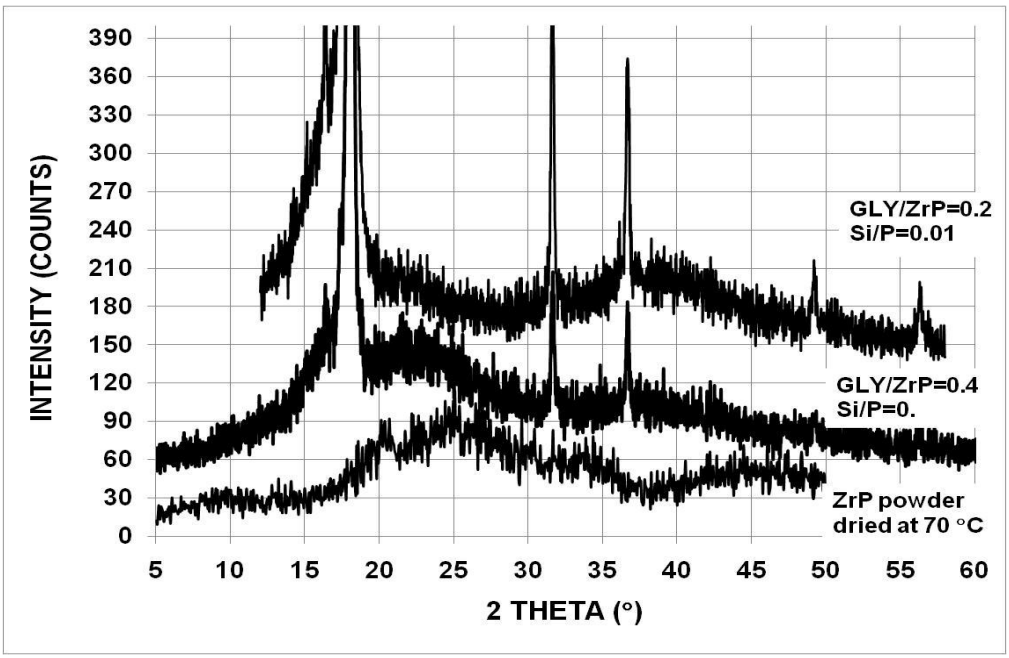

Fig . 11. XRD pattern for ZrP/PTFE/GLY and Si-ZrP/PTFE/GLY composite membranes at GLY/ZrP=0.2 and Si/P mass ratios as labeled, compared with the XRD pattern for a ZrP powder oven dried at 70 °C.

The XRD patterns of the unmodified ZrP/PTFE/GLY and Si-ZrP/PTFE/GLY composites were compared, in Fig. 11, with the pattern previously obtained for a ZrP powder, oven dried at 70 °C. With the exception of the PTFE peaks in the composites spectra that appeared at 2θ ~ 18 °, 31.5 °, and 2θ ~ 36.6 °, it can be seen that the materials have amorphous structure. There are two broad peaks in the ZrP powder spectrum at 2θ ~ 25 °and, 2θ ~ 45 ° that are consistent with the peaks in the crystalline ZrP [24]. It is evident that there is a shift in the broad peak appeared at 2θ ~ 25 ° in the ZrP powder XRD pattern, into a broad reflection at 2θ ~ 22 ° in the unmodified ZrP/PTFE/GLY and in the Si-modified composite membranes. It is not obvious in the Si-modified composite membrane but can be seen with careful examination of the XRD spectrum. There is a broad reflection at 2θ ~ 37 ° for both, the unmodified ZrP/PTFE/GLY and the Si– ZrP/PTFE/GLY composite

membranes. In general, the XRD spectra suggest that the amorphous ZrP material formed in the composite membranes possess some crystal structure.

5.4 Discussion of results

The morphology and the size of ZrP material changed as a result of the addition of silicic acid ($SiO_2.H_2O$) or sulphuric acid (H_2SO_4). In the absence of silicic acid or sulphuric acid, the ZrP particles were spheres with (250-500) nm in diameter. In contrast, plate-like particles of 1-5 μm were formed when "S" or "Si" was present as shown in SEM images.

Porosity is one of the important features of the membranes containing either sulphuric acid or silicic acid. The dense ZrP/PTFE/GLY membranes (Fig.1a) became porous membranes when either sulphuric acid (Fig. 1c) or silicic acid (Fig. 1b and Fig. 3c and d) was used during preparation. In some membrane samples (Fig. 2e), poor coverage of PTFE, by the modified ZrP material was observed. In a fuel cell, such porosity will permit the undesirable crossover of gases between the anode and the cathode. Composite membranes should be densely packed with particles to prevent gas crossover.

The XRD patterns confirmed the amorphous nature of the resultant composite membranes. The broad reflections at $2\theta \sim 22°$ and $2\theta \sim 37°$ for the unmodified ZrP/PTFE/GLY and the Si- ZrP/PTFE/GLY composite membrane suggest the presence of some crystal structure. The PTFE peaks ~ 31.5 °, and $2\theta \sim 36.6°$ in the Si– ZrP/PTFE/GLY membranes appeared to be more intense in the Si-modified membranes. This is consistent with the less coverage of PTFE by the Si-modified ZrP material.

Our hypothesis was that silicic acid would increase the number of OH groups in the ZrP structure and therefore, increase the conductivity. In contrast, sulphuric acid would decrease the number of OH groups, and therefore, decrease the conductivity. The conductivity observed in Fig. 6, supports our hypothesis. The conductivity increased with silicic acid addition, i.e., having more OH groups and decreased with sulphuric acid, i.e., fewer OH groups.

This work reported the conductivity enhancement upon the addition of silicic acid, $SiO_2.H_2O$. When silicic acid was in solution with phosphoric acid, at Si/P ratios of 0.004, it is possible that some of the "P" atoms in ZrP might have been replaced by some "Si" atoms. This increased the number of OH groups, therefore, provided more paths for the protons to hop. Proton conductivity enhancement might have been also caused by the possible formation of the Si-O-P bond, and the formation of water as seen in Eq.(3), thus, providing more water molecules and multiple paths for proton hopping.

When part of the silicic acid was in solution with phosphoric acid and, the other portion was in suspension, i.e., at Si/P mass ratio of 0.01, further enhancement in proton conductivity was observed. The proton conductivity increased reaching a maximum of (0.073 S cm^{-1}). $SiO_2.H_2O$ is a hydrophilic inorganic material. It is possible that the water content of silicic acid may have increased the number of water molecules in the composite membrane. Therefore, the enhancement in proton conductivity is explained by the increased proton hopping in all the preceding paths, in addition to the hopping on the surfaces of the hydrophilic, insoluble $SiO_2.H_2O$ particles.

The proton conductivity in the Si-ZrP/PTFE/GLY started to decrease at larger Si/P mass ratios (0.02). This is consistent with what have been previously studied and shown in literature. When an excessive addition of inorganic (e.g. SiO_2.) compounds occurred, it led to a decrease in proton conductivity [25]. This result is also consistent with our SEM observations for the Si–ZrP/PTFE/GLY membrane, at Si/P mass ratio of 0.02. The formation of a micron size ZrP particles in some regions, and the poor coverage of PTFE by the modified ZrP material in others, have decreased the total surface area of the ZrP, leading to a decrease in proton conductivity.

5. 5 Conclusions

Silicic acid ($SiO_2.H_2O$) was found to enhance the conductivity of ZrP/PTFE/GLY composite membranes when added to phosphoric acid prior to the in-situ precipitation reaction. Sulphuric acid was found to have a negative effect on the membranes proton conductivity, decreasing it by orders of magnitude. Both silicic acid and sulphuric acid had

an effect on the ZrP particles morphology. In the unmodified GLY/ZrP/PTFE composite membrane, the ZrP material was present as small spheres of (250-500 nm) [13]. When either silicic acid or sulphuric acid was used, the ZrP morphology was changed into a plate-like appearance of a larger size (1-5 μm).

When silicic acid ($SiO_2.H_2O$) was in solution with phosphoric acid, the enhancement in proton conductivity may have been caused by the increase in the number of OH groups and in the number of water molecules in the ZrP lattice. This may be explained by the increase in the number of possible proton hopping paths including, ZrP surface, the OH groups in glycerol, and the possible formation of the Si–O–P bond. When part of silicic acid was in solution with phosphoric acid and the other portion was in suspension (i.e. at Si/P mass ratio of 0.01), the enhancement in conductivity was attributed to the preceding reasons plus the proton hopping via the hydrophilic silicic acid particles.

The proton conductivity of the Si–ZrP/PTFE/GLY composite membranes (at Si/P mass ratio of 0.01) reached a maximum of 0.073 S cm^{-1} at 20°C, i.e., 73 % of the conductivity of a Nafion membrane. Increasing the Si/P mass ratio to 0.02, caused the proton conductivity to decrease. This was attributed to the poor coverage of PTFE, by the modified ZrP material hence, the reduction in the total ZrP surface area. When a sample of the Si-ZrP/PTFE/GLY composite membrane was processed at 200°C in the presence of a steam, under conditions typical of a direct propane fuel cell; the proton conductivity only decreased by 24 %.

Although the conductivity measurements reported here are very encouraging, because they approach that of Nafion's. Nevertheless, additional research will be required to develop techniques for preparing Si–ZrP/PTFE/GLY membranes that are dense enough to inhibit gas crossover.

5.6 Acknowledgments

The authors are grateful for the financial support from the Canadian federal government's Natural Sciences and Engineering Research Council and from the Ontario

provincial government's Ministry of Research and Innovation (Ontario Fuel Cell Research and Innovation Network).

5.7 References

1. B. Smitha, S. Sridhar, A.A. Khan, J. Membr. Sci., 259 , 2005, p.10.

2. Y. Chikashige, Y. Chikyu, K. Miyatake, M. Watanabe., Macromolecules, 38, 2005, p. 7121.

3. S. Kang, C. Zhang, G. Xiao', D. Yan , G. Sun., J. Membr. Sci., 334 , 2009, p. 91.

4. B. Kim, B. Jung, Macromol. Rapid Commun. , 25, 2004, p. 1263.

5. W. G. Grot, G. Rajendran, US Patent 5,919,583, 1999.

6. L. Chen, T. Yu, H. L Lin , S. H. Yeh, J. Membr. Sci., 307, 2008, p. 10.

7. F. Bauer1, M.W. Porada, Fuel Cells, 06, 2006, p. 261.

8. H. L. Tang, M. Pan, J. Phys. Chem. C, 112, 2008, p. 11556.

9. K. Li, G. Ye, J. Pan, H. Zhang , M. Pan, J. Membr. Sci.,347, 2010,p. 26.

10. F. Pereira, K. Vallé, P. Belleville, A. Morin, S. Lambert, C. Sanchez, Chem. Mater. 20, 2008, 1710.

11. C. C. Ke, X. J. Li, S. G. Qu, Z.G. Shao, B. L.Yi, Polym. Adv. Technol. , 2010, 1-7

12. C. Ferragina, R. D. Rocco, A. Fanizzi, P. Giannoccaro, L. Petrilli, J. Therm. Ana. Calorim. , 76, 2004, p. 871.

13. A. Al-Othman , A. Y. Tremblay, W. Pell, Y. Liu, B. A. Peppley , M. Ternan , J. Power Sources, 199, 2012, p. 14.

14. B. Gurau, E. Smotkin, J. Power Sources, 112, 2002, p. 339.

15. H.L. Lin, S.H. Yeh, T. L. Yu, L. C. Chen, J. Polym. Res 16, 2009, p. 519.

16. Y.J. Wang, Y. Pan, L. Chen, Mater. Chem. Phys. 92, 2005, p. 354.

17. Y. F. Lin, C. Y. Yen, C. C. M. Ma, S. H. Liao, C. H. Lee, Y. H. Hsiao, H. P. Lin, J. Power Sources, 171, 2007, p.388.

18. M. Casciola, G. Alberti, M. Sganappa, R. Narducci, J. Power Sources, 162, 2006, p. 141.

19. I.F. Amaral, P. L. Granja, M.A. Barbosa, J. Biomater. Sci. Polymer. Edn., 16, 2005, p.1575.

20. G. ILia, V.Parvulescu, A. Popa, S. Iliescu, J. Optoelectron. Adv. Mater, 10, 2008, p.3398.

21. L. V. So, J. J. Radioanal. Nucl. Chem., 98/2, 1986, p. 225.

22. S. J. Huang, H. K. Lee, and W.H. Kang Bull. Korean Chem. Soc., 26, 2005, p. 241.

23. V.M. Bouznik, S.D. Kirik, L.A. Solovyov, A.K. Tsvetnikov, Powder Diffr., 19, 2004, p.219.

24. A. Clearfield, J.A. Stynes, J. Inorg. Nucl. Chem. 26 , 1964, p. 117.

25. P. Bébin, M. Caravanier, H. Galiano, J. Membr. Sci. 278 , 2006, p. 35.

CHAPTER SIX-GENERAL DISCUSSION

Chapter 6 - General discussion

The high cost of polymer electrolyte membrane fuel cells (PEMFC) is one of the main obstacles that stand in the way of their commercialization. Most PEM fuel cells currently use hydrogen as a fuel. Hydrogen production, storage and transportation contribute to the high capital cost of PEMFC. Hydrocarbon fuels have several advantages over hydrogen because of their existing infrastructure and ease of storage. The use of hydrocarbon fuels is expected to have a large impact on reducing the cost of PEMFC if they are directly fed to the fuel cell. This will eliminate the fuel processor unit used to produce hydrogen that accounts for one third of the capital cost in a PEMFC system. For these reasons, there is a merit for using hydrocarbon technology instead of hydrogen in the current research project.

A high performance hydrocarbon (propane) fuel cell with platinum catalyst and phosphoric acid electrolyte was reported in 1964 by Grubb [1]. The cell operated in the temperature range of (150 –200) ºC. However, during the 1960's, it was difficult to predict the future of hydrocarbon fuel cells, but their theoretically higher efficiency, potentially lower initial cost have become motivations for future research [2].

The operation of a direct hydrocarbon PEMFC is illustrated using propane as an example. The anodic reaction taking place is:

$$C_3H_8+6H_2O = 3CO_2 + 20H^+ + 20e^{-1} \quad (1)$$

Oxygen or air enters at the cathode, and the following reaction takes place:

$$5\ O_2 + 20\ H^+ + 20\ e^{-1} = 10\ H_2O \quad (2)$$

And the overall reaction is: $C_3H_8 + 5\ O_2 = 3\ CO_2 + 4\ H_2O$ (3)

It is evident that water is a necessary reactant at the anode, and per one mole of propane electrochemically oxidized, six moles of water are consumed. Water reacts with propane at the anode to produce protons, carbon dioxide and 20 moles of electrons. Water

has been shown in this work to have a major effect on the hydration level of the proton conducting material, zirconium phosphate (ZrP).

The investigation of a high temperature membrane was performed on several stages. First, the degree of hydration of the electrolyte, zirconium phosphate, $Zr(HPO_4)_2.H_2O$ (ZrP) was studied and evaluated. ZrP was synthesized in its powder form, and investigated for its proton conducting properties at different temperatures, up to a maximum temperature of 200 ^oC. The synthesized ZrP powder characteristic were further studied and investigated using other techniques such as X-Ray diffraction (XRD) and thermogravimetric analysis (TGA). These techniques were used to evaluate the ZrP material structure and the water retention properties.

Second, a composite membrane was developed out of this powder because the ZrP material is brittle and lacks the mechanical integrity required in a PEMFC membrane. Porous polytetraflouroethylene (PTFE) was used as a support material for the ZrP electrolyte. More effort was then directed to improve the proton conductivity of the ZrP/PTFE composite membrane. The effect of the incorporation of glycerol (GLY) into the ZrP/PTFE membrane was investigated. A considerable enhancement of ZrP/PTFE proton conductivity was observed upon the addition of small amounts of GLY. As a result, a composite membrane composed of ZrP/PTFE/GLY was synthesized.

Third, the effect of the incorporation of a minor component "Si" or "S", i.e. via silicic acid ($SiO_2.H_2O$) and sulphuric acid (H_2SO_4) respectively, on the ZrP/PTFE/GLY composite membrane was studied. The synthesized modified membranes were evaluated for their morphology, structure and proton conducting properties. A considerable enhancement of proton conductivity was observed upon the addition of silicic acid.

6.1 Investigation of $Zr(HPO_4)_2.H_2O$ (ZrP)

Zirconium phosphate $Zr(HPO_4)_2.H_2O$ (ZrP) powder was investigated as a possible proton conducting material for direct hydrocarbon PEMFC. ZrP was synthesized by the precipitation reaction of $ZrOCl_2$ with aqueous H_3PO_4 solutions described in Eq. (1), at room temperature:

$$ZrOCl_2 \cdot 8H_2O + 2\ H_3PO_4 \rightarrow Zr(HPO_4)_2 \cdot H_2O + 2\ HCl + 8\ H_2O \quad (4)$$

At these conditions, amorphous ZrP powder was formed based on what was stated in literature [3] and based on our earlier work [4]. ZrP powder was dried at different temperatures and conditions. Some samples were oven dried while others were oven dried first then processed at the inlet conditions of a hydrocarbon (propane) fuel cell, i.e. temperature of 200 °C and an H_2O/N_2 molar ratio of 6.

Various analysis techniques were used to study and evaluate the properties of the prepared ZrP powder. The samples were studied using X-ray diffraction (XRD), thermogravemtric analysis (TGA), and electrochemical impedance spectroscopy (EIS). The proton conductivity of the various ZrP samples was evaluated using the four probe EIS technique.

This work reported that the proton conductivity of the synthesized ZrP materials processed at 200 °C, (with continuous H_2O injection at an H_2O/N_2 molar ratio of 6, in conditions similar to a direct hydrocarbon PEMFC), was one order of magnitude higher than the ZrP sample that was first oven dried at 70 °C.

In the same work, it was shown that it was possible to maintain a sufficient hydration level in the ZrP at 200 °C by having an appropriate water content in the vapour phase at the processing conditions, hence, increasing the proton conductivity. In our direct hydrocarbon fuel cell, it is possible to maintain these hydration conditions where water is being a stoichiometric reactant.

6.2 Synthesis of ZrP/PTFE/GLY composite membranes

This work has also investigated the synthesis of composite membranes composed of zirconium phosphate (ZrP) and porous polytetrafluoethylene PTFE as a mechanical support for ZrP. Therefore, zirconium phosphate $Zr(HPO_4)_2$, a proton conductor, was precipitated in situ within a porous PTFE membrane according to Eq.(1). PTFE membranes are characterized with their highly hydrophobic nature, hence, aqueous solutions of the chemical reagents were not used; instead, $ZrOCl_2$ alcoholic suspension was prepared. Ethanol and

isopropanol had a lower surface tension than water and they appeared to wet the PTFE surface quite well when first investigated in the laboratory.

The amount of ZrP needed to fill the voids of PTFE was calculated based on the void volume available in the sample sheet. Then, the corresponding amount of $ZrOCl_2$ (derived from the chemical reaction described in Eq.(1)) was added to the alcohol mixture. The $ZrOCl_2$ alcoholic suspension was then introduced to the pores of PTFE, followed by precipitation with phosphoric acid to form ZrP in the pores.

The result was an enhancement of proton conductivity from 10^{-3} S cm^{-1} as previously reported in literature for ZrP/PTFE composites [5] to 0.045 S cm^{-1}. This was accomplished by the incorporation of glycerol (GLY) into the $ZrOCl_2$ alcoholic suspension and ultimately, into the pores of PTFE. The results reported in this study showed that adding small amounts of GLY to an alcoholic suspension of $ZrOCl_2 \cdot 8H_2O$ produced a composite membrane with a conductivity of 0.02 – 0.045 S cm^{-1}.

Morphology studies using SEM on this membrane, including top view and cross sectional view studies showed ZrP spheres in the size range of (100 – 500 nm) in the composite membrane that were smaller than the PTFE pore diameters (1000 – 2000 nm). Proton conductivity studies on the other hand, showed an enhanced proton conductivity as well as a conductivity value that remained unchanged when the membrane was processed at the inlet conditions to a direct propane fuel cell (200°C and steam mole fraction y_{H2O} = 0.86).

In literature, a detailed description for the mechanism of proton conductivity in solids was provided [6]. In this thesis, we have also provided a description for the enhanced conductivity in ZrP/PTFE/GLY composite membranes. Furthermore, the effect of adding glycerol (GLY) on morphology and conductivity was examined.

It is possible that the enhancement observed in proton conductivity in our composite membranes may have been caused by, 1) proton transport at the interface between the small solid ZrP spheres and their glycerol coating, 2) proton transport though ZrP and proton transport thorough glycerol and, 3) presumably two surface phenomena, a combination of

proton transport on solid ZrP surfaces and proton hopping via the OH groups in glycerol. Furthermore, the successive wetting and drying cycles inside the confined hydrophobic pores of PTFE, have favored the formation of small aggregates of $ZrOCl_2$. These aggregates have been prevented from agglomeration due to the presence of glycerol that has a high surface tension. Thus, very small, relatively spherical ZrP particles were formed. These particles led to a high total surface area and hence, a highly conducting membrane.

6.3 Substitution of a minority component for phosphorus

In this work, novel composite membranes composed of modified S or Si–zirconium phosphate (ZrP), porous polytetrafluoethylene (PTFE) and, glycerol (GLY) were also synthesized. It was aimed at the substitution/modification of a minor component (S or Si) for phosphorus in the ZrP chemical structure. Thus, the modification was performed by introducing a certain amount of silicic acid or sulphuric acid into phosphoric acid. It was then aimed at studying the effect of having variable Si/P or S/P mass ratios in the acid solution/suspension.

The modification of ZrP/PTFE/GLY membranes was performed by introducing the $ZrOCl_2$ and GLY materials first into the PTFE pores, and then proceeding with the chemical reaction described in Eq. (1). At this phase, and prior to reaction, phosphoric acid was mixed with a specified amount of silicic acid or sulphuric acid. The amounts of both acids were varied in such a way that would result in a variable S/P or Si/P mass ratios in the silicic acid–phosphoric acid, or sulphuric acid–phosphoric acid. Sulphuric acid was always in solution with phosphoric acid, which was not the case with silicic acid. Silicic acid is a powder and had a limited solubility in phosphoric acid. Therefore, by having a variable Si/P mass ratios, silicic acid was in solution in some experiments. When the solubility limit was exceeded in other experiments, part of silicic acid appeared to be in suspension. Both of these situations effects on proton conductivity and morphology were indentified and studied.

Investigation of these modified ZrP/PTFE/GLY membranes showed that the Si–modified membranes had enhanced proton conductivity whereas the S–modified membranes showed a decreased conductivity value. Furthermore, a proton conductivity of 0.073 S cm^{-1} was obtained for the Si–ZrP /PTFE/GLY membrane that approached the conductivity of

Nafion (0.1 S cm^{-1}) at an Si/P mass ratio of 0.01. At higher mass ratios, i.e. Si/P mass ratio of 0.02, the conductivity declined.

Morphology studies using SEM on these composite membranes showed that the Si-ZrP/PTFE/GLY membrane with an Si/P = 0.01 in the phosphoric acid – silicic acid suspension had a different morphology of ZrP than observed in the unmodified composites. When all silicic acid was still in solution with phosphoric acid, plate-like ZrP particles of nearly 1 um in size were appeared. Adding more silicic acid resulted in a portion of it in solution, while the other portion appeared in suspension, thus, at Si/P mass ratios of 0.01, larger size ZrP material appeared, having the flaky shape with an average size of 2 μm. At Si/P mass ratios of 0.02 in the phosphoric acid – silicic acid suspension the plate like material continued to appear and poorer coverage on top of the composite membrane was observed. More strands of the polymers appeared to be entirely uncovered with ZrP at some regions whereas the particles appear to agglomerate in others. The poor coverage observed at higher Si/P ratios could be explained by a phase separation phenomenon.

The enhancement of proton conductivity in the modified Si-ZrP/PTFE/GLY composite membrane at Si/P mass ratios of 0.01 was explained in this thesis by, 1) the improvement in water retention properties of the composite membrane upon the introduction of silicic acid (hydrophilic), and 2) the possible formation of the Si–O–P bond that provided an extra path for proton hopping.

This work addressed the change of proton conductivity upon the addition of excessive amounts of silicic acid. It showed that there is a decrease in proton conductivity when the Si/P mass ratio was 0.02. This may be attributed to, 1) the formation of excessive amounts of water, hence, interruption of proton transport inside the membrane and, 2) the phase separation and the poor coverage of the proton conducting material in the resultant Si-composite membrane. As a result, this work showed that the composite membrane should have an appropriate silicic acid content, above which, the membrane conductivity starts to decrease.

6.4. References

1. W.T. Grubb, C.J. Michalski, J. Electrochem. Soc., 111(1964), p. 1015.

2. E.J. Cairns, Advances in Electrochemistry and Electrochemical Engineering, Vol. 8, C. W. Tobias, ed., Wiley-Interscience, New York, NY, 1971, p. 337.

3. Camino Trobajo, Sergei A. Khainakov, Ara´nzazu Espina, and Jose´ R. Garcı´a, On the Synthesis of r-Zirconium Phosphate, Chem. Mater., 12 (2000) , p. 1787.

4. A. Al-Othman, A.Y. Tremblay, W. Pell, S. Latief, T. J. Burchell, B. Pebbly, M. Ternan, J. Power Sources, 195 (2010), p. 2520.

5. Y. Park, K. Jae-Dong and M. Nagai. J. Mater. Sci. Lett., **19** (2000), p. 1735.

6. K. D. Kreuer, J. Mol. struct., 177 (1988), p. 265.

CHAPTER SEVEN-CONCLUSIONS

CONCLUSIONS

This section is devoted to address the conclusions drawn throughout this research project.

The decrease in zirconium phosphate proton conductivity that has been attributed to a loss in water content is consistent with our measurements of conductivity and water content analysis that were reported in this thesis. It was also shown that the vapour phase water content adjustment during processing at elevated temperatures 200 ºC enhanced the water content of the zirconium phosphate material. This hydration was accomplished by the gas phase in contact with the zirconium phosphate membrane that contained an H_2O/N_2 molar ratio of 6, which is similar to the stoichiometric feed ratio in a direct propane fuel cell. Furthermore, it has been shown that the conductivity of this ZrP material processed at 200 °C possessed an enhanced water content and proton conductivity. The proton conductivity reported from the elevated temperature test was one order of magnitude higher than that for the ZrP material dried at 70 °C in a relatively dry atmosphere. Thus, this thesis showed that it is possible to operate direct hydrocarbon fuel cells at elevated temperatures, without encountering degradation in the proton conductivity of the membrane and thereby take advantage of more rapid kinetics and greater current densities.

Glycerol (GLY) was found to enhance the proton conductivity when incorporated into a porous PTFE film. It was also found to enhance the proton conductivity when added to the ZrP/PTFE composite membrane. The inclusion of GLY in the ZrP/PTFE/GLY membrane made some changes on the composite membranes. First, it changed the morphology of the ZrP. Second; it enhanced the proton conductivity by orders of magnitude from being in the order of 10^{-5} S cm^{-1} to 0.045 S cm^{-1}. GLY addition resulted in the formation of nano-scale spherical ZrP particles, hence, increased the total surface area on the exterior of the small ZrP spheres, leading to an enhanced proton conductivity approaching that of Nafion. In this thesis, the technique of using glycerol (GLY) that has a high surface tension was combined with the successive wetting and drying cycles inside the hydrophobic pores of PTFE. This may have favored the formation of small, separate, particles of $ZrOCl_2$, thus, the formation of well defined, spherical nano-scale ZrP particles within the

confined environment existing in the PTFE pores. The improvement of proton conductivity may have been caused by a combination of proton transport on the increased surface area on the exterior of the small ZrP spheres plus proton hopping using both the OH groups in glycerol and the ZrP bulk. In this work, it was shown that the proton conductivity remained unchanged for a sample of this composite membrane processed at 200°C in the presence of a steam partial pressure typical of a direct propane fuel cell. This conductivity was orders of magnitude higher than that of Nafion at 130 °C. The results of this work offered a promising alternative for Nafion electrolyte, for fuel cell operations above the boiling point of water.

The effect of adding silicic acid ($SiO_2.H_2O$) was studied and it was found to enhance the proton conductivity of ZrP/PTFE/GLY composite membranes when added to phosphoric acid prior to reaction. Sulphuric acid, was found to have a negative effect on the membranes proton conductivity, decreasing it by orders of magnitude. The proton conductivity of Si–ZrP/PTFE/GLY composite membranes was 0.073 S cm^{-1}, i.e., 73 % of the conductivity of a Nafion membrane. The improvement of proton conductivity was explained by the increase in the number of OH groups, the increase in the number of water molecules and the possible formation of the Si-O-P bond that provided more paths for proton hopping. The proton conductivity however, decreased with excessive addition of silicic acid. This work reported the poor and the non-uniformly distribution of ZrP obtained when excessive amounts of silicic acid were introduced to the membrane and attributed the decrease in conductivity accordingly.

CHAPTER EIGHT- CONTRIBUTIONS TO ORIGINAL KNOWLEDGE AND RECOMMENDATIONS

CONTRIBUTIONS TO ORIGINAL KNOWLEDGE

The following is a list of the major contributions to original knowledge, resulted from this thesis.

1. Nafion–free, inorganic–organic composite membrane, with enhanced proton conductivity composed of zirconium phosphate, ZrP, (a solid proton conductor), porous polytetrafluoethylene (PTFE) and, glycerol (GLY) was successfully developed as a possible electrolyte for direct hydrocarbon fuel cells that might operate at temperatures approaching 200°C. To our knowledge, this is the first report of such membranes in the literature.

2. The presence of a water rich vapour phase was shown to produce a zirconium phosphate solid that was hydrated to a greater extent than the zirconium phosphate solids prepared in laboratory air. These conditions exist in a direct hydrocarbon fuel cell where water is present as a reactant, thus, providing water rich vapour phase.

3. Maintaining appropriate water content in the vapour phase at the processing conditions was shown to be successful in keeping the zirconium phosphate in a sufficiently hydrated state, so that the conductivity values could be improved by one order of magnitude.

4. The effect of glycerol (GLY) on the enhancement of proton conductivity in the prepared composite membranes was presented for the first time. Order of magnitude enhanced proton conductivity for the ZrP/PTFE/GLY composite membrane, was reported in this thesis. This value approached that of Nafion.

5. The effect of glycerol (GLY) addition on the improvement of PTFE conductivity, i.e, from being a non proton conducting material, to a material that possessed proton conductive properties, was reported in this thesis, and for the first time in the literature.

6. A technique was developed in this thesis, for the formation of nano–scale ZrP particles upon the addition of glycerol (GLY), combined with successive wetting and drying inside a confined hydrophobic environment (the pores of PTFE).

7. The enhanced proton conductivity caused by glycerol (GLY) in the ZrP/PTFE/GLY composite membranes was explained in this work by proton hopping via the OH groups in glycerol (GLY), in addition to two known phenomena: proton transport on the exterior surfaces of the ZrP solid spheres, proton hopping through the bulk of the ZrP.

8. The spherical shape of the ZrP particles obtained in the ZrP/PTFE/GLY composite membrane was explained in this thesis, based on the presence of glycerol (GLY). Isopropanol was used during preparation because (unlike water) it wets the PTFE porous membrane. GLY remained dissolved in isopropanol until it evaporated from the membrane leaving GLY in the PTFE pores with the hydrophilic zirconium oxychloride particles. At that point, micelles may have formed, with the hydrophobic portion directed toward the PTFE and the hydrophilic portion directed toward the zirconium oxychloride. Such an orientation may have favored the formation of the ZrP spherical particles.

9. The value of proton conductivity for the ZrP/PTFE/GLY composite membrane was shown to be maintained when the temperature was increased from 20 °C to 200°C provided the steam to feedstock ratio that was typical of that required for a direct propane fuel cell.

10. A method of modifying the composite membranes was described, by having additives such as silicic acid and sulphuric acid incorporated in the prepared ZrP/PTFE/GLY composite membrane.

11. An enhancement in proton conductivity was reported in this thesis by modifying the ZrP/PTFE/GLY composite membranes with silicic acid. The effect of silicic acid on the produced ZrP material morphology and surface coverage of the composite membrane was studied, evaluated and reported for the first time.

12. The enhanced proton conductivity reported in the Si–modified ZrP/PTFE/GLY composite membranes was explained in this thesis by a combination of proton hopping in glycerol (GLY), at the Si-ZrP surface, the Si-ZrP bulk, and at the surfaces of the hydrophilic silicic acid particles.

13. The value of proton conductivity for the Si–modified ZrP/PTFE/GLY composite membrane was shown to be maintained when the temperature was increased to 200°C provided the steam to feedstock ratio that was typical of that required for a direct propane fuel cell.

RECOMMENDATIONS FOR FUTURE WORK

This thesis presented a rigorous study for the high temperature ZrP/PTFE/GLY composite membrane synthesis. In this section, a few recommendations for future research on this type of composite membranes are presented.

1. This thesis investigated modified, Si–ZrP/PTFE/GLY composite membranes. However, this modification needs to be further addressed.

   This can be accomplished by the addition of silicic acid using a different technique, i.e. by adding specified amounts of silicic acid to the reaction mixture (the alcoholic $ZrOCl_2$ suspension) instead of adding it to phosphoric acid. In this case, new experiments can be performed to study the effect of introducing silicic acid into the pores of PTFE with GLY and $ZrOCl_2$ first, followed by reaction with phosphoric acid.

2. This thesis reported the effect of silicic acid addition on the enhancement of the composite membranes proton conductivity and morphology. The issues of having uniform and complete coverage of the proton conducting material need to be further investigated.

   Experiments can be performed using the successive wetting/drying technique used in this thesis to prepare the Si modified composite membranes. However, there is a certain void volume available in the PTFE sheet. Sufficient $ZrOCl_2$ was added in this work so that the produced amount of ZrP is enough to completely fill the pores of PTFE. Hence, future experiments can be performed to study the effect of having various (ZrP, GLY), to silicic acid mass ratios within the composite membrane. These mass ratios can be varied in such a way that the total amount of the three components is filling the pores available in the PTFE. These variations of components mass ratios are anticipated to have an effect on the membranes proton conductivity and morphology.

3. The composite membrane developed in this work should be tested and evaluated for its performance in a direct hydrocarbon fuel cell, by preparing a membrane electrode assembly (MEA) and obtaining a fuel cell polarization curve.

APPENDIX A

A1- DIRECT HYDROCARBON PROCESS FLOW SHEET AND FUEL CELL

A2- FUEL CELL'S GROOVE DEPTH CALCULATIONS

A3- FUEL CELL COMMISIONING AND START UP PROCEDURE

A-1 Direct hydrocarbon oxidation process flow sheet, fuel cell and, fuel cell test station.

The direct oxidation of hydrocarbon process flow sheet is shown in Fig. 1. It was designed and developed as part of the current research project. Propane is fed to the anode of the fuel cell. De-ionized water is also fed to the anode, via a peristaltic pump, out of a burette to provide the necessary water for the anode reaction.

The following reactions are taking place:

Anodic reaction: $C_3H_8 + 6\ H_2O = 3CO_2 + 20\ H^+ + 20\ e^{-1}$ (1)

Cathodic reaction: $5\ O_2 + 20\ H^+ + 20\ e^{-1} = 10\ H_2O$ (2)

And the overall reaction is: $C_3H_8 + 5\ O_2 = 3CO_2 + 4\ H_2O$ (3)

The exit steam at the anode is condensed in a flask to calculate the amount consumed inside of the fuel cell. Air is fed to the cathodic compartment. The flow rates of the inlet gaseous streams are measured with electronic flow meters.

The fuel cell is heated to a maximum of 200 °C via two heating elements purchased from Omega and mounted inside the graphite blocks. The temperature is controlled by two temperature controllers. The anodic and cathodic products (carbon dioxide, unreacted and partially reacted propane, steam and excess air) are measured by bubble flow meters. Differential pressure transducers are used between the exit carbon dioxide (CO_2), inlet de-ionized water and the inlet propane to monitor the pressure difference in such a way that a small differential pressure between streams is maintained. The fuel cell is connected to a potentiostat, and voltmeter to measure the potential difference and the current across the cell. The cell potential and other parameters, including reactants flow rates and temperatures are all monitored by LABVIEW.

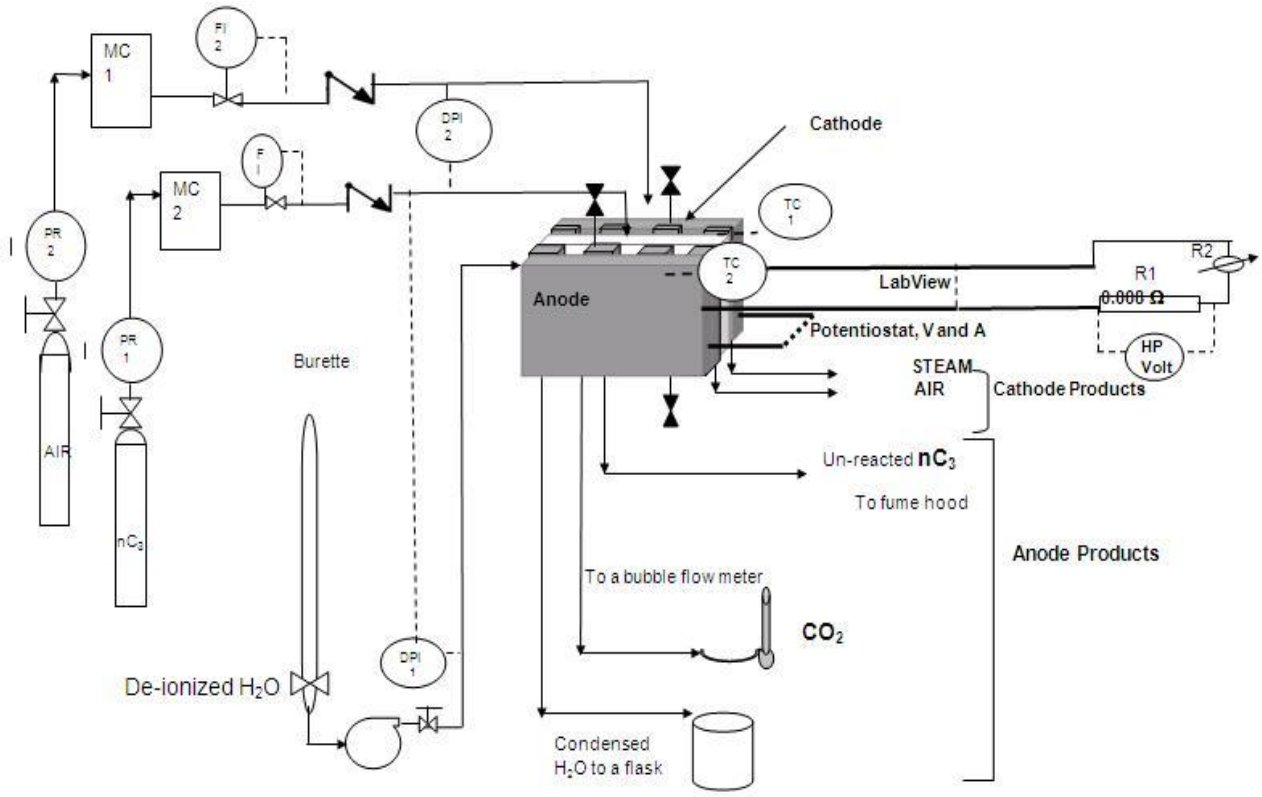

Fig. 1: Process flow sheet of direct propane electro-oxidation.

The fuel cell consists of two graphite blocks, in which a flow field is engraved. The fuel cell was custom made in our machine shop with a total machined geometrical cell area of 5 cm^2. The cell is also held together by two stainless steel plates that are gold-plated and a set of bolts. These two plates can be bolted together once the membrane electrode assembly is placed inside and further tightened by a torque wrench. The fuel cell is sealed by a Viton O-ring purchased from McMaster-Carr. The groove depth and dimensions were calculated then the groove was machined in the graphite plate accordingly. Fig. 2 shows a top view for a single graphite plate showing the locations of the flow field and the o-ring.

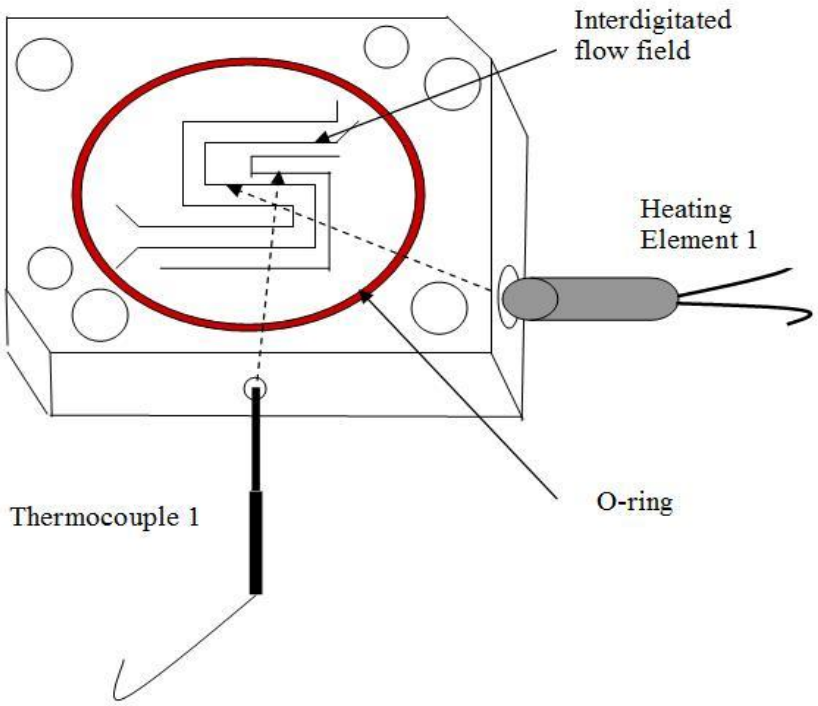

Fig.2: Top view of a single graphite plate.

A2- FUEL CELL'S GROOVE DEPTH CALCULATIONS

A-2 Groove depth calculations

The range of membrane thicknesses is from 0.17 - 0.34 mm. If we define the deformation (D) as: $D=1.78-H_o/1.78$ where H_o is the height of the O-ring.

Total Area of the O-ring = $(1.78/2)^2*\prod=2.488$ mm^2

This area is constant, and it equals to the area of the groove= 1.78*groove depth (y) = 2.488 mm^2. So, y =1.398 mm.

If the O-ring is to be completely pushed inside the groove, then, the deformation will be equal to = $1.78-H_o/1.78 = 1.78-1.39/1.78 =0.22$, where Ho is the height of the O-ring that is completely inside the groove.

Case A) The minimum value of the membrane thickness is 0.17 mm.

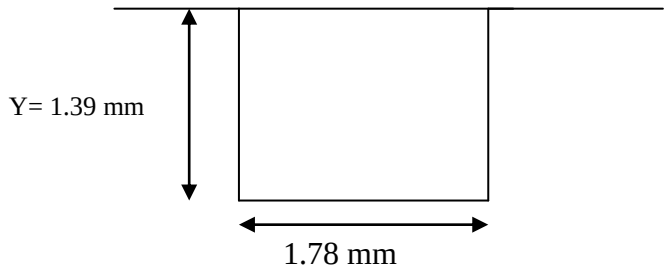

Figure 1: Case A.

If at a groove height of 1.39 mm, The O-ring surface will completely touch the upper plate surface and no space would be available for any membrane as shown in Figure 1, above. At a membrane thickness of 0.17 mm, the groove height has to be decreased maintaining the same deformation for the o-ring. The groove height would be: 1.39-0.17 = 1.22 mm, as shown in the Figure below. With a deformation that corresponds to 0.22 as calculated above.

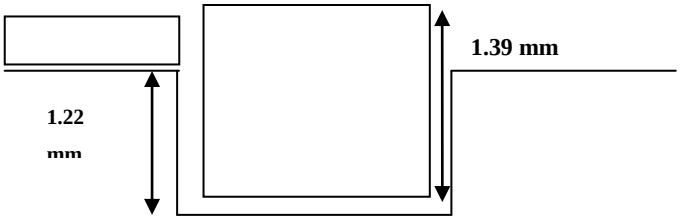

Case B) the maximum thickness of the membrane is 0.34 mm. At a groove height of 1.22, at the maximum value of 0.34 mm, then 1.22 +0.34 mm = 1.56 mm (this is the new height of the O-ring, i.e., less deformed to cover the increase in the membrane thickness while maintain the same groove height)

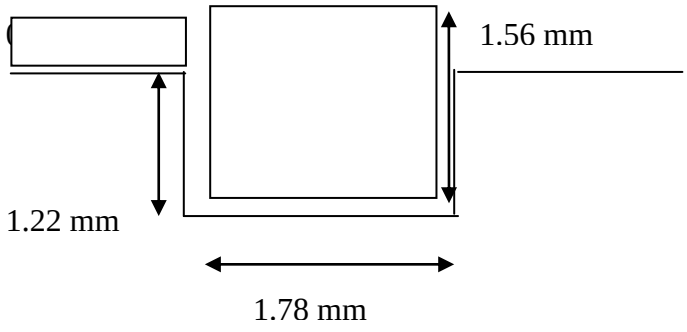

This corresponds to a deformation of: 1.78-1.56/1.78 = 0.1236

A value of 0.1 or even 0.04 is enough to make the seal. So, at a deformation of 0.1, the O-ring height would equal to:

D=1.78-H_o/1.78 = 0.1, so Ho= 1.602 mm, and at a groove height of 1.22, then the allowed membrane thickness that can fit in that space equals to : 1.602-1.22 = 0.382 mm.

In the same manner, and at a deformation of 0.04, then Ho = 1.708 mm, and the maximum membrane thickness that can be fit in there = 1.708-1.22 = 0.488 mm

Conclusion: a groove depth of 1.22 mm and 1.78 mm in width is willing to cover a membrane thickness from 0.17 – 0.488 mm, for the given O-ring dimensions, (1.78 mm width).

A3- FUEL CELL TEST STATION COMMISIONING AND START UP PROCEDURE

A-3: DHFC test station–start up procedure

Fig.1: Fuel cell test station located in D219.

A) LabView

1. **Self Calibration:** Click on **Measure and Automation** icon on the desktop, then **Configure**, **devices and interface**. Right click on: **NI-PCI-6010** and choose: **Self test then self calibrate.**

2. Open Labview main screen (there is a shortcut on the desktop).

3. Ensure that both sides of DPI's are at atmospheric pressure , this is done by:
   3.1 closing the cylinder shut off valve of the propane and the air cylinders
   3.2 verifying that the water pump has been shut off.
   3.3 opening the anodic reaction products, propane and air rotameter valves. This ensures that there is no back pressure in the lines upstream of these valves.
   3.4 open the on-off valves adjacent to the gas cylinder regulators
   3.5 verify that the air and propane gas cylinders have discharge pressure of **0** psig.

4. **RUN** labview first, then **ZERO** the LabView readings for the differential pressure indicators (DPI's): P1 (water – propane white line on labview) and P2 (air-propane purple line on labview) when atmospheric pressure is on both sides of the DP cells. Then close the air and propane rotameter valves. To "Zero" the DP readings, go to the bar located to the left of "zero DP" label, copy data from there and paste it in the "zero DP" bar. Then go to EDIT, set current value as default. Go to **FILE** and save. The click on **PAUSE**.

5. Adjust the mass controllers "set points" to the desired values should be done **step-wise**, 0.5 volts at a time, followed by a waiting time of 2 minutes. It is also done when the process is on RUN mode and gases are flowing. Targets are: 5 Volts for

propane (F1) (as calibrated- 2.2 mL/min air at NTP) and 4 Volts for Air (F2) (as calibrated-1.3 mL/min air at NTP), i.e. set them at their full scale.

Note that P1 is the square cole-parmer pressure transmitter (0-1 PsiD), part #: 68071-52. And P2 is one of the Baratron pressure transducers, from MKS, # 223BD-00100AAB.

B) Fuel Cell Assembly Procedure

1. Place the MEA inside the fuel cell; put the various plates in the proper order (See Fig. 2 for the order) and once all the layers are properly aligned insert the bolts, and gently hand tighten the bolts.

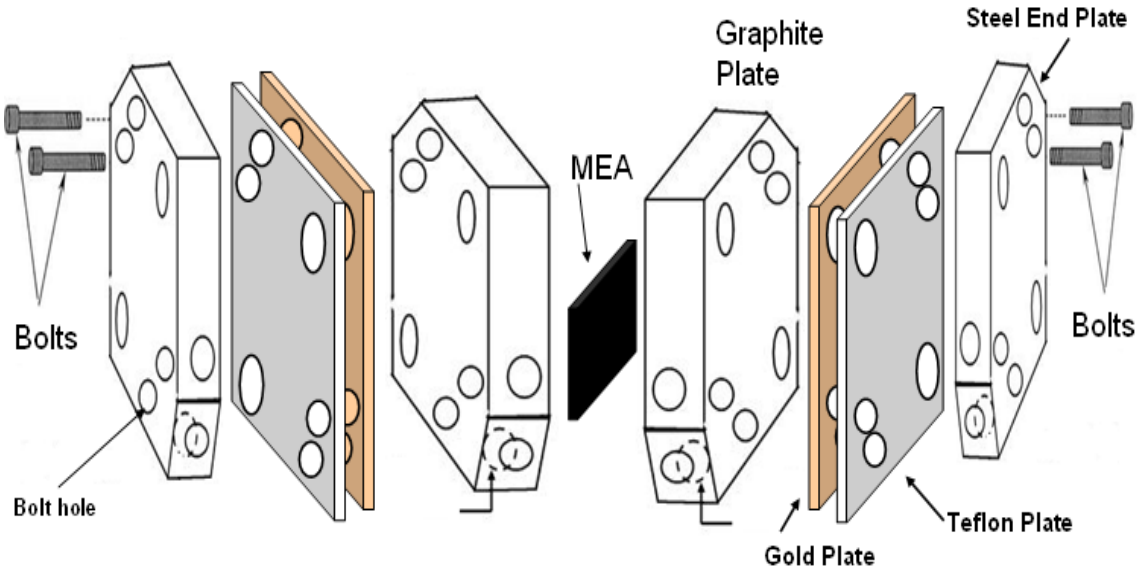

Fig. 2: Fuel Cell Assembly-Layers order.

2. Start tightening the bolts using a torque wrench. This is done by (referring to Figure 3) slightly turning bolt number 1 for example at one corner followed by turning the bolt on the opposite side of fuel cell (number 2) to obtain the same magnitude of force as bolt #

1. Then returning back to bolt number 3 followed by bolt number 4 and so on until all bolts are tightened.

3. Use the torque wrench to obtain a torque of 10 in-lb_f value initially. Then increase torque vales to 30-40 in-lb_f (a general accepted torque values are 30 - 40 in-lb_f for 1/4" bolts and 20 - 30 inch lbs for screws [1]), and in some fuel cell studies a value of 125 inches lbs (on the torque wrench) is recommended [2].

4. Inspect connections (on the fuel cell) : propane inlet (1A-inlet), water inlet (2A-inlet), air inlet (1C-inlet), reaction product and unreacted propane outlet (1A-outlet), steam outlet (2A-outlet), air steam outlet (1C-outlet) and the cathode reaction product (2C-outlet).

5. Ensure that (a) the anode reaction product outlet goes to a bubble flow meter, (b) the propane and air outlets go to the fume hood to an erlenmeyer flask (500 mL) that contains 4 cm's of water, and (c) the cathode product (steam-air mixture) outlet goes to a flask to be weighed. (Note that the empty flask must be weighed before the experiment begins). Rather than dead-ending any of the streams, the feed lines to the fuel cell (propane and air) were submerged in a few cm's of water (4 cm of water in a 500 mL flask). This makes the feed lines dead-ended unless the pressure in the lines exceeds a few cm of water. In those cases, the feed gases will bubble through the water. The head of water acts as a pressure relief or safety valve and prevents excessive pressure in the lines.

6. Set the heaters and thermocouples in place and adjust the set points to the desired values for the temperature controllers (120 °C). In order to adjust the set points on the temperature controllers these steps are followed, referring to Figure 4 below and when the temperature controller is ON:

6.1 Press the arrows △ or ▽ in order to adjust the SV value to the desired set point SV. Then press ↵

6.2 Press  to make sure that the controller is in the RUN position. This can be verified when the function r-5 on the PV screen is at RUN. If not you can adjust that using the arrows then by pressing enter ↵

6.3 Press ↵ again until a function (At) is shown on the PV screen. Then by △ adjust the value on SV screen to be ON. At that moment the **At** will start flashing on the temperature controller, this means it began to heat to the desired set point. Press ↵ again.

6.4 To stop the temperature controller from heating you can press  , and then adjust the r-5 function on the PV screen to the STOP condition by using the arrows.

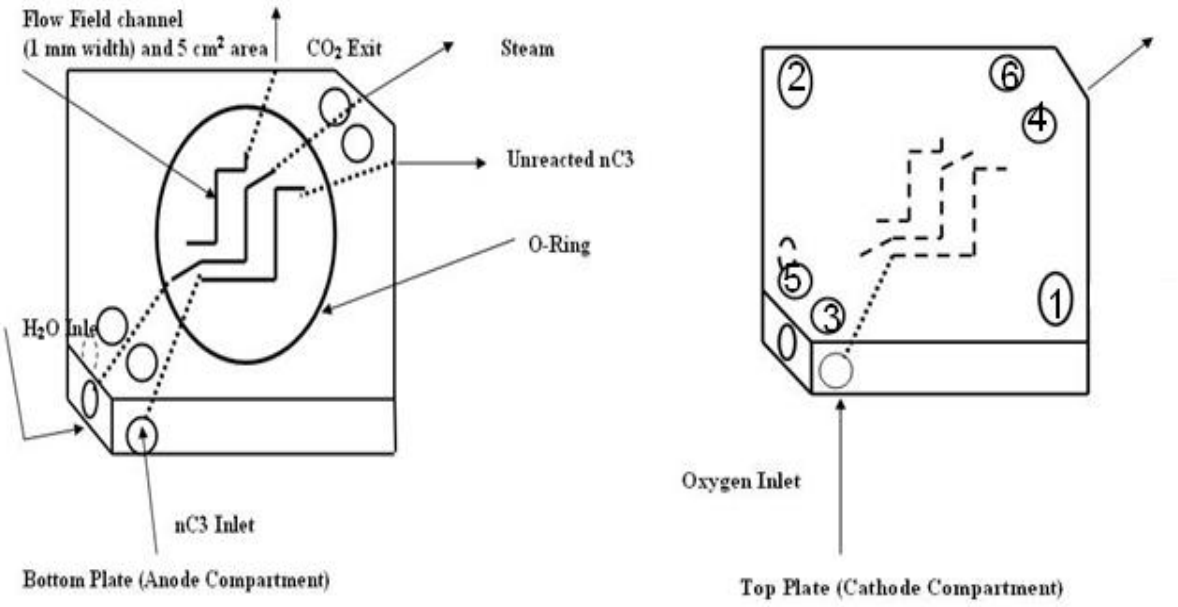

Fig.3: Top view of the anode and cathode

Fig.4: Temperature controller

C) Process Start up and Operation

1. Inspect the electrical connections by referring to the wiring diagram (see Fig. 5 below). Note that : (a) Connections C and D on the analog interface card transmit the fuel cell potential to LabView, and (b) Connections E and F transmit either a current measurement (Potentiostat method) or the potential across the standard resistance (Standard resistance method) to LabView.

Measurements using the standard resistance

- Wires C and D from the analogue signal interface card should be connected to wires C and D at the fuel cell anode and cathode for fuel cell potentiostat measurement.

- Wires C’ and D’ at the fuel cell anode and cathode should remain unconnected to anything.

- Wires E and F from the analogue signal interface card should be connected to wires G and H that are across the standard resistance.

Measurements using the potentiostat

- Wires C and D from the analogue signal interface card should be connected to positions C and D on the potentiostat.

- Wires E and F from the analogue signal interface card should be connected to positions E and F on the potentiostat.

- Wires E and F at the fuel cell anode and cathode should be connected to wires E’ and F’ that go to the potentiostat. Wires E and F to the Standard Resistance should not be connected to anything.

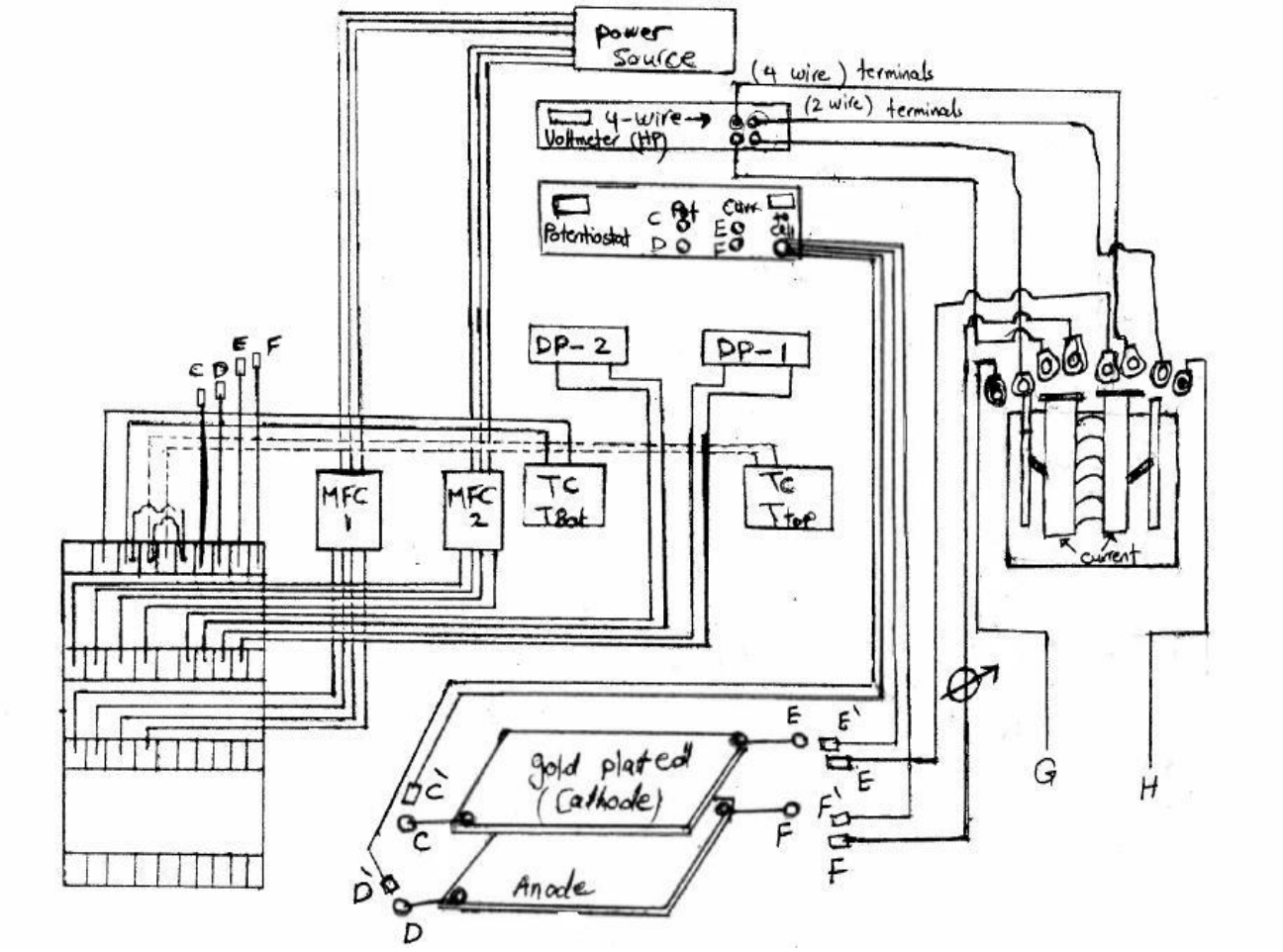

Fig. 5: Wiring diagram.

Calibration of the standard resistance using the HP meter.

Connections C, D, E, and F on the analog interface card should not be connected to anything.

1. Using the 4-wire measurement (shown in Fig.5 for the HP voltmeter), the value of the standard resistance is determined under the lab conditions. A standard resistance of 0.01 Ohm was obtained from NRC.

a) The 4-wire connection to the HP voltmeter (referring to Fig.5) is established. The outermost wires from the standard resistance should be connected to the HP voltmeter terminals where the current [1] is generated [Ω Signal (4-wire)] and the innermost wires from the standard resistance are to be connected to the HP voltmeter terminals that measure potential [2] [Input (2-wire)]. Values from [1] and [2] above shall be used to calculate the resistance.

b) Once the resistance is known, disconnect the 4-wire connection wires and connect them with E and F. Press the function button on the HP voltmeter to change measurement to "potential symbolized by V". The HP voltmeter will now shift the function to measure the potential. If you do not notice a change in function from Ω Signal to V signal, press "Hold/Manual" button to change.

c) Record V initially before any gas flow.

2. On the test station rack, turn the main power switch **ON.** This will cause the heaters to begin heating and controlling at their set points.

3. Click **RUN** button on labview.

4. Inspect the gas cylinders connections (all connectors are tightened and no leaks). Close all the rotameter valves. Close the on/off exit valves near the gas cylinder regulators. Adjust the propane gas cylinder discharge pressure (head pressure) (before the mass controller F1 (propane) to a value of 10 psig. Adjust the air gas cylinder discharge pressure (head pressure) (before air mass controller F2) to a value of 10 psig.

5. Establish the **air** flow first.

5-1 Close the on-off valve adjacent to the air regulator. Adjust the air cylinder regulator so that the air cylinder discharge pressure is 10 psig. Open the on-off

valve adjacent to the air regulator. Maintain the cylinder discharge pressure at 10 psig, by adjusting the air regulator.

5-2 With the air cylinder discharge pressure at 10 psig, and the on-off valve adjacent to the air regulator completely open, adjust the air rotameter valve to establish air flow to the cathode side of the fuel cell. Carefully watch the reading of the differential pressure transducer, DP2 (purple line, air-propane). It should have atmospheric pressure on the propane side and on the air side it should have a maximum differential pressure of 3 mm H_2O. This is a pressure slightly above atmospheric pressure on the air side. This reading represents the ΔP across the membrane electrode assembly. Experiments have indicated that MEA's rupture occurs at a value of $\Delta P = 3.4$ mm H_2O.

5-3 Measure the air flow rate with the bubble meter. Adjust the air rotameter to increase the air flow rate to the smaller value of either (a) 4 V (1.0 mL /min NTP) on the air mass flow controller or (b) 3 mm H_2O on the DP2 cell. Make a note of the numerical reading on the rotameter scale.

6. Establish **propane** flow.

6-1 Close the on-off valve adjacent to the propane regulator. Adjust the air cylinder regulator so that the propane cylinder discharge pressure is 10 psig. Open the on-off valve adjacent to the propane regulator. Maintain the cylinder discharge pressure at 10 psig, by adjusting the propane regulator. With the propane cylinder discharge pressure at 10 psig, and the shut off valve completely open, adjust the propane rotameter valve to establish propane flow to the anode side of the fuel cell. Carefully watch the reading of the differential pressure transducer, DP2 (purple line, air-propane) prior to adjusting the propane rotameter valve. Initially, the air side should have a maximum differential pressure of 3 mm H_2O (labview reading of 0.005). As the pressure on the propane side increases, the differential pressure should decrease toward zero. This reading represents the ΔP across the membrane

electrode assembly. If the reading is positive, the pressure on the air side will be greater than the pressure on the propane side. If reading is negative the pressure on the propane side will be greater than that on the air side. Note that the flow rates of propane and air should be adjusted using rotameter valves until acceptable flow rates are obtained. In all cases the maximum differential pressure should not exceed ± 3 mm H_2O.

6-2 Measure the propane flow rate with the bubble meter. Adjust the propane rotameter to increase the propane flow rate on the propane mass flow controller, F2, to the smaller value of either (a) 5 V (1.0 mL /min NTP) on the propane mass flow controller or (b) ± 3 mm H_2O (Labview reading of 0.003) on the DP1 cell. Make a note of the numerical reading on the rotameter scale. It should have atmospheric pressure on the water side and slightly above atmospheric pressure on the propane side. Ideally, and after the final adjustment at a propane flow rate of 5 Volts, F1 and DP2 pressure difference of ± 3 mm H_2O or slightly less is wanted.

6-3 Make a note of the reading of the differential pressure transducer (air-propane). It should have changed. Now the propane side should be slightly above the air side. It now should be the opposite of item 5-2 above. Propane must flow through a long tube to the bubbler in the fume hood.

7. Establish the **water** flow.

7-1 Turn on the water pump to the smallest flow rate with a hose clamp completely sealing off the water tube. Then start adjusting the clamp position to allow water to flow very SLOWLY. Now, the water pressure should rise automatically to approximately match the propane pressure, but be slightly less than the propane pressure, if the water channel is closer to the anode product channel than the propane channel. We need to monitor the differential pressure between the propane and water (DP1). Depending on the interdigitated channels used, one of the streams (propane) will be at a greater pressure than water in order to ensure that propane pressure is greater than water pressure, i.e., the DP1 reading is positive or negative and has a value of approximately 2 mm H_2O.

8. Click SAVE on Labview to record measurements.
9. All the saved files can be found on my computer, C, DATA. They will be shown according to the date.

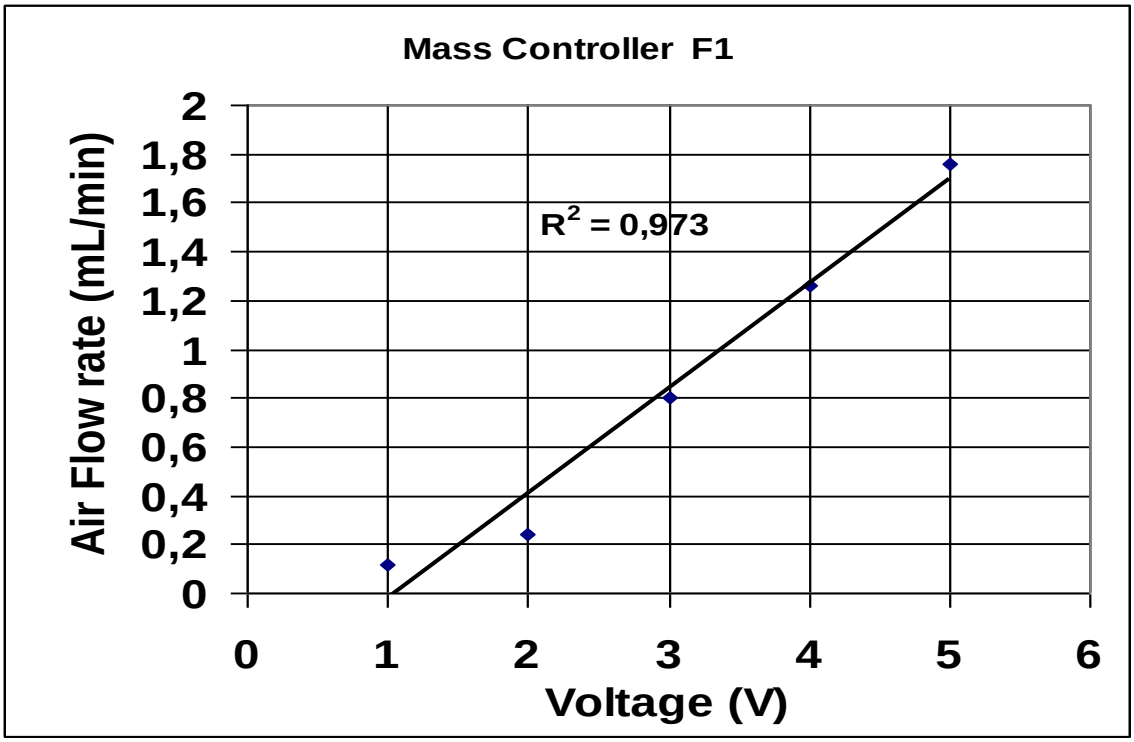

Fig. 6: Calibration of mass controller 1 at head pressure of 10 psig using Air.

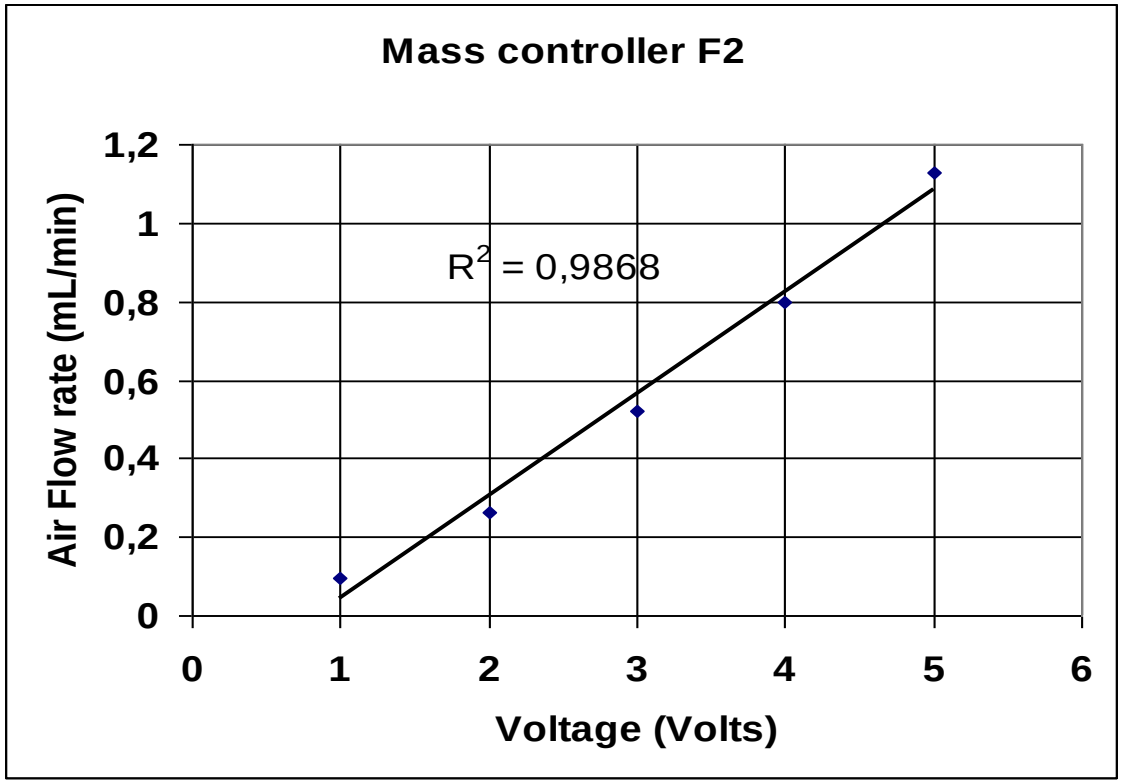

Fig. 7: Calibration of Mass controller 2 at head pressure of 10 psig using Air.

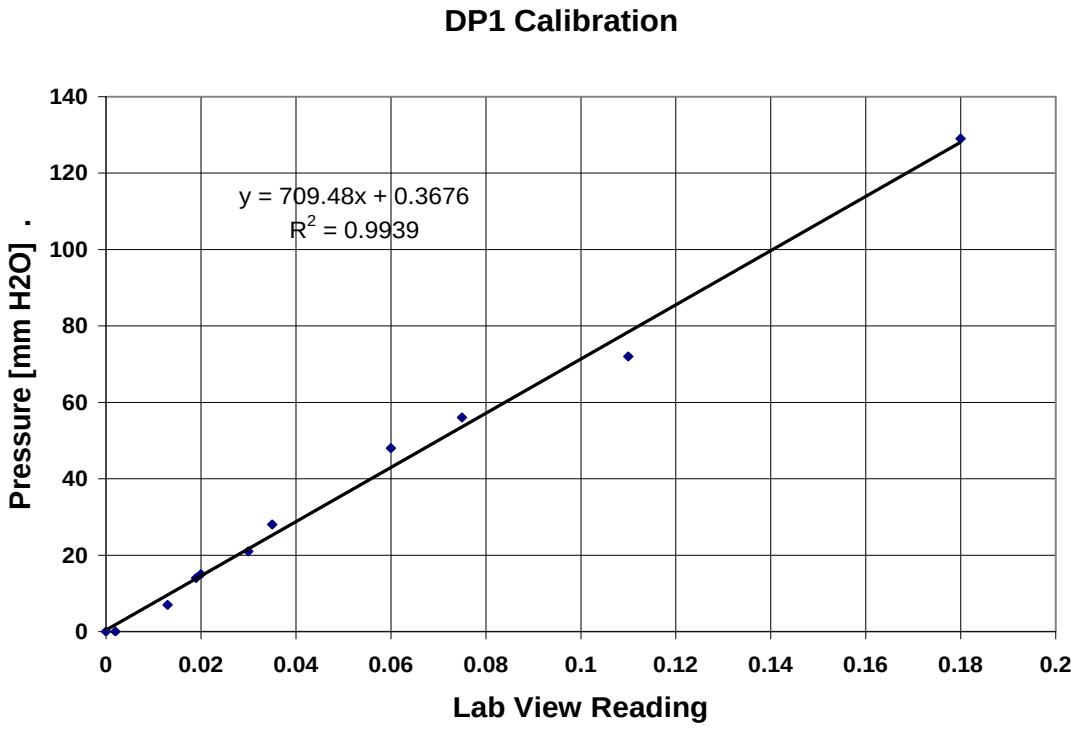

Fig. 8: Calibration of pressure transducer 1 (HC-H_2O).

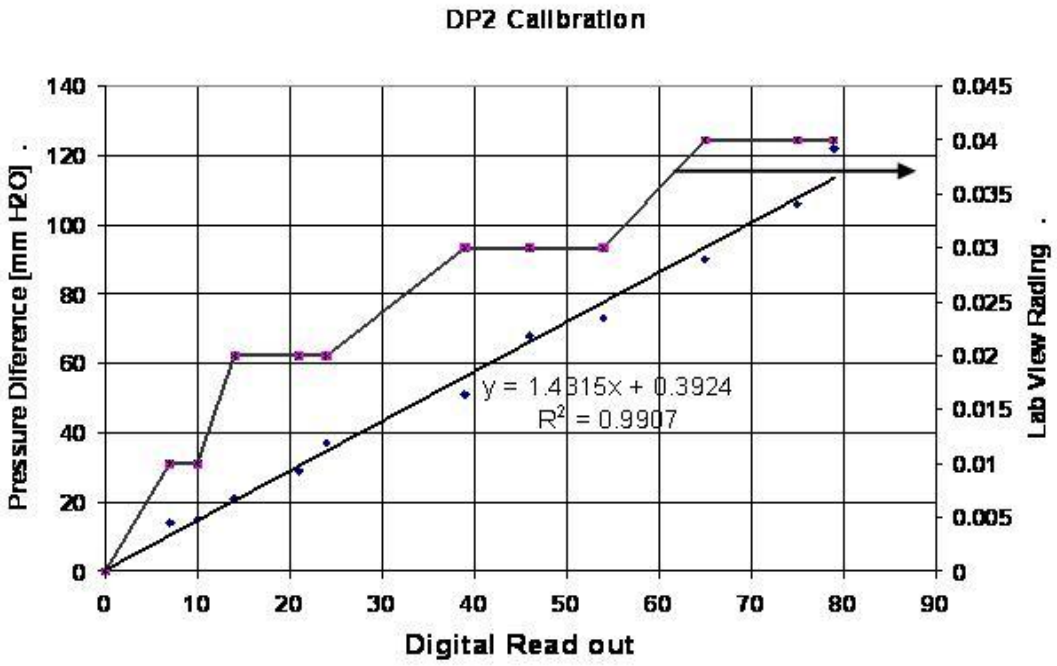

Fig. 9: Calibration of DP2 (HC-Air)

References

1. http://www.eaglefuelcells.com/tips.html
2. W. K. Lee et al. J. Power Sources, 84 (1999), p.45.

APPENDIX B

REVIEW OF PREVIOUSLY USED TECHNIQUES TO PREPARE ZrP/PTFE COMPOSITES

Appendix B: Review of the techniques previously used to prepare ZrP/PTFE composites-morphology studies

Several studies were conducted in this work to synthesize ZrP/PTFE composite membranes. The objective was to have a mechanically stable and conductive composite membrane by filling the pores of PTFE with the electrolyte material (ZrP). This could be accomplished by the in-situ precipitation of ZrP according the chemical reaction shown in Eq (1) below:

$$ZrOCl_2 \cdot 8H_2O + 2\ H_3PO_4 \rightarrow Zr(HPO_4)_2 \cdot H_2O + 2\ HCl + 8\ H_2O$$

An SEM image for zirconium oxychloride ($ZrOCl_2.8H_2O$) is shown in Fig. 1. The material consists of cuboid shaped particles of 100 + μm length and 50 μm width. Zirconium oxychloride ($ZrOCl_2.8H_2O$) is an off-white solid characterized by being a highly hygroscopic material.

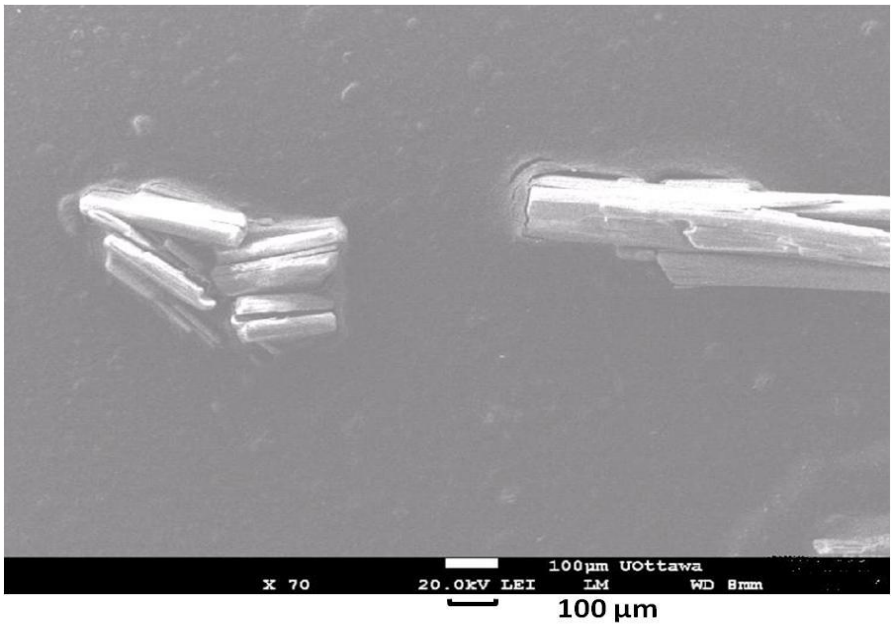

Fig. 1. SEM image of zirconium oxychloride ($ZrOCl_2.\ 8H_2O$).

Composite membranes were first prepared by painting a previously sonicated alcoholic suspension of $ZrOCl_2$/isopropanol on top of the porous PTFE in all directions. The PTFE was then rapidly dried in the oven after each painting step. The procedure was repeated several times to ensure a complete filling of the pores with $ZrOCl_2$. Glycerol (GLY) was added to H_3PO_4 to prior to the in-situ reaction to overcome the effect of surface tension and ensure the full coverage of the acid on top of the membrane. Electrochemical impedance analysis of this type of composite membrane was performed and the results showed an enhanced proton conductivity in the range of 0.03 S/cm. However, the amount of glycerol (GLY) in the membrane was not yet determined because GLY was added to the acid and the membrane was rinsed after the reaction. Despite the enhanced proton conductivity, SEM analysis of this membrane showed a non uniform coverage of the ZrP material on top of the membrane. Fig.2. shows a top view for the membrane prepared by painting the $ZrOCl_2$/isopropanol suspension, followed by reaction with concentrated (20 mL of H_3PO_4) that contained 0.2 g of GLY. Image (a) shows the ZrP material covering the surface of the membrane; however, it also shows the non–uniform distribution of the material on–top of the composite membrane. In particular, and as seen in image (b), a large agglomerate of ZrP particles appeared on some regions of the PTFE, whereas, other regions of the PTFE appeared to be uncovered. The previous observations showed that painting produced a non uniform coverage of the ZrP material.

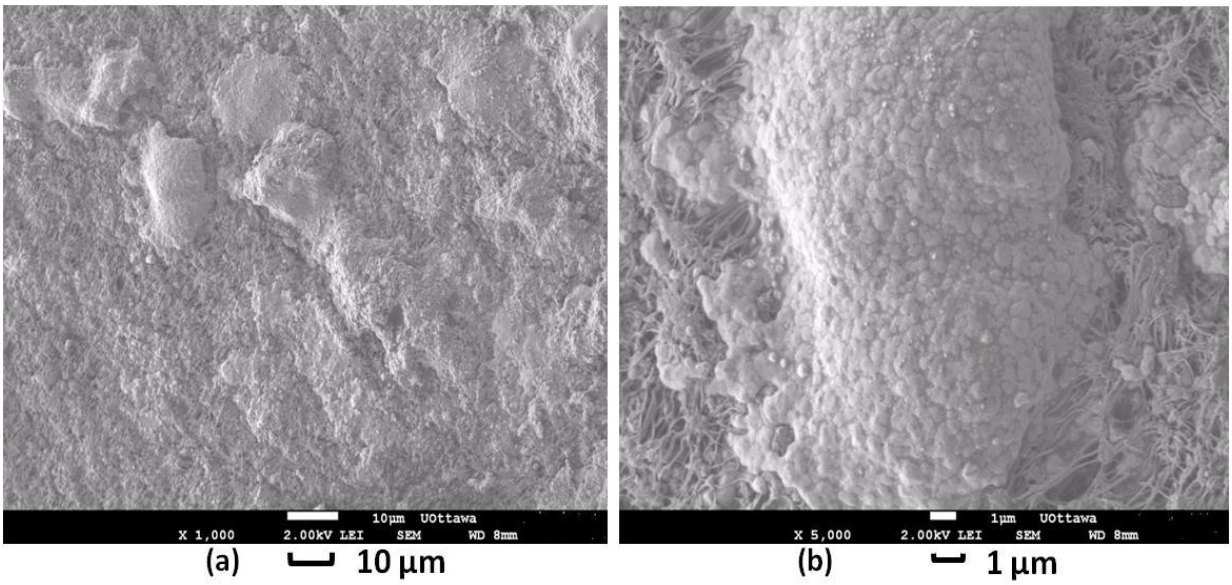

Fig. 2. SEM image of ZrP/PTFE composite membranes when 0.2 g GLY was added to 20 mL H_3PO_4

Nano–size ZrP particles were also prepared in this research project. The objective was to prepare the ZrP material first, then introduce it into the PTFE pores. ZrP nano particles were prepared by titrating a 25 mL of 0.5 M of $ZrOCl_2$ into a stirred 50 mL of Decane (n-Decane, practical from J.T. Baker Inc.). Titration of $ZrOCl_2$ was performed under stirring for 30 minutes followed by the titration of a 25 mL of 1 M H_3PO_4 into the stirred emulsion. The emulsion was then kept under vigorous agitation for 2 hours. A sample was taken and analyzed for the particle size distribution using Malvern zetasizer nano analyser. The results are shown in Fig. 3. A narrow particle size distribution was obtained with an average diameter of 5560 nm. A sample of this emulsion was decanted for several times by adding isopropanol. Then the emulsion was painted on-top of the PTFE sheet in all direction followed by drying in the oven at 130 ºC. The painting and the oven drying was repeated several times. SEM analysis was made for a membrane sample prepared by this method. The results are shown in Fig. 4.

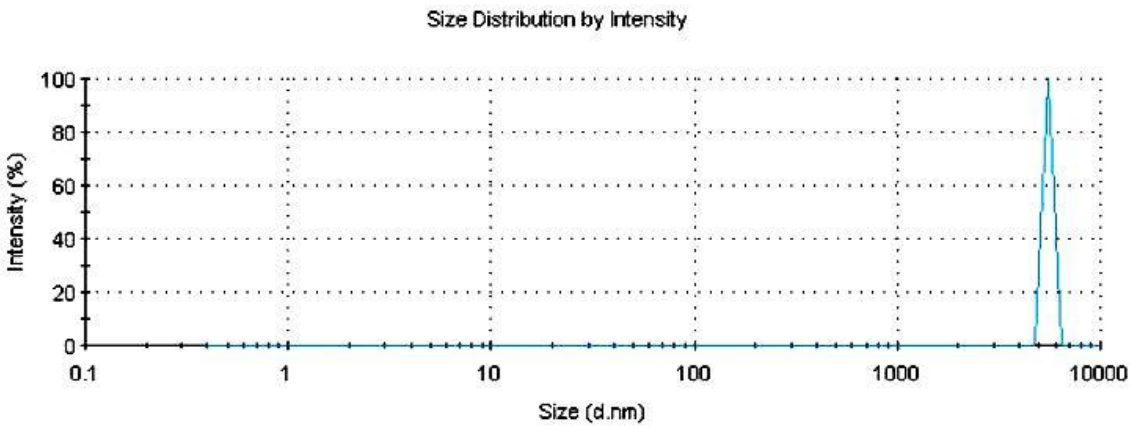

Fig. 3. Size distribution of the formed ZrP nano particles.

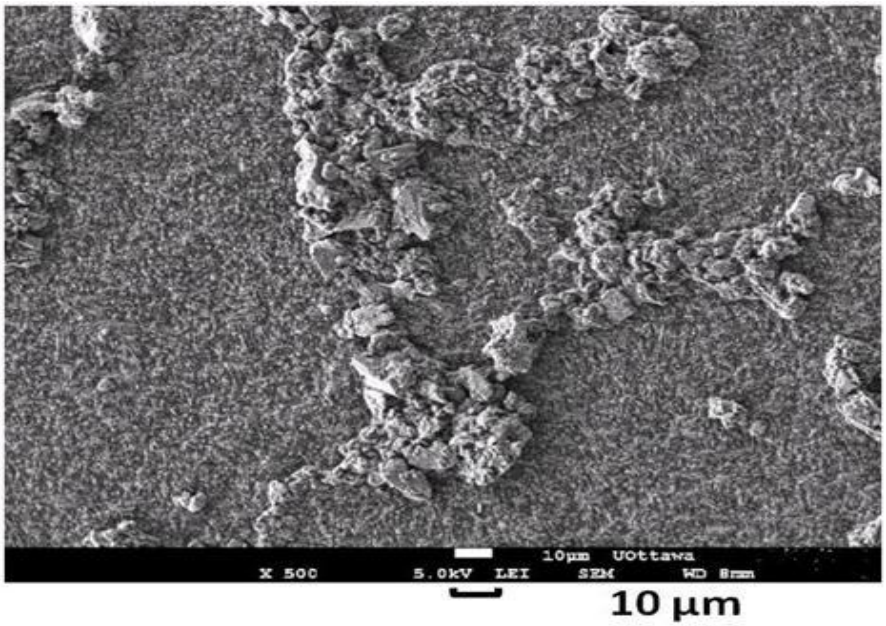

Fig. 4. SEM image of ZrP nano particle emulsion painted then dried on a PTFE porous sheet.

Fig.4. shows that the ZrP nano particles agglomerated into larger clusters upon drying, hence, prevented the ZrP from entering the small pores of PTFE. Consequently, subsequent research efforts in this work were directed toward the preparation of stirred and heated alcoholic suspension of $ZrOCl_2$. This alcoholic suspension contained a specified amount of glycerol. Then, the suspension was introduced into the pores of PTFE as previously explained in chapter 4 of this thesis.